SRNL-STI-2012-00404

Evolution of Chemical Conditions and Estimated Solubility Controls on Radionuclides in the Residual Waste Layer During Post-Closure Aging of High-Level Waste Tanks

M.E. Denham

M.R. Millings

August 2012

Savannah River National Laboratory
Savannah River Nuclear Solutions
Aiken, SC 29808

Prepared for the U.S. Department of Energy Under Contract Number DE-AC09-08SR22470

SRNL
SAVANNAH RIVER NATIONAL LABORATORY

DISCLAIMER

Printed in the United States of America

Prepared for
U.S. Department of Energy

REVIEWS AND APPROVALS

Authors

_____

M. E. Denham, Environmental Restoration Technologies Date

_____

M. R. Millings, Environmental Restoration Technologies Date

Technical Reviewers

_____

S.H. Reboul, Process Technology Programs Date

_____

R. L. Nichols, Environmental Restoration Technologies Date

Approvals

_____

H.H. Burns, Environmental & Chemical Processing Research Programs Date

_____

R. S. Aylward, Environmental Stewardship Date

_____

S. L. Marra, Environmental Stewardship

Date

_____

K. H. Rosenberger, SRR Closure and Disposal Assessment

Executive Summary

This document provides information specific to H-Area waste tanks that enables a flow and transport model with limited chemical capabilities to account for varying waste release from the tanks through time. The basis for varying waste release is solubilities of radionuclides that change as pore fluids passing through the waste change in composition. Pore fluid compositions in various stages were generated by simulations of tank grout degradation.

The first part of the document describes simulations of the degradation of the reducing grout in post-closure tanks. These simulations assume flow is predominantly through a water saturated porous medium. The infiltrating fluid that reacts with the grout is assumed to be fluid that has passed through the closure cap and into the tank. The results are three stages of degradation referred to as Reduced Region II, Oxidized Region II, and Oxidized Region III. A reaction path model was used so that the transitions between each stage are noted by numbers of pore volumes of infiltrating fluid reacted. The number of pore volumes to each transition can then be converted to time within a flow and transport model.

The bottoms of some tanks in H-Area are below the water table requiring a different conceptual model for grout degradation. For these simulations the reacting fluid was assumed to be 10% infiltrate through the closure cap and 90% groundwater. These simulations produce an additional four pore fluid compositions referred to as Conditions A through D and were intended to simulate varying degrees of groundwater influence. The most probable degradation path for the submerged tanks is Condition C to Condition D to Oxidized Region III and eventually to Condition A. Solubilities for Condition A are estimated in the text for use in sensitivity analyses if needed. However, the grout degradation simulations did not include sufficient pore volumes of infiltrating fluid for the grout to evolve to Condition A. The numbers of pore volumes of reacting fluid required to reach each stage of grout degradation are shown below.

Tanks Above the Water Table		Tanks Below the Water Table	
Chemical Stage	Pore Volumes Reacted	Chemical Stage	Pore Volumes Reacted
Reduced Region II	0 - 523	Condition C	0 – 1787
Oxidized Region II	524 - 2119	Condition D	1788 – 2442
Oxidized Region III	>2119	Oxidized Region III	>2442

Solubility controls for use in a flow and transport model were estimated for 27 elements in each of the chemical stages generated in the grout simulations plus local groundwater. The grout simulations were run with the initial infiltrating fluid in equilibrium with atmospheric oxygen to account for degradation of the reduction capacity of the grout. However, a lower Eh was used in pore fluids in the oxidizing conditions used to estimate solubilities to be more consistent with measured Eh values and natural systems. Solubilities of plutonium are affected by this decision,

but those of other elements are not. In addition, the baseline for H-Area tanks is that they will be washed with oxalic acid prior to being filled with grout. Hence, oxalate was included in the pore fluids by assuming equilibrium with calcium oxalate. The pore fluid compositions used for the solubility estimates are shown below.

Parameter	Tanks Above the Water Table			Tanks Below the Water Table			
	Red. Reg. II	Ox. Reg. II	Ox. Reg. III	A	B	C	D
pH	11.1	11.1	9.2	5.4	8.8	8.8	8.8
Eh (volts)	-0.47	0.24	0.29	0.37	0.36	-0.31	0.36
Ca+2 (molar)	4.0E-3	4.0E-3	6.6E-5	6.2E-5	4.0E-4	3.90E-4	3.9E-4
DIC	6.7E-7	6.9E-7	7.5E-5	9.8E-5	2.8E-5	3.2E-5	3.0E-5
SO4-2	1.0E-5	1.0E-5	1.0E-5	6.3E-6	1.5E-5	2.0E-5	6.9E-6
Na+	1.0E-3	1.0E-3	1.0E-3	4.4E-5	3.9E-5	4.0E-5	4.0E-5
Cl-	1.0E-3	1.0E-3	1.0E-3	8.5E-5	8.1E-4	7.8E-4	8.0E-4
Oxalate	4.1E-6	4.1E-6	4.4E-5	4.2E-5	9.5E-6	9.5E-6	9.5E-6

Solubility estimates were done by equilibrating a solubility controlling phase for each element with the pore fluid compositions using The Geochemist's Workbench®. Condition B pore fluids are similar to Condition D. Therefore, solubilities for Condition B were not estimated, but assumed to be the same as in Condition D. In general solubility controlling phases were selected to bias solubilities to higher values. Several elements had no solubility controls and solubility estimates for other elements were omitted because the elements had short half-lives or were present in residual waste in very low amounts. For these it is recommended that release from the tank be instantaneous when the tank liner is breached.

There is considerable uncertainty in this approach to enabling a flow and transport model to account for variable waste release. Yet, it is also flexible and requires much less computing time than a fully coupled reactive transport model. This allows some of the uncertainty to be addressed by multiple flow and transport sensitivity cases.

Some of the uncertainties are addressed within this document. These include uncertainty in infiltrate composition, grout mineralogy, and disposition of certain components during the simulations. Uncertainty in the solubility estimates is addressed in part by examining sensitivity of solubilities for four key elements to uncertainty in thermodynamic data, pH, Eh, total inorganic carbon concentration, and oxalate concentration. In addition, the solubilities for the elements estimated here are compared to two other compilations of solubilities in cementitious materials.

Contents

Table of Figures

Table of Tables

Introduction

Release of contaminants from residual waste in closed high level waste tanks will depend on the chemical composition of pore fluids passing through the residual waste layer. The composition of these fluids will vary, causing solubilities of key radionuclides to vary, as infiltration water flows through the tank fill grout. Geochemical modeling is described here that enables a flow and transport model with limited chemical capabilities to simulate this. The simplifications that allow implementation of the model are documented and justified. In the most general sense, the model assumes that the residual waste remains as a discrete layer at the bottom of the tanks after they are filled with reducing grout. Henceforth, this discrete layer is referred to as the residual waste layer. Infiltration from the surface or groundwater that passes through the tanks interacts with the grout driving changes to grout mineralogy and causing fluids emerging from the grout into the residual waste layer to have a composition that reflects these interactions. Release of contaminants from the tanks is controlled primarily by solubility of assumed contaminant-bearing solid phases in the varying fluid composition. Hence, this waste release model imposes chemical constraints on contaminant release that vary as the grout degrades. Varying physical controls such as hydraulic driving forces and hydraulic conductivity can be imposed by the flow and transport model that draws input from this waste release model.

Development of the waste release model was done in two stages – the modeling of the grout degradation and the estimation of solubilities of 27 elements at the various chemical conditions suggested by the grout modeling. Of the 27 elements, Np, Pu, Tc, and U, are considered to be the most likely risk drivers based on process knowledge and previous Performance Assessment modeling. These are given extra attention in development of the waste release model.

Simulations of Tank Grout Degradation

Estimated Chemical Evolution of Reducing Grout

Figure 1 shows a diagram depicting the conceptual model of waste release from high level waste tanks. Water infiltrating through the cover system enters the grout, reacts with grout minerals, and ultimately passes through the residual waste layer beneath the grout. As reactions in the grout progress and minerals dissolve or precipitate, the pore water chemistry exiting the grout changes. The changing pore water chemistry passing through the residual waste layer results in varying solubility of contaminants.

The simulation treats the tank grout as a porous medium. It is recognized that fracturing could lead to heterogeneous flow patterns and that “fast” flow paths might occur within the tank. Yet, there is very little certainty about the nature and effects of fracturing over the thousands of years of tank aging. In particular, there is uncertainty surrounding the extent to which water passing through fractures interacts with the grout and, importantly, how water that reaches the residual layer through a fracture interacts with that layer. The differing effects of fractures and fast-flow

paths are addressed in sensitivity analyses within the Performance Assessment using information selected from the waste release model and implemented with the flow and transport modeling.

The Geochemist's Workbench® (Bethke, 2005) was used to simulate the major changes in pore fluid chemistry by modeling infiltrating fluid passing through a hypothetical one cubic meter block of tank grout. The simulations were done in the "Flush" mode to simulate plug flow through a porous medium. Each pore volume of fluid that enters the grout block completely replaces the previous reacted pore volume of fluid. This results in a reaction path model in which each pore volume of reacting fluid changes the mineralogy of the grout. The changes are reflected in the chemical composition of the fluid exiting the grout. The nature of this type of modeling produces step changes in the major chemical parameters of interest such as Eh and pH. These occur when a mineral that exerts the

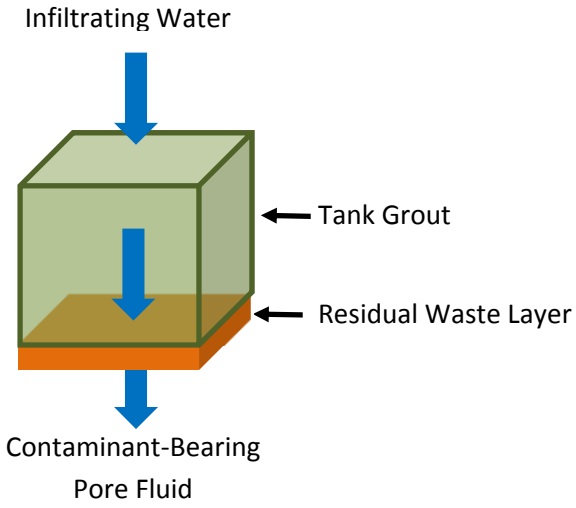

Figure 1: Conceptual model of pore fluid evolution and plutonium dissolution from the residual waste layer.

dominant control on a parameter is completely dissolved from the grout. Minor changes in these parameters may occur when a previously stable mineral begins to dissolve or a mineral begins to precipitate.

The advantage of this type of modeling is its flexibility. The only grout properties required are the mineralogy and the porosity. This frees the flow and transport model to run numerous simulations varying flow conditions without the computational burden of solving the equilibrium chemistry at each node.

The initial mineralogy of the hypothetical grout block was estimated from the proposed grout formulation using a normative calculation. The normative mineralogy is simply a way to assign the chemical components of the bulk composition of the grout to mineral phases. The actual mineralogy is unknown so representative phases used in published cement simulations (e.g., Höglund, 2001; Lothenbach and Winnefeld, 2006) were chosen for the normative mineralogy. The grout formulation was from Stefanko and Langton (2011) and is shown in Table 1. The effect of small deviations from these nominal values on rates of grout degradation would be small relative to the effects of other uncertainties. Chemical analyses of each of the major cementitious constituents in the formulation were taken from Langton (2009, Attachment 2). These are shown in Table 2 along with the calculated bulk composition of the proposed grout.

Table 1: Proposed Tank 18 grout formulation (Stefanko and Langton, 2011).

Grout Component	Pounds Per Cubic Yard
Cement Type I/II	125
Slag Grade 100	210
Fly Ash Class F	363
Quartz Sand	1790
Gravel No. 8	800
Water	405

Table 2: Chemical compositions of major grout constituents (Langton, 2009) and bulk composition of proposed grout.

Component	Cement Type I/II (Wt.%)	Slag Grade 100 (Wt.%)	Fly Ash Class F (Wt.%)	Proposed Grout (g/m^3)
Al2O3	4.91	10.1	28.4	77388
CaO	64.3	35.8	1.41	95326
Fe2O3	3.5	0.36	7.99	20252
K2O	0.37	0.27	2.99	7050
MgO	0.95	12.6	1.0	18557
Na2O	0.09	0.22	0.44	1288
SO3	2.64	1.99	0.1	4653
SiO2	21.0	39.1	53.1	178647

The normative mineralogy of the grout was calculated by assigning major chemical components to cementitious minerals (Appendix 1 shows chemical formulas of all minerals considered):

- All SO_3 was assigned to gypsum ($CaSO_4 \cdot 2H_2O$) with the requisite CaO
- All remaining CaO was assigned to JenH ($Ca_{1.33}Si_{1.0}O_{3.33} \cdot 2.17H_2O$) with the requisite SiO_2
- All MgO was assigned to OH-Hydrotalcite ($Mg_4Al_2(OH)_{14} \cdot 3H_2O$) with the requisite Al_2O_3
- All remaining Al_2O_3 was assigned to gibbsite ($Al(OH)_3$)
- All Fe_2O_3 into was assigned to magnetite (Fe_3O_4)
- All remaining SiO_2 was assigned to amorphous silica (SiO_2)

The alkalis were assumed to remain soluble in the pore fluid, to be leached out with the first pore volume of infiltrating fluid.

The normative mineralogy is shown in Table 3. The normative mineralogy is assumed to be completely hydrated because of the time lag between closure cap degradation and breaching of the liner. Amorphous silica in the mineralogy represents the silica glass associated with blast furnace slag and fly ash. There is an excess of silica relative to portlandite ($Ca(OH)_2$), and thus all portlandite is assumed to react to the C-S-H phase JenH (Kulik, 2011). Iron likely exists in several phases, but magnetite was chosen here because it is a common phase in fly ash (e.g., Hower et al., 1999) and the Portland cement has a measured reduction capacity. Nevertheless, only one gram of magnetite was put in the "Basis" mineralogy for the grout simulations so that only reduction capacity from the slag would be considered – a bias toward a shorter duration of reducing conditions. Pyrite (FeS_2) was assigned to account for this because pyrrhotite, which has been observed in various types of slag quickly oxidizes to pyrite during grout simulations (Denham, 2007, Rev. 2).

Table 3: Calculated normative mineralogy of proposed grout and the equilibrium mineralogy as recalculated by The Geochemist's Workbench.

Minerals in System	Normative Mineralogy (g/m^3)	Recalculated (g/m^3)
Calcite	--	2.82E-1
Ettringite	--	2.58E4
Gibbsite	1.01E5	9.72E4
Gypsum	1.00E4	--
JenH	2.15E5	9.69E4
TobD	--	1.21E5
Magnetite	1.96E4*	1.04E0
OH-Hydrotalcite	5.10E4	5.10E4
SiO2	1.05E5*	--
Pyrite	8.16E2	8.16E2
Inert	1.54E6	1.54E6

*Not used in base case simulation – see uncertainty section

When setting up a simulation in The Geochemist's Workbench® the normative mineralogy and pore fluid are entered into the "basis". From this starting point, The Geochemist's Workbench® recalculates the basis so that the fluid and minerals are in equilibrium. This may involve precipitation or dissolution of minerals. In the recalculated mineralogy in Table 3, a small amount of calcite and larger amounts of ettringite ($Ca_6Al_2(SO_4)_3(OH)_{12}\cdot 26H_2O$) and TobD ($Ca_{0.88}Si_{0.67}O_{2.22}\cdot 1.83H_2O$) were added at the expense of carbonate in the original pore fluid and minerals containing calcium, sulfur, aluminum, and silica.

Pyrite was included in the mineralogy to account for the reducing capacity of the grout. It is important to note that pyrite is used simply as a method to account for the measured reducing capacity of the grout and is not meant to imply that grains of pyrite in the grout are the primary

source of reducing capacity. To the contrary, the main source of reducing capacity is likely reduced sulfur incorporated in the silica glass of the blast furnace slag (Pabalan et al., 2009). However, this cannot be represented in the model in a way that is mechanistically true. So, a distinct solid phase, in this case pyrite, is used to account for the reducing capacity.

The reducing capacity of the grout was calculated from the amount of slag in the formulation and the measured reducing capacity of slag (Roberts and Kaplan, 2009). This was done as shown in Figure 2. Other iron was left out of the mineralogy with the exception of one gram of magnetite to hold a place for iron in the basis.

Calculation of Amount of Pyrite (accounts for reducing capacity of slag)

Measured reducing capacity of slag = 819 ueq/g (SRNL-STI-2009-00637 (Roberts and Kaplan, 2009))

Pyrite oxidation reaction: $FeS_2 + 3.75O_2 + 0.5H2O = Fe^{+3} + 2SO_4^{-2} + H^+$

15 moles electrons exchanged/mole pyrite oxidized MWpyrite=119.967 g/mole

15/119.967 = 0.125 moles electrons exchanged/gram pyrite oxidized

reduction capacity of pyrite = 125,000 ueq/gram

124,591 grams slag/m^3 of reducing grout

total reduction capacity= 124,591 g slag/m^3 grout x 819 ueq/ g slag = 1.02E8 ueq/m^3 grout

Figure 2: Calculation of amount of pyrite in normative mineralogy to account for measured reducing capacity.

The chemical composition of the infiltrating water that was reacted with the tank grout is shown in Table 4. It was derived by equilibrating an average rainwater composition (Strom and Kaback, 1992) with kaolinite and amorphous silica using The Geochemist's Workbench®. This was used to simulate rainwater that had passed through soil and the closure cap. The dissolved oxygen and carbon dioxide concentrations were calculated by equilibrating this water with atmospheric oxygen (PO2=0.2 atm) and carbon dioxide (PCO2=3.2E-4 atm). It is assumed here that the pore water composition remains constant throughout the grout aging simulation. At some point, perhaps within the modeling period, the infiltration would revert to the composition of rainwater. Assuming rainwater composition in the SRS area in the future is similar to the composition reported in Strom and Kaback (1992), the primary difference would be lower dissolved aluminum and silica concentrations. The rainwater pH and the dissolved gas concentrations would be the same. Reaction of the infiltrating water with grout was closed with respect to atmospheric gases. A porosity of 21% (Stefanko and Langton, 2011) defined the pore volume of the grout block.

Table 4 : Infiltrating water composition used in grout evolution simulations.

Constituent	Concentration
pH	4.68
$O_{2(aq)}$	2.19E-4 moles/liter
$CO_{2(aq)}$	1.07E-5 moles/liter
Cl^-	2.74E-5 moles/liter
Na^+	8.69E-6 moles/liter
Ca^{+2}	2.06E-6 moles/liter
Mg^{+2}	1.34E-6 moles/liter
Al^{+3}	8.43E-7 moles/liter
$H_4SiO_{4(aq)}$	1.90E-3 moles/liter
SO_4^{-2}	1.35E-5 moles/liter

The simulations of the chemical evolution of tank grout were run using The Geochemist's Workbench® in a manner similar to Denham (2007, Rev. 2), with some notable exceptions. The current simulations used a different set of cementitious minerals with different thermodynamic data obtained from Lothenbach and Winnefeld (2006) and Kulik (2011). The PHREEQC thermodynamic database (provided with The Geochemist's Workbench® as "thermo_phreeqc") was used as the framework to build a thermodynamic database suitable for simulations of cementitious materials. In addition to cementitious minerals, the thermodynamic data for the iron minerals pyrite, magnetite, and maghemite were updated. The minerals allowed in the simulations are shown in Table 5 and the thermodynamic data are presented in Appendix 1.

Table 5: Minerals allowed in simulations of tank grout chemical evolution.

Brucite	Gibbsite	Monocarboaluminate
C4AH13	Gypsum	OH-Hydrotalcite
Calcite	JenD	Portlandite
Ettringite	JenH	SiO2(am)
Fe(OH)3(am)	Maghemite	TobD
Fe-Ettringite	Magnetite	TobH

It should be noted that an inherent assumption in these simulations is that the minerals that make up the residual waste layer do not strongly influence the composition of the pore fluids. Hay (2012) has observed gibbsite, hematite, cejkaite, calcite, a nitrated sodium aluminum silicate, and a uranyl hydrogen fluoride hydrate in Tank 18 residual waste. The hematite is assumed here to convert to magnetite prior to the tank liner breaching because of contact with the reducing grout pore fluids. The grout pore fluids are in equilibrium with gibbsite and calcite throughout the simulation, so the presence of these in the residual waste layer do not affect the pore fluid composition. The effect of the other phases is unknown. Nonetheless, the residual waste layer is

approximately 2.9 cm thick on average (U-ESR-F-00041) compared to the approximate 10 meter thick layer of grout above it. Hence, one pore volume of fluid passing through the grout equates to approximately 345 pore volumes of the residual waste layer (assuming a similar porosity). So, the mineralogy of the residual waste layer should quickly approach equilibrium with the grout pore fluids.

Figures 3 and 4 show the evolution of Eh and pH in fluids eluting from the tank grout over 2500 pore volumes. Figure 5 shows the evolution of the mineralogy of the grout that dictates the pH and Eh transitions. A nomenclature modified from Bradbury and Sarott (1995) to include redox aspects of the grout is used to describe the chemical evolution of the tank grout. The grout evolves through three distinct regions beginning with Reduced Region II (Figure 3). In this region the Eh is predominantly -0.47 volts and is poised by the presence of pyrite. When pyrite is completely oxidized at pore volume 523, there is a step change to Oxidized Region II with an Eh of +0.56 volts. The mineral JenH initially controls pH at pH=11.6 but is converted to TobD by 67 pore volumes of fluid reacted. Throughout the remainder of Reduced Region II and all of Oxidized Region II,TobD controls pH at a value of 11.1 (Figures 4 and 5). At pore volume 2119 the mass of TobD is exhausted and the grout moves into Oxidized Region III. This region has an Eh of +0.68 volts and a pH of 9.2. The Eh is poised by equilibrium with dissolved oxygen and the pH is controlled by OH-hydrotalcite. An increase in dissolved inorganic carbon also occurs in Oxidized Region III as calcite begins to dissolve.

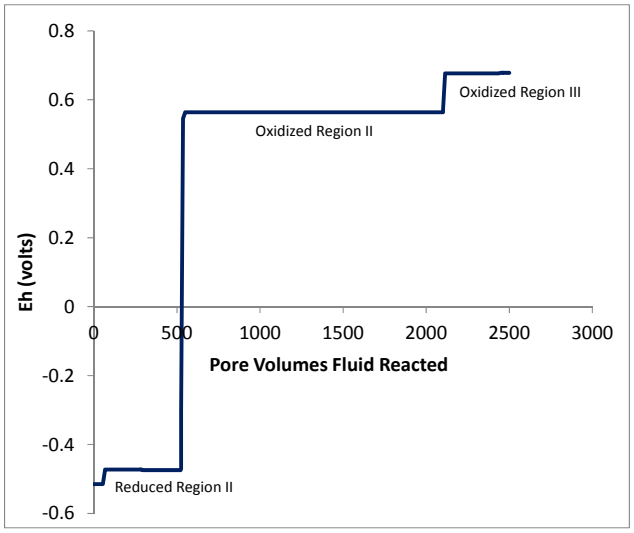

Figure 3: Eh evolution during simulated grout aging.

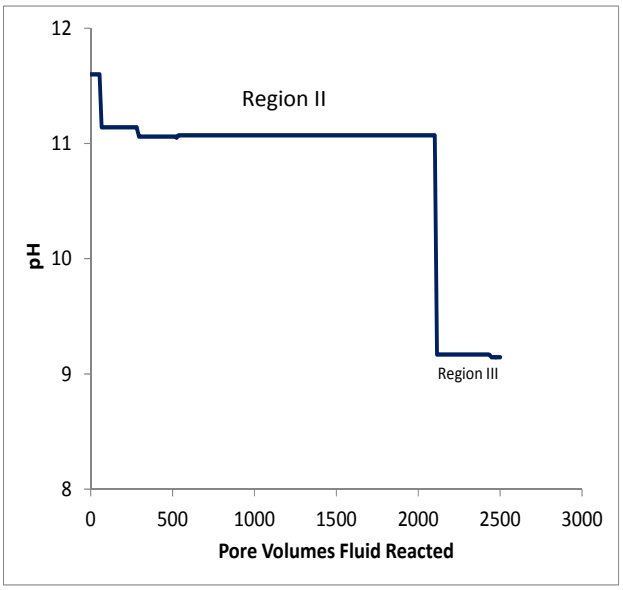

Figure 4: Simulated evolution of pH in grout pore fluids entering residual waste layer.

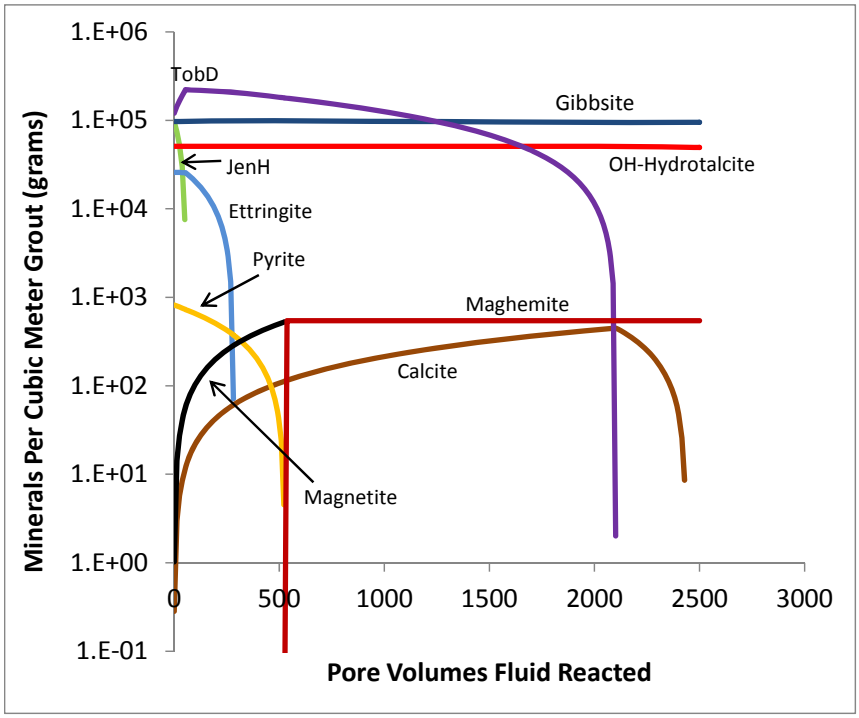

Figure 5: Simulated evolution of mineralogy in tank grout.

The simulation results provide the basis for choosing chemical conditions for calculating solubility of various radionuclides throughout the Performance Assessment modeling period. These are shown in Table 6.

Table 6: Eh, pH and dissolved inorganic carbon at different chemical conditions during simulated evolution of tank grout.

Chemical Condition	Eh (volts)	pH	Ca(molar)	Total Carbonate (molar)
Reduced Region II	-0.47	11.1	0.004	6.7E-7
Oxidized Region II	+0.56	11.1	0.004	6.9E-7
Oxidized Region III	+0.68	9.2	6.6E-5	7.5E-5

Pore Fluid Conditions for Submerged Tanks

For several tanks in H-Area the residual waste layer is below the water table (Hamm and Collard, 2010). For the purposes of this document all tanks that have a portion at or below the water table are called "submerged tanks". In submerged tanks, once the tank liner fails the pore fluid passing through the waste layer will be influenced by the chemistry of groundwater. For these tanks it was conservatively assumed here that lateral flow of groundwater through the tank grout will predominate over vertical flow from infiltrate (Flach and Jordan, 2010). To evaluate the potential influence of groundwater on radionuclide solubility, four different chemical conditions were simulated that show varying degrees of groundwater influence. The basis for these is shown in Figure 6. The groundwater composition used (Table 7) is from a background water table well, designated P27D (Strom and Kaback, 1992), approximately 450 meters east of Tank 43.

Table 7: Groundwater composition used to mix with grout pore fluids to produced Conditions B, C, and D.

Parameter	P27D Groundwater
pH	5.4
Eh (volts)	0.37
Ca+2 (moles/liter)	6.2E-5
DIC	9.8E-5
SO4-2	6.3E-6
Na+	4.4E-5
Cl-	8.5E-5

Condition A: Groundwater flows laterally directly into the residual waste layer with no effect of outer concrete.

Condition B: Groundwater equilibrates with outer concrete, assumed to be fully carbonated, before passing through the residual waste layer where it mixes with a small amount of Oxidized Region II grout pore fluid

Condition C: Groundwater flows laterally directly into the residual waste layer with no effect of outer concrete and mixes with a small amount of Reducing Region II grout pore fluid

Condition D: Groundwater flows laterally directly into the residual waste layer with no effect of outer concrete and mixes with a small amount of Oxidizing Region II grout pore fluid

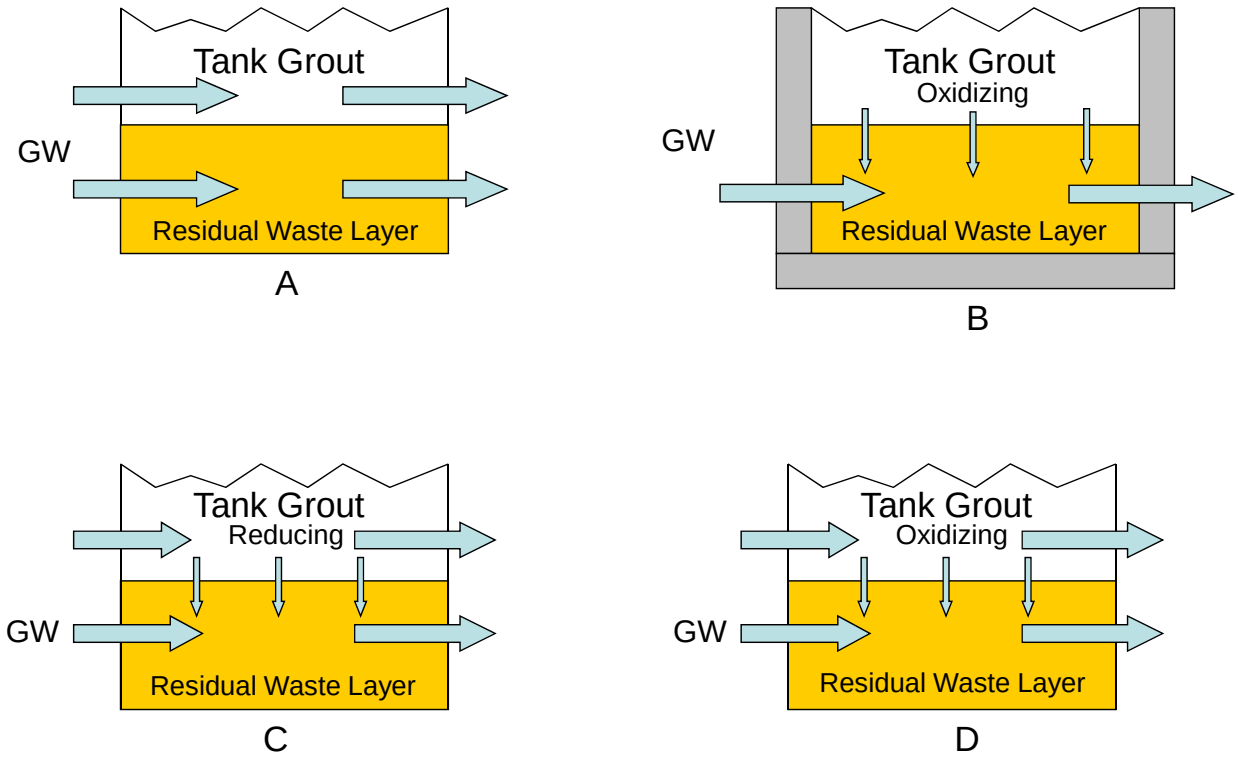

Figure 6: Basis for four conditions controlling pore fluid chemistry in residual waste layer of partially submerged tanks.

To calculate the compositions for Conditions B, C, and D, The Geochemist's Workbench® was used in the flash mode to mix the two endmember fluid compositions. The Eh of the Oxidizing Region II endmember was set to 0.24 volts for reasons discussed below. Mixing of compositions using Eh to represent the redox state can lead to spurious results – the endmember Eh values can be altered in the final mixing results. To overcome this, the fugacities of oxygen in equilibrium with the Eh were used to account for the redox state of the endmembers.

Figure 7 shows pH and Eh mixing curves for Conditions B, C, and D and Table 8 shows the compositions of the pore fluids for each Condition. Composition of 90% groundwater and 10% grout pore fluid were chosen for Conditions B, C, and D, consistent with the flow and transport modeling. Equilibrium with precipitating calcite causes similarity in pH, Ca concentrations, and dissolved inorganic carbon concentrations between Conditions B, C, and, D.

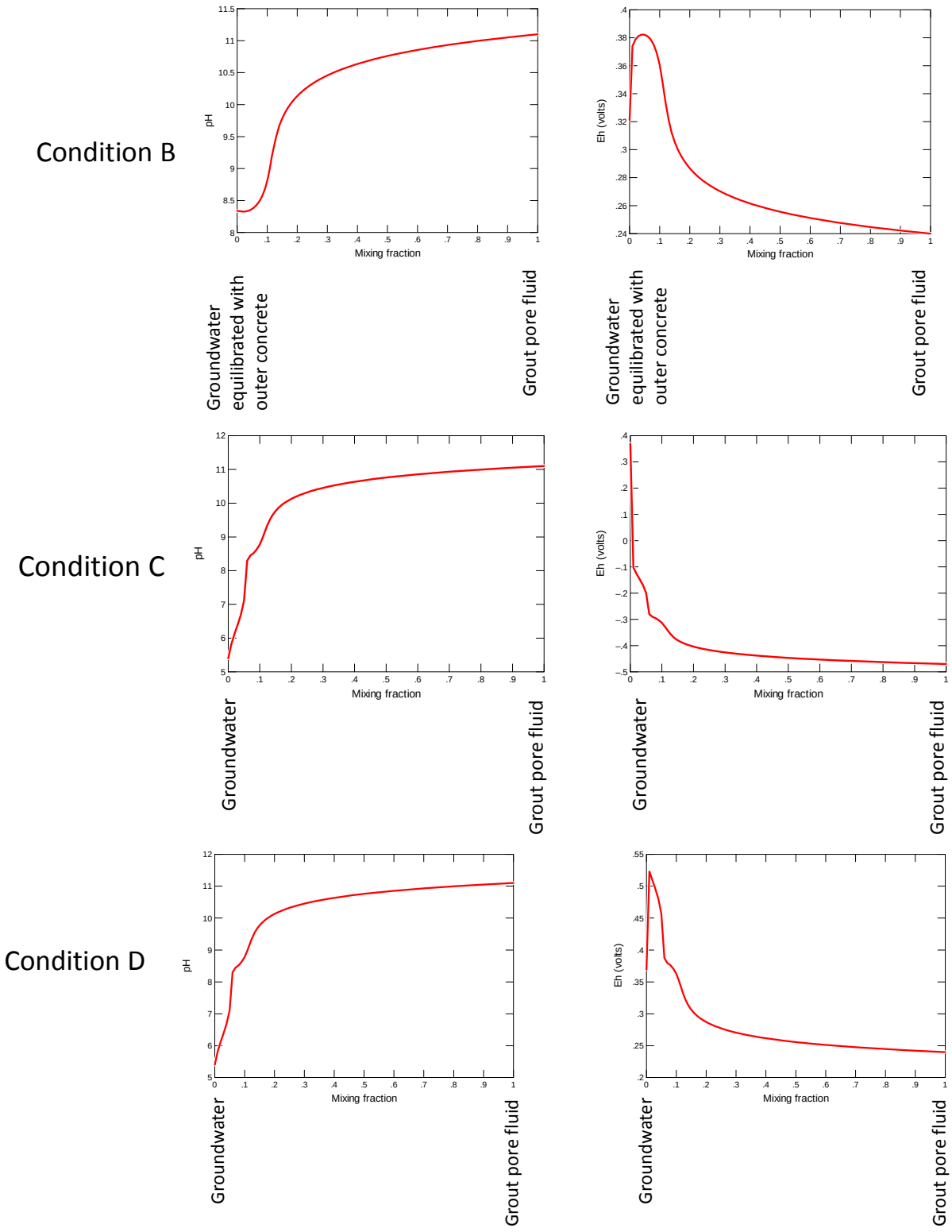

Figure 7: pH and Eh curves resulting from mixing endmember pore fluid compositions for Conditions B, C, and D.

Table 8: Chemical Compositions of contaminated zone pore fluids for Conditions A, B, C, and D.

Parameter	Condition A	Condition B	Condition C	Condition D
pH	5.4	8.8	8.8	8.8
Eh (volts)	0.37	0.36	-0.31	0.36
Ca+2 (moles/liter)	6.2E-5	4.0E-4	3.9E-4	3.9E-4
DIC	9.8E-5	2.8E-5	3.2E-5	3.0E-5
SO4-2	6.3E-6	1.5E-5	2.0E-5	6.9E-6
Na+	4.4E-5	3.9E-5	4.0E-5	4.0E-5
Cl-	8.5E-5	8.1E-4	7.8E-4	8.0E-4

Grout Degradation in Submerged Tanks

The evolution from one condition to another during grout degradation of the submerged tanks is not as straightforward as for the non-submerged tanks. The most probable progression would be from Condition C to Condition D to Oxidized Region III and eventually to Condition A. The number of pore volumes of infiltrating fluid used in the grout simulations was insufficient for the grout to evolve to Condition A and no specific transition is listed. Solubilities are included for Condition A for comparison to the other conditions. Grout degradation simulations were run for submerged tanks using the The Geochemist's Workbench and the same conceptual model as for the non-submerged tanks, but with a different infiltrating fluid. For these simulations the infiltrating fluid for the non-submerged tanks was mixed with groundwater using the "Flash" mode in The Geochemist's Workbench. The mix composition for 90% groundwater and 10% original infiltrate was used as the grout degrading fluid. Figure 8 shows the pH and Eh transitions from the simulations. Eh transitioned from -0.47 v to 0.54 volts after 1826 pore volumes. The reason for the longer transition time compared to the non-submerged tanks is the low dissolved oxygen concentration (3.8E-5 molar) in the background well nearest the H-Tank Farm. The pH transitioned from 11.3 to 9.3 at 2445 pore volumes of fluid reacted. Within the waste layer, a pore fluid composition of Condition C would be applicable to 1826 pore volumes fluid reacted, Condition D would be applicable to 2445, followed by Oxidized Region III.

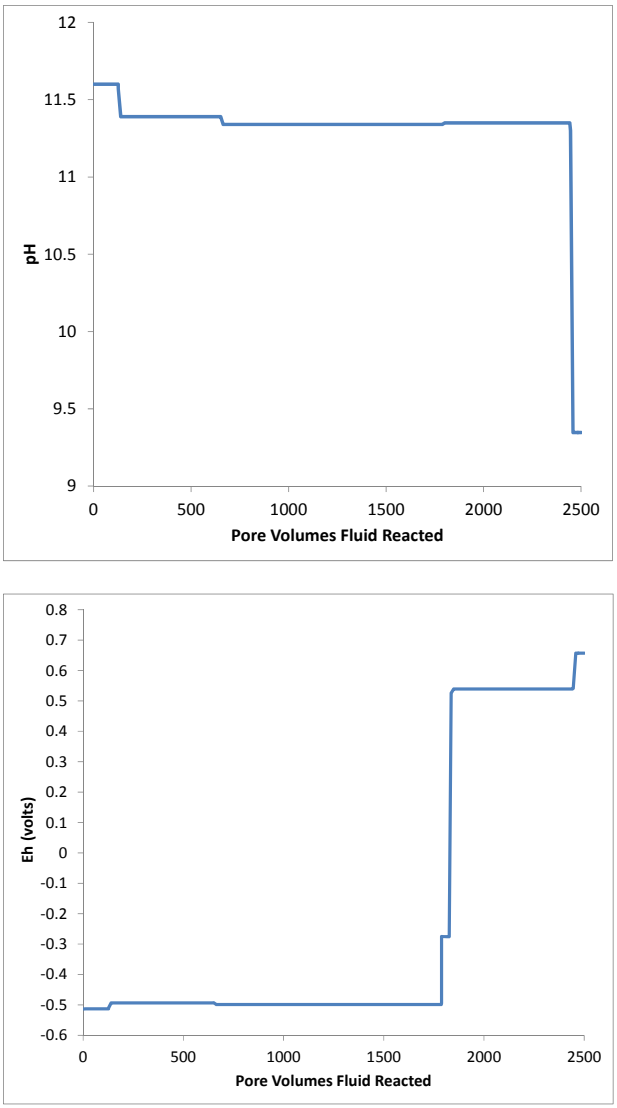

Figure 8: pH and Eh transitions in grout pore fluid as grout degrades in submerged tanks.

Uncertainties

Simulation of Chemical Evolution of Tank Grout

This simulation of the chemical evolution of tank grout is meant to provide a basis for Performance Assessment modeling to reflect potential changes in the solubilityof radionuclides in the residual waste layer in response to evolution of the layers pore fluid composition as tank grout ages. There is considerable uncertainty in this approach that cannot be quantified. This is primarily driven by uncertainty inthe physical condition of the grout at the time the liner is breached and thereafter. To date Performance Assessment modeling of the F-Area tanks has nominally treated the grout as a porous medium and the variable effect of fast flow paths and other phenomena have been assessed in sensitivity analyses. The simulation of the chemical evolution of tank grout presented here is to support flow and transport modeling of the grout as a

porous medium and does not explicitly account for physical degradation of grout or heterogeneity in chemical or flow properties, including fracturing.

Uncertainty in simulations of chemical degradation of grout persists because of a lack of pertinent experimental data. Yet, it is worth considering the validity of extrapolating short-term grout degradation experiments to the very long time frames involved in Performance Assessment modeling. In a detailed study of the microfabric and chemistry of 20 year old cement blends stored at 98% relative humidity, Luke and Lachowski (2008) observed indications that the blends had not yet reached “steady-state equilibrium”. Most experimental studies are done on cements aged a fraction of that time. In contrast, the grout in tanks will age at 100% relative humidity for several hundred to thousands of years before the steel liner will be breached and radionuclides released. For these simulations it is assumed that the grout is fully hydrated and at equilibrium and is likely to behave differently than cementitious materials in short-term laboratory experiments. Likewise, it is difficult to extrapolate results from column studies to actual flow through the tank grout. This is because the contact time with cementitious material for any aliquot of effluent in a column study is typically much shorter than the contact time infiltration will have with tank grout materials. This is not an argument against experiments, but rather a caution that it is very difficult to extrapolate experimental results to the actual processes that will control grout degradation over very long timeframes. Pabalan et al. (2009) suggest the same for several degradation mechanisms. In the absence of experimental data, but with the necessity to demonstrate performance, modeling proceeds with appreciation of the uncertainties involved. Some of these uncertainties are discussed below.

Effective Reduction Capacity

The Eh transition is primarily controlled by the amount of slag used in the grout formulation, its reduction capacity, the amount of that reduction capacity imparted to the grout, and the thermodynamic data used for pyrite. It is assumed here that all reduction capacity measured in the slag is imparted to the grout over time. It is possible that not all of this reduction capacity would be available to pore waters and the effective reduction capacity would be less than predicted by the amount of slag in the grout. Then the Eh transition would occur at fewer pore volumes of infiltrating fluid. Two factors help to mitigate the effects of this possibility.

1) In the current simulations only reduction capacity contributed by blast furnace slag is considered. Both the Portland cement and fly ash have substantial reduction capacity as well (Roberts and Kaplan, 2009). Fly ash has 36% of the reduction capacity of blast furnace slag, but is present at 1.7 times the mass of blast furnace slag in the tank grout. Figure 9 shows the results of the simulation using slag alone and adding in the reduction capacity of the fly ash using the mineral magnetite. In this simulation, the Eh mimics the original simulation (Figure 3) until 523 pore volumes of fluid have reacted. Then, the Eh rises to -0.26 volts and is maintained for an additional 352 pore volumes. At 875 pore volumes, the Eh rises to +0.56 volts.

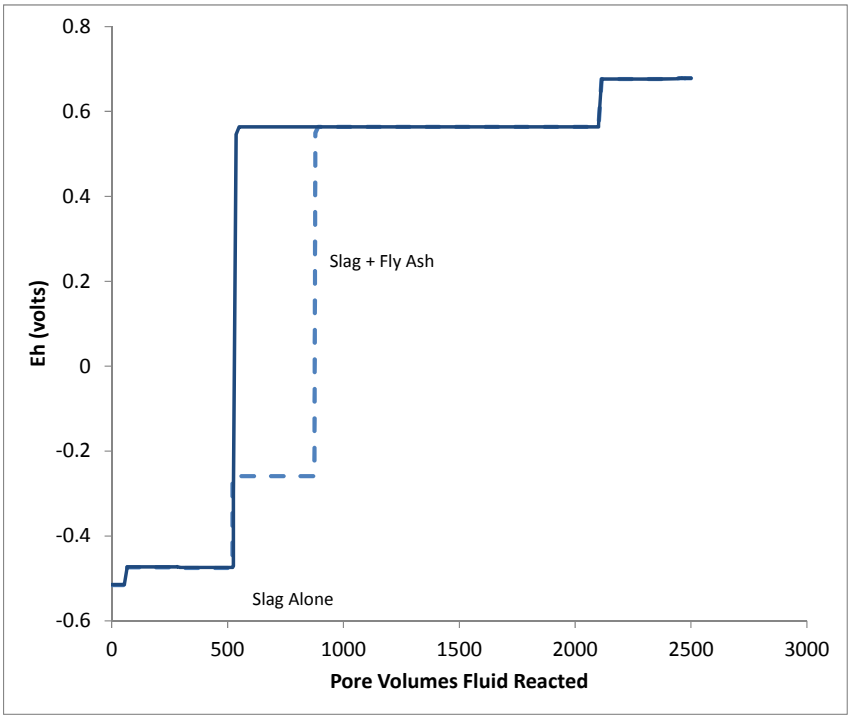

Figure 9: Comparison of Eh transition accounting for reduction capacity of slag (as pyrite) alone and slag (as pyrite) plus fly ash (as magnetite).

2) Roberts and Kaplan (2009) found that the reduction of Saltstone and Saltstone vault concrete exceeded that expected based on the amount of slag in these cementitious forms. It could be argued that for Saltstone, the simulant fluids used in the formulation had high concentrations of nitrite that could act as a reductant. However, the nitrite concentrations in the different simulants varied by a factor of 4, with no corresponding variation in reduction capacity of the Saltstone. Furthermore, nitrite does not explain the elevated reduction capacity of the vault concrete. Thus, it is possible that the total reduction capacity in a cementitious waste form is greater than the sum of that measured in its components.

Thermodynamic Data for Pyrite

The equilibrium constant for the reaction:

$FeS_2 + 2H^+ + 2e^- = Fe^{+2} + 2HS^-$

varies by 2 orders of magnitude depending on the thermodynamic database used. In Denham (2007, Rev. 2) the thermodynamic database "thermo.com.V8.R6+" was used with logK= -16.23 for the pyrite dissolution reaction. Newer thermodynamic databases use lower logK values for

pyrite dissolution. Hummel (2002) used logK= -18.50, while the HATCHES database uses a value of logK= -17.49. The value from the HATCHES database was chosen here because it is in between the two extremes. It also agrees with the value reported for this reaction by the HSC v.7.0 thermodynamic database. This accounts for some of the difference between the value of the Eh change in the current simulations compared to those in Denham (2007, Rev.2). In that previous document the transition occurred at 371 pore volumes rather than 523. Use of 7 mg/L dissolved oxygen in the simulations, rather than 8 mg/L, accounts for some of the difference. The remainder is the result of underestimating the amount of pyrrhotite required to account for the reducing capacity of the slag in Denham (2007, Rev. 2). The grout formulation used in that report does not differ significantly in the fraction of slag from that used in the current simulations.

Dissolved Oxygen in Infiltrate

The timing of the redox transition is dependent on the dissolved oxygen concentration in the assumed infiltrating water. The concentration used was in equilibrium with atmospheric oxygen – the highest possible concentration. The number of pore volumes required to reach the redox transition is inversely proportional to the dissolved oxygen concentration in the infiltrating water. Hence, at lower dissolved oxygen concentrations the number of pore volumes of infiltrating fluid required to cause the redox transition would be proportionally higher. A survey of dissolved oxygen concentrations in SRS background wells screened in the water table aquifer showed that they are close to saturation with atmospheric oxygen (Millings, 2012a). Nevertheless, there were wells that had concentrations that were nearly 40% less than saturation. Thus, the value of dissolved oxygen concentration assumed for infiltrating water is reasonable, but it should be noted that it could be lower. Assuming a lower dissolved oxygen concentration would decrease the number of pore volumes of reacting infiltrate required to reach the Eh transition from Reducing Region II to Oxidizing Region II.

Dissolved Carbon Dioxide in Infiltrate

The pH transition (Region II to Region III) is controlled primarily by the amount of hydrous calcium silicates present in the grout, but other factors have secondary effects. The dissolved inorganic carbon concentration in the infiltrate exerts some control on the pH transition. In the grout aging simulations it was assumed that the infiltrating water was in equilibrium with atmospheric CO_2 ($LogPCO_2=10^{-3.5}$ atm). Millings (2012b) surveyed Savannah River Site groundwater and vadose zone data for dissolved carbonate concentrations and partial pressures of CO_2. Partial pressures of CO_2 in the vadose zone and in equilibrium with water table aquifer groundwater fall mostly within the range of $10^{-1.85}$ to $10^{-2.23}$ atm. Figure 10 shows the results of using infiltrate equilibrated with these partial pressures of CO_2 in the grout aging simulations. Infiltrate equilibrated with $PCO_2=10^{-1.85}$ atm results in the transition from Oxidized Region II to Oxidized Region III occurring at 1777 pore volumes rather than 2119.

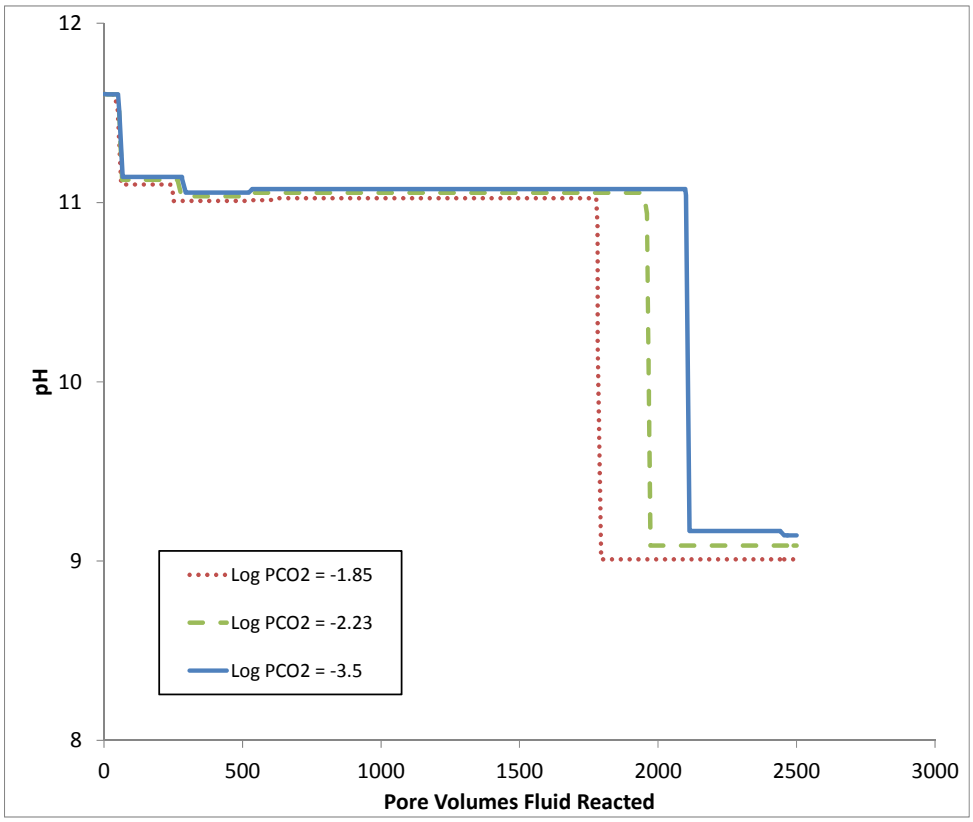

Figure 10: Simulation of the pH transition in aging grout using infiltrate equilibrated with different values of PCO_2.

Dissolved Silica in Infiltrate

The concentration of dissolved silica in the infiltrating water has a more significant influence on the pH transition by enhancing the dissolution of hydrous calcium silicates. The infiltrating water was assumed to be in equilibrium with amorphous silica, which produces the highest reasonable dissolved silica concentration. Were it in equilibrium with a lower solubility form of silica such as cristobalite, the number of pore volumes of infiltrating fluid required to reach the pH transition would be 16% higher. The transition would occur at a still higher number of pore volumes if the infiltrating water were assumed to be in equilibrium with quartz.

It is counterintuitive that higher dissolved silica concentrations in infiltrating water would enhance dissolution of hydrous calcium silicate. Yet, this can be understood in two ways. One is that above a pH of approximately 9.8 the dominant species of dissolved silica is $H_3SiO_4^-$. Hence, in Region II dissolved silica in the infiltrate undergoes the following reaction as it enters the tank grout, creating acid that promotes dissolution of hydrous calcium silicate:

$$H_4SiO_4° = H_3SiO_4^- + H^+$$

Alternatively, the reaction of the hydrous calcium silicate TobD with infiltrating H_4SiO_4 can be considered:

$TobD + 0.99H_4SiO_4° = 0.83Ca^{+2} + 1.32H_2O + 1.66H_3SiO_4^-$

The ion activity product (IAP) is:

$$IAP = \frac{(aCa^{+2})^{0.83} \times (aH3SiO4^{-})^{1.66}}{(aH4SiO4)^{0.99}}$$

As $H_4SiO_4°$ reacts with TobD an equivalent amount of $H_3SiO_4^-$ is produced, but within the IAP the $H_4SiO_4°$ is raised to the 0.99 power whereas $H_3SiO_4^-$ is raised to the 1.66 power. Thus, higher concentrations of dissolved silica entering the grout results in a higher IAP, driving the reaction in the direction of dissolution of TobD. Hence, the assumption that infiltrating water is in equilibrium with amorphous silica favors shorter times to transition from Oxidized Region II to Oxidized Region III.

Silica in Original Grout Mineralogy

A more influential control on the pH transition is the disposition of silica in the simulation. The base case simulation was done assuming free silica remaining after the normative mineralogy calculation was essentially inert and free silica was thus not an input into the initial mineralogy of the simulation. This has various effects depending on the assumed form of the silica. Figure 11 shows the effects of different scenarios involving silica compared to the base case in which silica was not included in the initial mineralogy. When silica is added it complicates the pH transition because three distinct pH regions occur, the duration and pH values varying with the form of silica. If silica from the normative mineralogy calculation is added as amorphous silica, the first pH transition from 11.0 to 9.8 occurs at approximately 50% fewer pore volumes of fluid reacted. The second transition from a pH value of 9.8 to 9.1 occurs at 4198 pore volumes. However, if kaolinite is allowed to precipitate the first transition occurs at transition at only 13% fewer pore volumes. If the form of silica is the more stable cristobalite, there is a minor pH transition from 11.0 to 10.7 at 1109 pore volumes, but the major transition from 10.7 to 9.3 occurs at 2389 pore volumes. If quartz is assumed to account for the silica, the transitions are very near those of cristobalite. Given the time frame of hundreds to thousands of years, silica in the original grout may recrystallize as cristobalite or quartz. In any event, a middle ground was taken by eliminating a free silica phase from the initial mineralogy of the simulation.

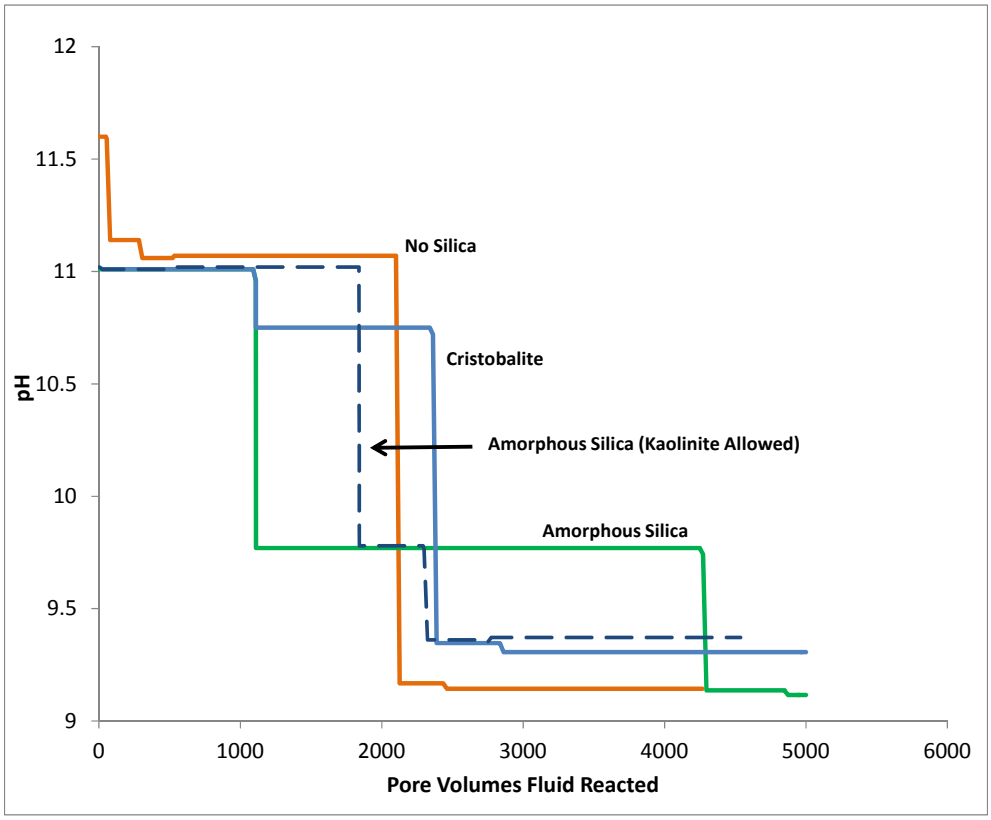

Figure 11: Results of different scenarios for inclusion of the normative silica in the grout evolution simulation.

Variations in Normative Mineralogy

When different normative mineralogies calculated from the same bulk chemical composition are used in the grout aging simulations small variations in Eh and pH can occur. The extent of variation is constrained by the constant bulk composition and the recalculation of an equilibrium mineral assemblage by The Geochemist's Workbench®. Table 9 shows an alternative normative mineralogy and the recalculated equilibrium mineral assemblage. The recalculated mineralogy is similar to that in Table 3 as expected. Figure 12 shows simulations of the pH and Eh evolution in aging grout using the alternative normative mineralogy in Table 9. The pH values are slightly lower for the alternative mineralogy than for the original mineralogy in Region II and slightly higher in Region III. The Eh values are essentially identical.

A related and pertinent issue is the effect on solubilities of key radionuclides of Eh and pH values that vary from those predicted. This is addressed in the section titled "Radionuclide Solubility Estimations".

Table 9: Alternative normative mineralogy and the mineralogy as recalculated by The Geochemist's Workbench.

Alternative Mineralogy		Recalculated Mineralogy	
Mineral	**Amount (g/m^3)**	**Mineral**	**Amount (g/m^3)**
Brucite	2.69E4	Hydrotalcite	5.10E4
Silica (Chalcedony)	1.36E5	--	--
Ettringite	2.43E4	Ettringite	2.41E4
Gibbsite	1.15E5	Gibbsite	9.75E4
Pyrite	8.16E3	Pyrite	8.16E3
Magnetite	--	Magnetite	5.52E-1
JenD	1.79E5	TobD	8.16E3
TobH	--	TobH	2.13E5

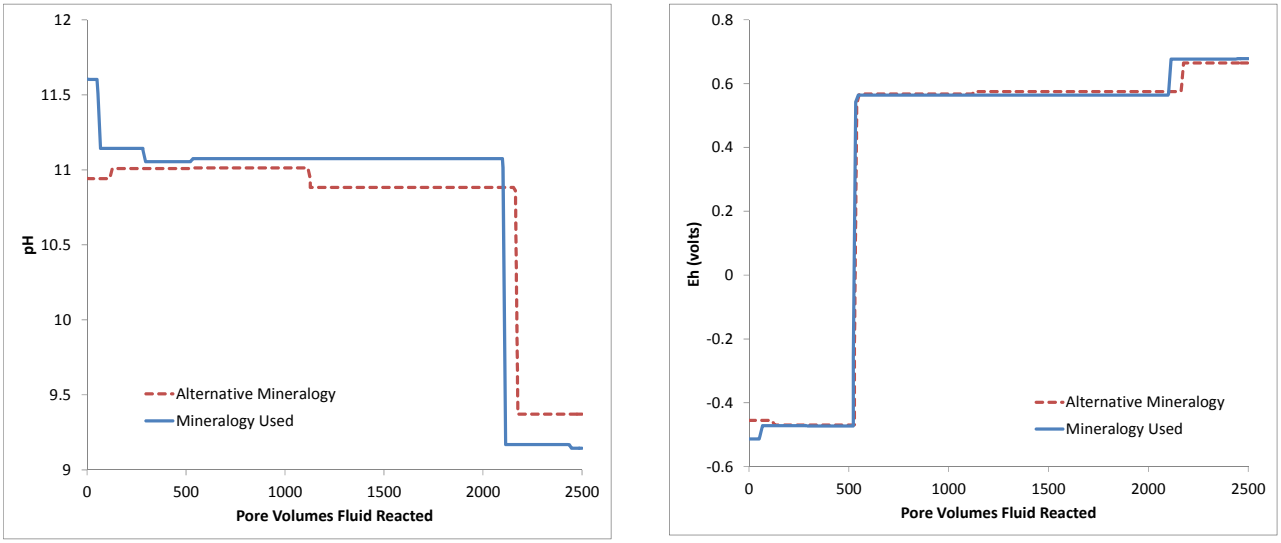

Figure 12: Comparison of simulated pH and Eh transitions in aging grout using an alternative normative mineralogy to those using the mineralogy in Table 3.

1-D Simulations of Grout Chemical Degradation

To examine how the reaction path model used with a flow and transport model compares to actual coupled reactive transport models several 1-D simulations were run with The Geochemist's Workbench. These simulations used the same mineralogy and infiltrating fluid as the reaction path model. Specific discharge was set at 30 cm/yr, the same as is used in the flow and transport model for the period after the steel liner fails. The grout domain is 4 meters long

and one meter on each side and the simulation begins with an unlimited reservoir of infiltrate at the left side of the domain.

Figure 13 shows simulated movement of the oxidation front through the grout. Results are shown for the oxygen concentration (2.19E-4 molar) in the infiltrate that was used in the reaction path simulations and for a lower oxygen concentration (1.75E-4 molar) representing the lower part of the range found by Millings (2012a). For the higher oxygen concentration the oxidation front advanced 216 cm in 800 years or at a rate of 0.3 cm per year. In the closure design of the tanks infiltration will pass through approximately 10 meters of reducing grout. Hence, the 1-D simulation predicts that the redox front will pass through the grout completely in 3300 years. This agrees well with the Base Case Performance Assessment modeling done with a flow and transport model and the reaction path simulations. The simulation using the lower oxygen concentration results in the oxidation front advancing at a rate of 0.2 cm/yr and a transition from Reducing Region II to Oxidized Region II at 5,000 years after the steel liner fails.

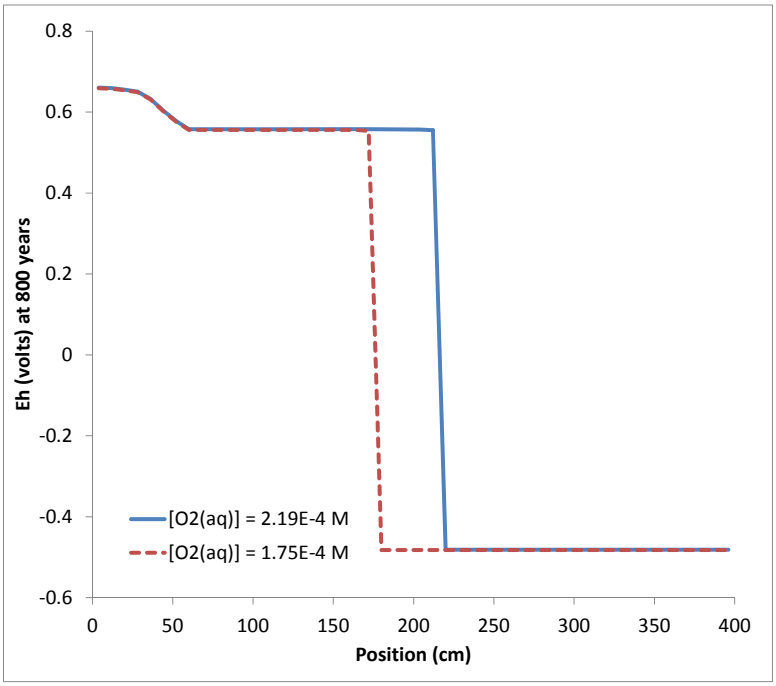

Figure 13: 1-D simulation of the advance of an oxidation front through the tank grout.

The 1-D simulations were run with the infiltration in equilibrium with three different partial pressures of carbon dioxide: $10^{-3.5}$, $10^{-2.23}$, and $10^{-1.85}$ atm (Figure 14). A partial pressure of $10^{-3.5}$ atm was used for the reaction path simulations. Use of this PCO_2 in the 1-D simulations causes the pH front to advance at a rate of 0.05 cm/yr. This corresponds to a time span of 20,000 years from when the tank liner fails to the transition from Oxidized Region II to Oxidized Region III which is consistent with the Performance Assessment modeling. At $PCO_2 = 10^{-1.85}$, the high end of the range of CO_2 partial pressures recommended by Millings (2012b), the front advances at a rate of 0.07 cm/yr. These rates are comparable to the advance rate of a carbonation front for tank

grout calculated by Langton (2007) using an analytical solution and assuming the grout to be 50% water saturated.

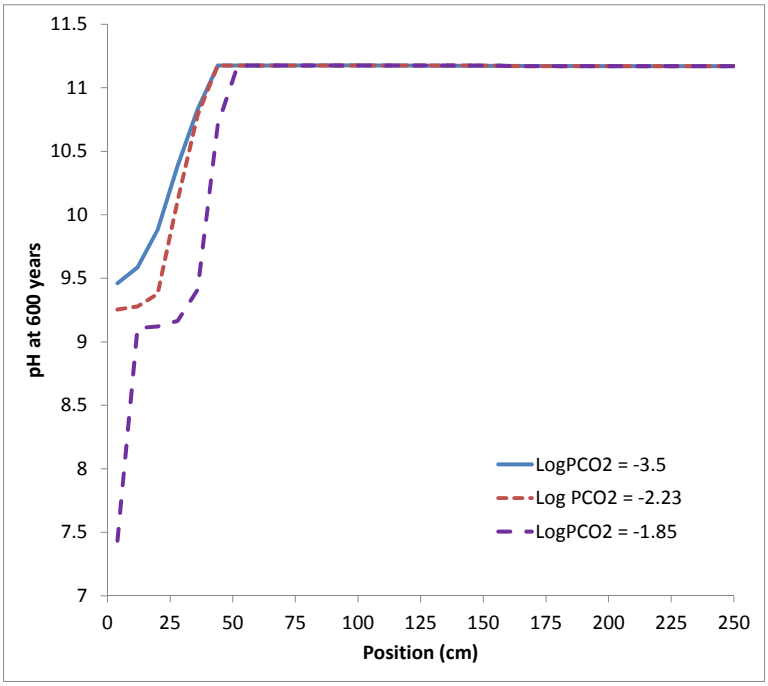

Figure 14: 1-D simulations of the advance of a pH front through tank grout with the infitrate in equilibrium with different partial pressures of CO_2.

Summary of Uncertainty in Grout Degradation Simulations

There are several sources of uncertainty in simulating chemical degradation of the reducing tank grout. Some of these such as variations in dissolved oxygen and CO_2 in the infiltrate, thermodynamic uncertainty, and disposition of silica can be quantified. Others such as the effective reactivity of the grout minerals are difficult to quantify. Some of the assumptions used in the simulations bias the results toward shorter durations of Reduced Region II and Oxidized Region II (Conditions C and D for submerged tanks). Yet, quantifying the uncertainty in these durations was not attempted. Instead, rather large uncertainties are recommended as bounding values. An uncertainty of ±30% of pore volumes is recommended for the duration of Reduced Region II. An uncertainty of ±50% is recommended for the duration of Oxidized Region II. Similar uncertainties are recommended for the durations of Conditions C and D.

Radionuclide Solubility Estimations

Radionuclide solubility estimations were done using The Geochemist's Workbench. This involved selecting an appropriate thermodynamic database, selecting an appropriate solubility

controlling phase for each radionuclide, and then equilibrating these phase(s) with the fluid compositions from Tables 6 and 7.

For the elements Am, Ni, Np, Pu, U, Tc, and Th thermodynamic data for aqueous hydroxyl and carbonate complexes, as well as appropriate solid phases were obtained by direct download from the Nuclear Energy Agency (http://www.oecd-nea.org/). The Nuclear Energy Agency (NEA) is part of the Organisation for Economic Co-Operation and Development (OECD) and has published several thorough reviews of thermodynamic data for radionuclides and compiled internally consistent traceable datasets. The data was converted to a format suitable for use by The Geochemist's Workbench using the Gibbs free energies of the solids and aqueous complexes of interest and their associated components to calculate LogK values for dissociation constants. These were entered into the "thermo_phreeqc" database available with The Geochemist's Workbench. For the other elements the thermodynamic database available from the Japanese Atomic Energy Agency (http://www.jaea.go.jp/english/) was used. It uses NEA data for some elements but includes many more elements than the NEA database. The JAEA database is also well reviewed, internally consistent, and traceable. For a few specific calculations other sources of thermodynamic data were used and these are noted in the text.

Selecting Solubility Controlling Phases

A fundamental part of establishing solubility controlled waste release rates is selection of a solubility controlling phase for each radionuclide. For some of the radionuclides of interest there are studies in the literature that can guide selection of solubility controls. For other radionuclides selection of solubility controlling phases was generally conservative, meaning that where multiple phases of a radionuclide were possible, selection was biased toward higher solubilities.

There are two factors that determine the solubility of a phase – the composition and the structure. For phases with the same composition, amorphous forms usually have higher solubilities than crystalline forms. Thus, where thermodynamic data existed, the amorphous forms were selected for solubility controls. For most, hydroxides were chosen over oxides because the hydroxide of an element usually has a higher solubility than the oxide. Carbonate phases were selected for Sr, Ca, and, under relatively high carbonate conditions, some trivalent species. Carbonate phases normally precipitate easily from solution (example, Noyes, 1994) and their occurrence in the grouted tanks was considered to be plausible.

The selection of solubility controlling phases followed the general process shown in Figure 15. For each radionuclide the process began with an examination of the literature for occurrence of a stable phase with reliable thermodynamic data at conditions prevalent in the tanks or cementitious systems. If one was found, it was selected. If none was found, a list of other phases that contain components found in the tanks and having reliable thermodynamic data was assembled. The stability fields of these phases were examined and phases stable at conditions corresponding to those of the conceptual model were retained. If there were appropriate geologic or industrial process analogues cited in the literature they were considered. Examples are radium

sulfate and strontium carbonate. If there were no analogues cited in the literature, but the hydroxide was stable, it was retained. If reliable thermodynamic data was available for the amorphous hydroxide then it was selected. The process attempted to balance scientific knowledge with the need to be cautious and biased toward higher solubilities.

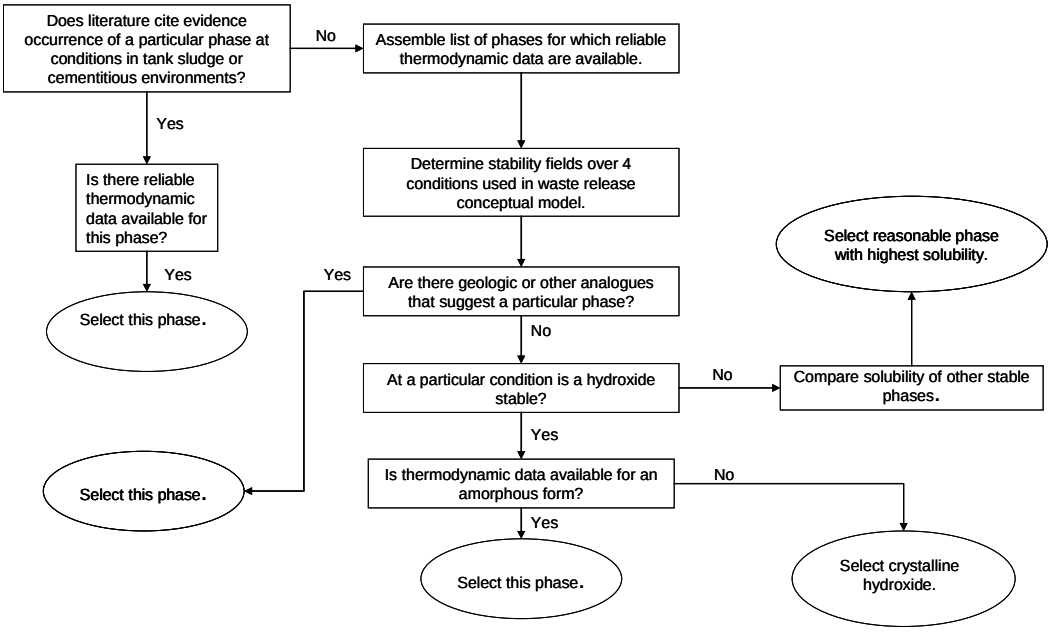

Figure 15: General flow for selection of solubility controlling phases.

Solubility Estimates

Solubility estimates for 16 elements were calculated using The Geochemist's Workbench by equilibrating a selected solubility controlling phase with the composition of the pore fluid representing each chemical condition. The pore fluid compositions are listed in Table 10. Not all

Table 10: Pore fluid compositions used for solubility estimates for each chemical condition.

Parameter	Tanks Above the Water Table			Tanks Below the Water Table			
	Red. Reg. II	Ox. Reg. II	Ox. Reg. III	A	B	C	D
pH	11.1	11.1	9.2	5.4	8.8	8.8	8.8
Eh (volts)	-0.47	0.24	0.29	0.37	0.36	-0.31	0.36
Ca+2 (molar)	4.0E-3	4.0E-3	6.6E-5	6.2E-5	4.0E-4	3.90E-4	3.9E-4
DIC	6.7E-7	6.9E-7	7.5E-5	9.8E-5	2.8E-5	3.2E-5	3.0E-5
SO4-2	1.0E-5	1.0E-5	1.0E-5	6.3E-6	1.5E-5	2.0E-5	6.9E-6
Na+	1.0E-3	1.0E-3	1.0E-3	4.4E-5	3.9E-5	4.0E-5	4.0E-5
Cl-	1.0E-3	1.0E-3	1.0E-3	8.5E-5	8.1E-4	7.8E-4	8.0E-4
Oxalate	4.1E-6	4.1E-6	4.4E-5	4.2E-5	9.5E-6	9.5E-6	9.5E-6

of the elements that were in the pore fluid compositions produced by the grout modeling were used in the solubility estimates. Therefore, the compositions listed in Table 10 are not in perfect charge balance. This was accounted for in the solubility estimates for all conditions except Condition A by adjusting the chloride concentration to achieve charge balance. Charge balance could not be achieved for Condition A by varying chloride, sulfate, or sodium. So, solubility estimates in Condition A were run without balancing charge. To test whether this made a difference a more complete composition was used for Condition A and charge balanced using chloride. There were no significant differences in solubilities between the estimates with or without charge balance.

For relatively soluble elements, here defined as greater than 1E-5 molar, a different approach was used for calculating solubilities. Rather than equilibrating a solubility controlling phase with a pore fluid composition, the element was added to the pore fluid composition until saturation with a controlling phase was reached.

Eh Values Used in Solubility Estimates

In the grout degradation simulations the Eh at oxidizing conditions is controlled by equilibrium with the dissolved oxygen. Yet, Eh values of natural waters are rarely in equilibrium with dissolved oxygen despite being exposed to oxygenated groundwater for thousands of years. This may be due to predominantly slow reaction kinetics for oxidation by dissolved oxygen (Langmuir, 1997). Figure 16, from Langmuir (1997), shows Eh-pH regimes for different types of natural waters. The added red ovals are at pH values of approximately 9.2 and 11.1 and suggest the range of Eh values that would be reasonable for calculating solubilities at these pH values. The disparity between measured Eh and that in equilibrium with dissolved oxygen is also observed in SRS groundwater. Eh measurements of groundwater from 6 water table wells reported in Stom and Kaback (1992) are shown on an Eh-pH diagram in Figure 17. The Eh values are lower than would be expected for equilibrium with dissolved oxygen (cross-hatched region) and their position suggests they reflect the ferric-ferrous iron couple. Others have suggested that Eh values used for modeling metal solubility and speciation in cements at pH=12.5 should be near +0.2 volts (Glasser, 1997; Krupka and Serne, 1998), rather than the +0.48 volts that would be in equilibrium with dissolved oxygen. Atkins and Glasser (1992) reported that Eh values of ordinary Portland cement should be between 0.0 and +0.1 volts. Likewise, Fuhrmann and Gillow (2009) measured Eh values for a West Valley grout of approximately +0.15 v. Therefore, it is reasonable to assume that Eh values controlling solubility in the oxidized regions simulated here would be lower than those resulting from the grout simulations (i.e., lower than equilibrium with the dissolved oxygen).

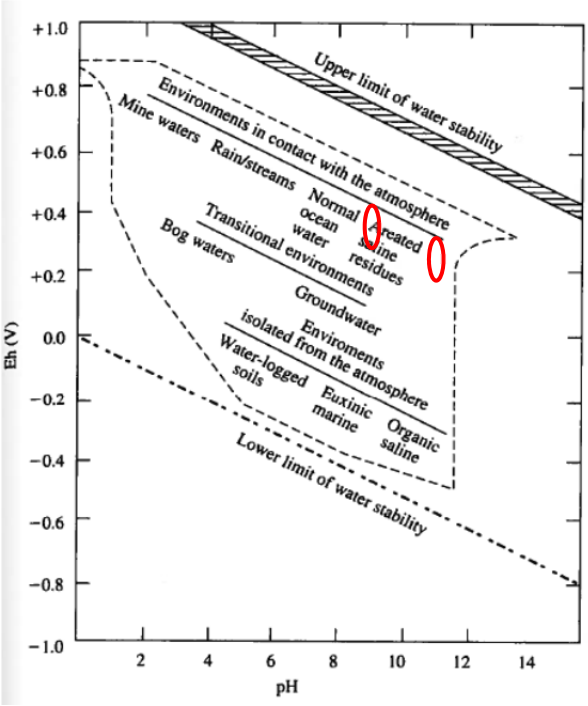

Figure 16: Eh-pH diagram from Langmuir (1997) showing typical regimes for various natural waters; red ovals are overlaid to suggest range of realistic Eh values for calculating solubilities in Oxidized Region II and III.

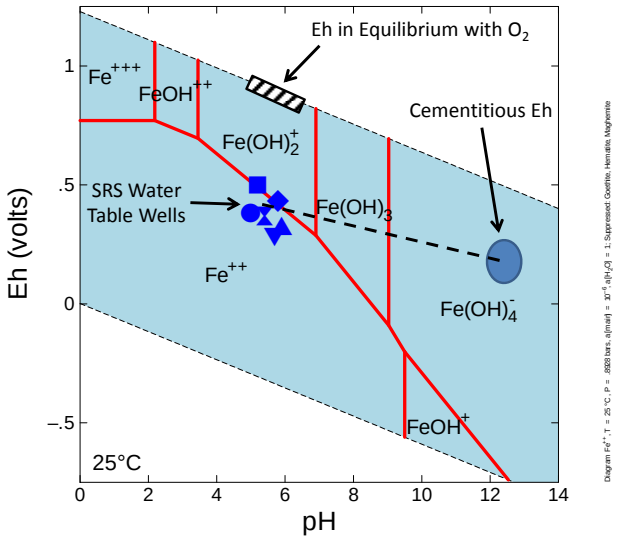

Figure 17: Eh-pH diagram showing Eh of SRS background water table wells in relation to iron speciation.

Here, Eh values of +0.24 and +0.29 volts were chosen for Oxidized Regions II and III. This was based on extrapolating the groundwater values from Figure 17 to the appropriate pH values of 11.1 and 9.2 along a line intersecting the point pH=12.5, Eh=+0.2 v, similar to the method of Krupka and Serne (1998).

Oxalate in the Residual Waste

Washing the tank with oxalic acid is the baseline for tank closure. The oxalate ion can chelate some radionuclides, enhancing their solubility. Thus, oxalate was considered in the estimates of contaminant solubilities. Poirier (2008) measured an oxalate concentration of 1000 mg/L in the final wash of Tank 5F. However, calcium oxalate has a relatively low solubility and will control the solubility of oxalate in the calcium-rich pore fluids associated with the tank grout. Thus, the solubility of calcium oxalate was estimated for each pore fluid condition by equilibrating it with the composition of the various pore fluids using The Geochemist's Workbench. Table 10 lists the pore fluid compositions, including oxalate, used for solubility estimates at each chemical condition.

Estimated Solubilities

Table 11 shows solubility values and controlling phases for all of the elements of interest at each of the chemical states of interest. Several of the elements have either a very small inventory or a short half-life and are unlikely to be an issue at exposure points. In addition, some of the elements have no identified solubility controls and it is recommended that their release be modeled as instantaneous (within the first pore volume). Solubilities for six conditions are shown because the composition of the Condition B pore fluid is so similar to that of Condition D that only solubilities for Condition D are reported.

Table 11: Estimated solubilities for discrete phases in pore fluids of six conditions expected during grout degradation of non-submerged and submerged tanks.

Reduced Region II				Oxidized Region II		
	Controlling Phase	**Solubility (moles/liter)**			**Controlling Phase**	**Solubility (moles/liter)**
Ac	$Ac(OH)_{3(am)}$	1E-09		**Ac**	$Ac(OH)_{3(am)}$	1E-09
Am	$Am(OH)_{3(am)}$	1E-09		**Am**	$Am(OH)_{3(am)}$	1E-09
Ba	$BaSO_4$ (barite)	3E-05		**Ba**	$BaSO_4$ (barite)	3E-05
Bk	short half-life	-		**Bk**	short half-life	
C	$CaCO_3$ (calcite)	2E-06		**C**	$CaCO_3$ (calcite)	2E-06
Cf	small inventory	-		**Cf**	small inventory	
Cm	$Cm(OH)_{3(am)}$	1E-09		**Cm**	$Cm(OH)_{3(am)}$	1E-09
Co	CoS(beta)	3E-02		**Co**	no solubility control	
Cs	no solubility control	-		**Cs**	no solubility control	
Eu	$Eu(OH)_{3(am)}$	8E-07		**Eu**	$Eu(OH)_{3(am)}$	8E-07
I	no solubility control	-		**I**	no solubility control	
Nb	no solubility control	-		**Nb**	no solubility control	
Ni	$NiS_{(c)}$alpha	2E-09[1]		**Ni**	$Ni(OH)_2$ (beta)	1E-07
Np	$NpO_{2(am,hyd)}$	1E-09		**Np**	$NpO_{2(am,hyd)}$	3E-07
Pa	no solubility control	-		**Pa**	no solubility control	
Pu	$PuO_{2(am,hyd)}$	3E-11		**Pu**	$PuO_{2(am,hyd)}$	3E-11
Ra	$RaSO_4$	3E-05		**Ra**	$RaSO_4$	3E-05
Rh	short half-life	-		**Rh**	short half-life	
Se	$FeSe_{2(cr)}$	2E-05		**Se**	no solubility control	-
Sm	$Sm(OH)_{3(am)}$	1E-09		**Sm**	$Sm(OH)_{3(am)}$	1E-09
Sn	$SnO_{2(am)}$	4E-04		**Sn**	$SnO_{2(am)}$	4E-04
Sr	$SrCO_3$	3E-03		**Sr**	$SrCO_3$	3E-03
Tc	$TcO_2.1.6H_2O$	1E-08		**Tc**	no solubility limit	
Te	short half-life	-		**Te**	short half-life	
Th	$ThO_{2(am,hyd,aged)}$	1E-09		**Th**	$ThO_{2(am,hyd,aged)}$	1E-09
U	$UO_{2(am,hyd)}$	5E-09		**U**	$UO_3 \cdot 2H_2O$	5E-05
Y	$Y(OH)_{3(c)}$	4E-13[2]		**Y**	$Y(OH)_{3(c)}$	4E-13

[1] An alternate value is 1E-7 moles/liter because NiS (alpha) is sensitive to Eh in Reduced Region II

[2] Note that ^{90}Y is the yttrium isotope of concern and that its transport is controlled by transport and decay of ^{90}Sr

Table 11: (cont.) Estimated solubilities for discrete phases in pore fluids of six conditions expected during grout degradation of non-submerged and submerged tanks.

Oxidized Region III				Condition A		
	Controlling Phase	**Solubility (moles/liter)**		**Element**	**Controlling Phase**	**Solubility (moles/liter)**
Ac	$Ac(OH)_{3(am)}$	6E-08		**Ac**	No solubility control	-
Am	$AmCO_3OH{\cdot}0.5H_2O$	2E-09[3]		**Am**	$AmCO_3OH{\cdot}0.5H_2O$	3E-04
Ba	$BaSO_4$ (barite)	1E-05		**Ba**	$BaSO_4$	3E-05
Bk	short half-life	-		**Bk**	Short Half-life	-
C	$CaCO_3$ (calcite)	1E-03		**C**	No solubility control	-
Cf	small inventory	-		**Cf**	Small inventory	-
Cm	$CmCO_3OH{\cdot}0.5H_2O$	2E-09		**Cm**	$CmCO_3OH{\cdot}0.5H_2O$	3E-04
Co	no solubility control	-		**Co**	No solubility control	-
Cs	no solubility control	-		**Cs**	No solubility control	-
Eu	$EuOHCO_{3(cr)}$	3E-08		**Eu**	$EuOHCO_{3(c)}$	2E-03
I	no solubility control	-		**I**	No solubility control	-
Nb	no solubility control	-		**Nb**	No solubility control	-
Ni	$NiCO_3$	1E-05		**Ni**	No solubility control	-
Np	$NpO_{2(am,hyd)}$	2E-06		**Np**	$NpO_{2(am,hyd)}$	3E-05
Pa	no solubility control	-		**Pa**	No solubility control	-
Pu	$PuO_{2(am,hyd)}$	3E-11		**Pu**	$PuO_{2(am,hyd)}$	2E-10
Ra	$RaSO_4$	1E-05		**Ra**	$RaSO_4$	3E-05
Rh	short half-life	-		**Rh**	Short half-life	-
Se	no solubility control	-		**Se**	No solubility control	-
Sm	$SmCO_3OH{\cdot}0.5H_2O$	2E-09		**Sm**	$SmCO_3OH{\cdot}0.5H_2O$	3E-04
Sn	$SnO_{2(am)}$	7E-07		**Sn**	$SnO_{2(am)}$	3E-08
Sr	SrCO3	1E-04		**Sr**	No solubility control	-
Tc	no solubility limit	-		**Tc**	No solubility control	-
Te	short half-life	-		**Te**	No solubility control	-
Th	$ThO_{2(am,hyd,aged)}$	1E-09		**Th**	$ThO_{2(am,aged)}$	2E-05
U	$UO_3{\cdot}2H_2O$	4E-06		**U**	$UO_3{\cdot}2H_2O$	4E-05
Y	$Y(OH)_{3(c)}$	2E-09		**Y**	No Solubility Control	-

[3] An alternative value is 6E-8 moles/liter for $Am(OH)_{3(am)}$ as the controlling phase; used in Denham and Millings (2012)

Table 11: (cont.) Estimated solubilities for discrete phases in pore fluids of six conditions expected during grout degradation of non-submerged and submerged tanks.

Condition C				Condition D		
	Controlling Phase	**Solubility (moles/liter)**			**Controlling Phase**	**Solubility (moles/liter)**
Ac	$Ac(OH)_{3(am)}$	2E-07		**Ac**	$Ac(OH)_{3(am)}$	2E-07
Am	$AmCO_3OH{\cdot}0.5H_2O$	4E-09		**Am**	$AmCO_3OH{\cdot}0.5H_2O$	4E-09
Ba	$BaSO_4$	7E-06		**Ba**	$BaSO_4$	2E-05
Bk	Short Half-life	-		**Bk**	Short Half-life	-
C	$CaCO_3$	4E-04		**C**	$CaCO_3$	4E-04
Cf	Small inventory	-		**Cf**	Small inventory	-
Cm	$CmCO_3OH{\cdot}0.5H_2O$	4E-09		**Cm**	$CmCO_3OH{\cdot}0.5H_2O$	4E-09
Co	beta-CoS	1E-04		**Co**	No solubility control	-
Cs	No solubility control	-		**Cs**	No solubility control	-
Eu	$EuOHCO_{3(c)}$	3E-08		**Eu**	$EuOHCO_{3(c)}$	4E-08
I	No solubility control	-		**I**	No solubility control	-
Nb	No solubility control	-		**Nb**	No solubility control	-
Ni	alpha-NiS	6E-11		**Ni**	beta-$Ni(OH)_2$	6E-07
Np	$NpO_{2(am,hyd)}$	1E-09		**Np**	$NpO_{2(am,hyd)}$	2E-05
Pa	No solubility control	-		**Pa**	No solubility control	-
Pu	$PuO_{2(am,hyd)}$	3E-11		**Pu**	$PuO_{2(am,hyd)}$	3E-11
Ra	$RaSO_4$	7E-06		**Ra**	$RaSO_4$	2E-05
Rh	Short half-life	-		**Rh**	Short half-life	-
Se	$FeSe_2$	5E-08		**Se**	No solubility control	-
Sm	$SmCO_3OH{\cdot}0.5H_2O$	4E-09		**Sm**	$SmCO_3OH{\cdot}0.5H_2O$	4E-09
Sn	$SnO_{2(am)}$	3E-07		**Sn**	$SnO_{2(am)}$	3E-07
Sr	$SrCO_3$	1E-03		**Sr**	$SrCO_3$	1E-03
Tc	$TcO_2{\cdot}1.6H_2O$	4E-09		**Tc**	No solubility control	-
Te	No solubility control	-		**Te**	No solubility control	-
Th	$ThO_{2(am,aged)}$	1E-09		**Th**	$ThO_{2(am,aged)}$	1E-09
U	$UO_{2(am)}$	4E-09		**U**	$UO_3{\cdot}2H_2O$	2E-06
Y	$Y(OH)_3$	1E-08		**Y**	$Y(OH)_3$	1E-08

Solubilities of Np, Pu, and U at Eh in Equilibrium with Dissolved Oxygen

Table 12 shows the estimated solubilities and controlling phases for Np, Pu, and U for Eh values in equilibrium with dissolved oxygen in Oxidized Regions II and III. Pu is the only one significantly affected by the assumption that Eh is not in equilibrium with dissolved oxygen.

Table 12: Estimated solubilities of Np, Pu, and U in Oxidized Regions II and III at Eh values in equilibrium with dissolved oxygen.

	Oxidized Region II		Oxidized Region III	
Element	Phase	Solubility (M)	Phase	Solubility (M)
Np	$NpO_2OH_{(am, aged)}$	7E-7	$NpO_2OH_{(am, aged)}$	5E-5
Pu	$PuO_{2(am, hyd)}$	5E-8	$PuO_{2(am, hyd)}$	8E-8
U	$UO_3 \cdot 2H_2O$	6E-5	$UO_3 \cdot 2H_2O$	4E-6

Apparent Solubilities for Coprecipitated Elements

The term coprecipitated here includes radionuclides bound in the crystal lattice of solid iron phases and mixed with iron phases such that the access of pore fluids to the plutonium is occluded by the host phase. Technetium is very soluble at the conditions of tank washing, and thus it is suspected that technetium that remains in the residual waste after the washing process is coprecipitated with iron or other phases. Several studies provide evidence of Tc coprecipitated with iron phases. Cantrell et al. (2006) observed that a significant fraction of Tc-99 in Hanford waste tank sludge was relatively insoluble, 20% in one sample and 80% in another, and that the insoluble Tc-99 was correlated with iron oxides in selective extraction experiments. Krupka et al. (2009) also observed Tc co-precipitated with ferric iron phases in Hanford tank waste. The experiments of Wakoff and Nagy (2004) further indicate that coprecipitation of Tc in ferric iron phases is likely. They conducted experiments with perrhenate, an analogue for pertechnetate, under Hanford tank sludge conditions and concluded that up to 14% of the Tc-99 in tank sludges may be irreversibly sorbed, possibly coprecipitated, in iron and aluminum solids. Gu et al. (2003) also hypothesized that Tc-99 was removed from solution during titration experiments of acidic groundwater by co-precipitation with iron and aluminum phases.

There is indirect evidence to suggest that plutonium would be coprecipitated with iron phases. Coprecipitation with ferric iron phases has been the basis for various methods of removal of plutonium from solution (e.g., Gävfert et al., 2002; Slater et al., 1997; Lozano et al., 1997). Site specific evidence is presented in a review of Tank 18 history and chemistry by Hobbs (2012). He concludes that it is likely that a portion of plutonium remaining in the residual waste after cleaning is coprecipitated.

There is also evidence in the literature that neptunium may readily coprecipitate with ferric iron oxides. Grigoriev et al. (2001) found that Np(V) and Np(VI) sorb strongly to ferric oxyhydroxides at high pH, while Np(IV) forms true mixed oxide co-precipitates. If neptunium sorbed strongly to ferric iron phases as they formed, and these particles settled to the bottom of

the tanks to form a lithified heel, the neptunium would be effectively co-precipitated. Its release to pore fluids would require dissolution of the ferric iron phases. Likewise, Nakata et al. (2002) observed that Np(IV) sorbed strongly on magnetite in anaerobic conditions, while Np(V) sorbed strongly to hematite under aerobic conditions.

An apparent solubility of a coprecipitated radionuclide can be estimated if it is assumed that a coprecipitated radionuclide would be released as the host iron phase dissolved at the same molar X:Fe ratio at which it exists in the solid. Molar ratios of Np, Pu, Tc, and U in H-Area tanks were calculated from the estimated final inventories listed by Dean (2012). These and the solubilities of an assumed host iron phase were used to estimate apparent solubilities for Np, Pu, Tc, and U. A similar method was used by Cantrell et al. (2006) to calculate release of Tc-99 from an iron phase.

The iron phases used here to estimate the apparent solubility of coprecipitated plutonium throughout the post-closure aging of the tanks are magnetite (Fe_3O_4) and maghemite (Fe_2O_3). X-ray diffraction analysis of Tank 18 residual waste samples by Hay (2012) show that hematite is a dominant iron phase in the tank today. For the grout simulations presented here it is assumed that exposure to reducing pore fluids after closure, but before the liner is breached, would convert the hematite to magnetite. Magnetite is assumed to be prevalent in Reducing Region II and oxidizes to maghemite at the transition to Oxidized Region II. Denham (2007, Rev. 2) assumed prevalence of hematite in Oxidized Region II and III, but maghemite is a more likely oxidation product of magnetite because of their similar crystal structures. In addition, maghemite is more soluble than hematite and biases the apparent solubilities of plutonium to higher values.

The solubilities of magnetite and maghemite were calculated at the chemical conditions of Reduced Region II, Oxidized Region II, and Oxidized Region III using The Geochemist's Workbench®. Thermodynamic data for magnetite was obtained from the HATCHES database (Heath, 2007). For comparison, the solubility of magnetite using a value for logK from the HSC v.7 database (Roine, 2009) was slightly higher (6.8E-6 versus 4.0E-6) than that from Geochemist's Workbench®. The value from the HATCHES database was used because it is expected to be more consistent with the NEA thermodynamic data. Neither the HATCHES nor the NEA databases contain data for maghemite. Thus, the thermodynamic data for this phase was obtained from the HSC v. 7 database. Table 13 shows the solubility of the iron host phase and Table 14 shows the estimated apparent solubilities of Np, Pu, Tc, and U.

Table 13: Solubility of host iron phases the pore fluids of the different chemical conditions.

Condition	Phase	Fe Solubility (moles/liter)
Reducing Region II	Magnetite	7.30E-11
Oxidized Region II	Maghemite	7.10E-10
Oxidized Region III	Maghemite	1.40E-11
Condition A	Maghemite	1.11E-08
Condition C	Magnetite	2.27E-08
Condition D	Maghemite	8.54E-12

Table 14: Apparent solubilities of potentially coprecipitated elements.

	Apparent Solubilities (moles/liter)			
Condition	**Pu**	**Np**	**U**	**Tc**
Reducing Region II	8E-13	5E-15	2E-12	1E-14
Oxidized Region II	7E-12	4E-14	2E-11	1E-13
Oxidized Region III	1E-13	9E-16	5E-13	2E-15
Condition A	2E-10	3E-13	9E-11	1E-12
Condition C	3E-10	6E-13	2E-10	3E-12
Condition D	1E-13	2E-16	7E-14	1E-15

Uncertainty in Solubility Estimates

Several sources contribute to uncertainty in the solubility estimates presented here. Uncertainty in the thermodynamic data and choice of solubility controlling phase are inherent to any solubility estimate. Uncertainty in the solubility controlling phase primarily reflects lack of available information on kinetics of nucleation and is the reason the choices here are mostly biased toward higher solubilities. Most other sources relate to the uncertainty in the chemical conditions of the fluid in which the solubility controlling phase is dissolving. This section explores some of these uncertainties and their effect on solubility values.

The first subsection examines uncertainty in solubilities of Np, Pu, U, and Tc introduced by uncertainty in the thermodynamic data. In the following subsections sensitivities to choice of controlling phase, pH, Eh, dissolved inorganic carbon, and oxalate are presented for each element. This is done using diagrams of solubility versus the parameter of interest. In these

diagrams the other parameters for each condition are held constant and correspond to values in Table 10. The diagrams show the log of the activity of the basis species of the contaminant on the y-axis. In the reactions that make up the diagrams all species of the contaminant are written in terms of the basis species. Thus, assuming near ideal behavior, the y-axis represents the total concentration of the contaminant. The x-axis is the log of the activity of the individual species in the axis label. Again, ideal behavior is assumed and the term concentration is used rather than activity to refer to values on the x-axis. The diagrams are simplified systems and are meant to illustrate trends in solubility. Therefore, the solubilities shown on the diagrams may differ slightly from those listed in Table 10.

The discussion centers on Reduced Region II, Oxidized Region II, and Oxidized Region III. In the oxidized regions comparisons are made between the sensitivities at the assumed Eh of 0.24 volts and those at Eh values in equilibrium with dissolved oxygen, +0.56 volts for Oxidized Region II and +0.68 volts for Oxidized Region III. Diagrams for Conditions C and D are presented in Appendix 3, but not discussed in the main text because their trends in sensitivities are similar to those in Reduced Region II and Oxidized Region III at an Eh of 0.29 volts.

It is important to note that some conditions that appear on the diagrams are not feasible. For example, it is not possible to maintain a high carbonate concentration in Ca-rich water at a pH of 11.1. If there is no buffering of pH by grout or waste minerals calcite will precipitate and the pH will go down. If there is buffering the pH may remain high even though calcite will precipitate. Likewise, maintaining a high oxalate concentration in the presence of Ca-rich pore fluids is not feasible.

Thermodynamic Data

Uncertainty in thermodynamic data is the product of uncertainty in experimental results from which the thermodynamic data is derived. In many cases equilibrium constants for aqueous species and solid phases are estimated from measurement of an equilibrium constant of a related entity. In these cases uncertainty is introduced by the estimation method. For the NEA database, uncertainties for all reactions were estimated from evaluation of the experimental data by the NEA Committee. Four elements, Np, Pu, Tc, and U, are considered most likely to contribute to significant doses based on inventories, knowledge of their behavior, and previous Performance Assessment modeling. Uncertainties in the solubilities for these were estimated here using the uncertainties listed by the NEA for the formation reactions of the solubility controlling phase and the dominant aqueous species. The dominant aqueous species were defined from the solubility runs of The Geochemist's Workbench as the species with the highest concentrations and those with concentrations within an order of magnitude of the highest. Solubility runs were then done in which the equilibrium constants of the formation reactions for the controlling solid and the aqueous species were varied in opposite directions by the uncertainty listed by the NEA for each reaction. In other words to estimate the maximum solubility within the uncertainty the solid phase was made less stable and the dominant aqueous species were made more stable. The

opposite was done to estimate the minimum solubility. This gives a range that can be considered the maximum uncertainty in solubility.

Uncertainties were estimated for the four elements in the six different pore fluid compositions and are shown in Figure 18. In general, the uncertainties are between 1 and 2 orders of magnitude. The uncertainties in solubilities for other elements addressed in this report are probably similar, though uncertainties for elements that have a long history of experiments may be less.

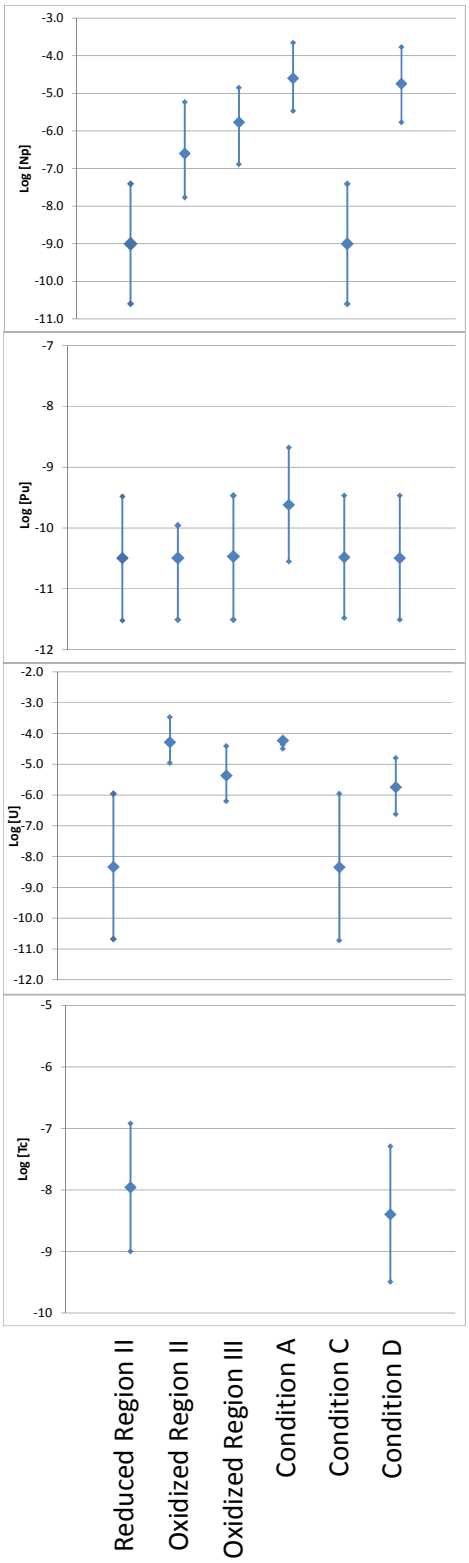

Figure 18: Uncertainty in solubility estimations for Np, Pu, U, and Tc under the six contaminant zone pore fluid conditions.

Neptunium

Solubility Controlling Phase

Two solid phases were selected to control solubility of neptunium at different redox conditions. At highly oxidizing conditions $NpO_2OH_{(am,aged)}$ is a thermodynamically stable Np(V) phase. $NpO_{2(am,hyd)}$ is an Np(IV) phase stable at other conditions. Figure 19 shows Eh-pH diagrams for neptunium at Regions II (Figure 19a) and III (Figure 19b). Crystalline phases such as $NpO_{2(c)}$, Np_2O_5 and $NpO_2(OH)_{2(c)}$ were avoided in favor of the more soluble amorphous phases.

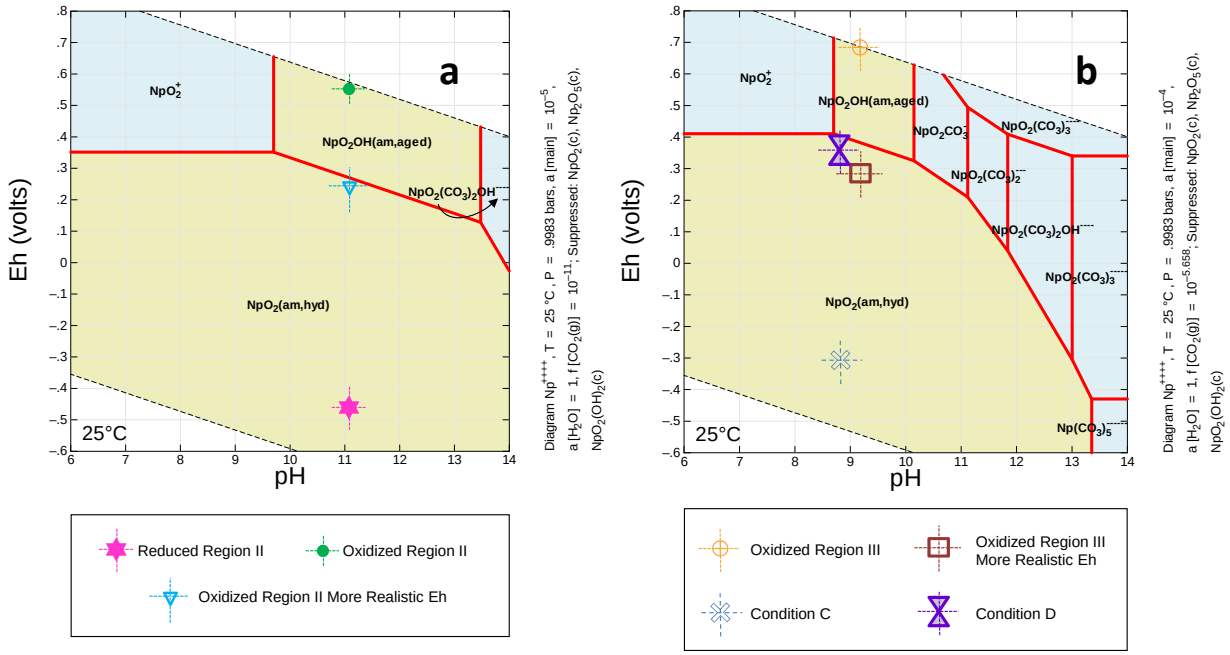

Figure 19: Eh-pH diagrams of neptunium speciation; a) Region II and b) Region III.

Sensitivity to pH

The effect of pH variation depends strongly on the Eh assumed. In Reduced Region II (Eh=-0.47 v), the solubility of $NpO_{2(am,hyd)}$ is constant over the pH range of 8 to13 (Figure 20). Figure 21 shows the solubility versus pH for Oxidized Region II at Eh values of +0.56 v (equilibrium with atmospheric oxygen) and +0.24 v (more realistic). The variation is greater at the more oxidizing condition for which $NpO_2OH_{(am,aged)}$ is the dominant solid phase. The minimum solubility is at a pH of approximately 11.3. Hence, as pH increases from 11.1 the solubility decreases to the minimum and is then constant to a pH of 12. At pH>12 solubility of $NpO_2OH_{(am,aged)}$ increases with increasing pH. At pH<11.1 solubility increases one order of magnitude per unit decrease in pH. At an Eh of +0.24 v the stable phase is $NpO_{2(am,hyd)}$ that has a constant solubility over the pH range of 8 to 11.3. The solubility increases slightly as pH increases beyond 11.3, until $NpO_2OH_{(am,aged)}$ becomes the more stable phase at pH=11.6. The solubility is constant between pH=11.6 and pH=12.3 and then rises to approximately 1.3E-6 moles/liter at pH=13.

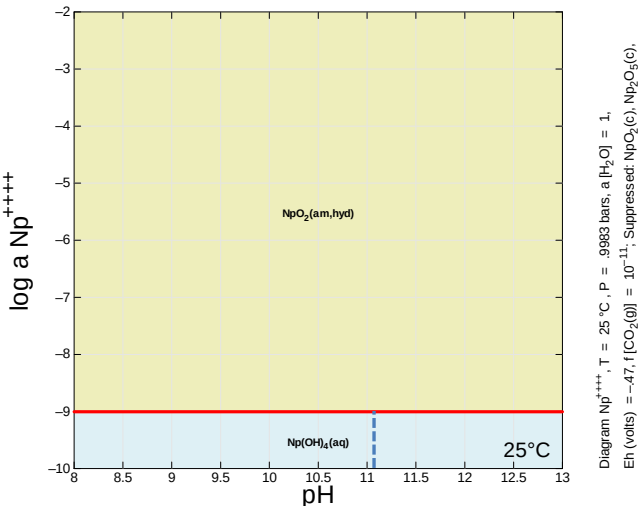

Figure 20: Solubility vs. pH for NpO2(am,hyd) in Reduced Region II. Dashed line shows approximate pH in Reduced Region II.

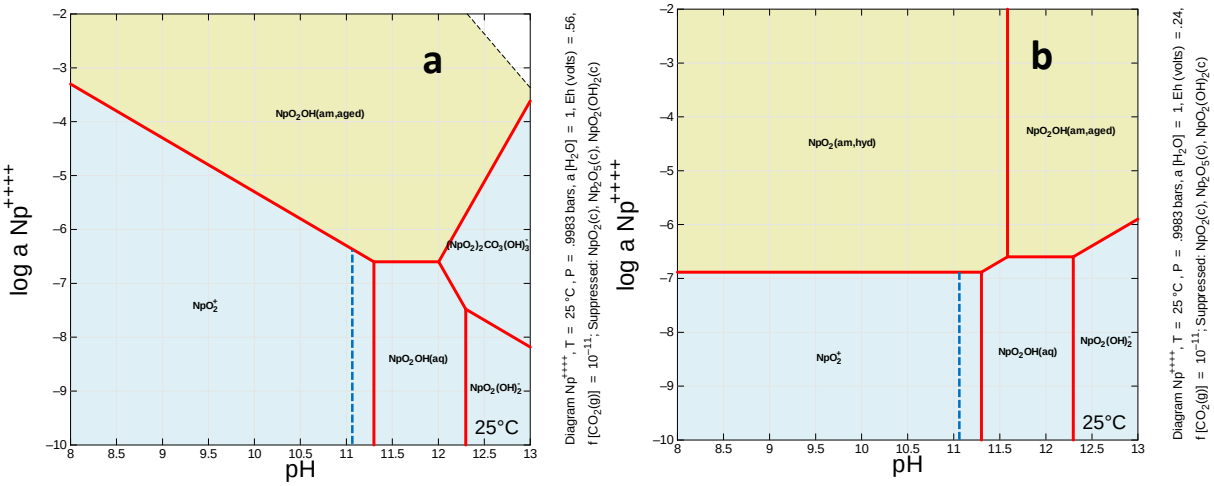

Figure 21: Solubility of NpO_2OH(am,aged) and $NpO_{2(am,hyd)}$ versus pH for Oxidized Region II with a) Eh=+0.56 v and b) Eh=+0.24 v. Dashed line shows approximate pH at each condition.

In Oxidized Region III, solubility of neptunium phases is affected more by pH because of the influence of carbonate complexing (Figure 22). At an Eh in equilibrium with dissolved oxygen (Figure 22a) the minimum solubility of $NpO_2OH_{(am,aged)}$ occurs at a pH~9.4. Therefore, an increase from pH=9.2 initially results in a decrease in solubility, but beyond pH~9.4 the solubility decreases with continued increase in pH. At pH<9.2 the solubility increases. At Eh=0.29 volts (Figure 22b) $NpO_{2(am,hyd)}$ is the more stable phase at pH<10.7. The solubility is lower and constant from pH~9.4 to 8.0. As pH increases beyond 9.4, solubility increases.

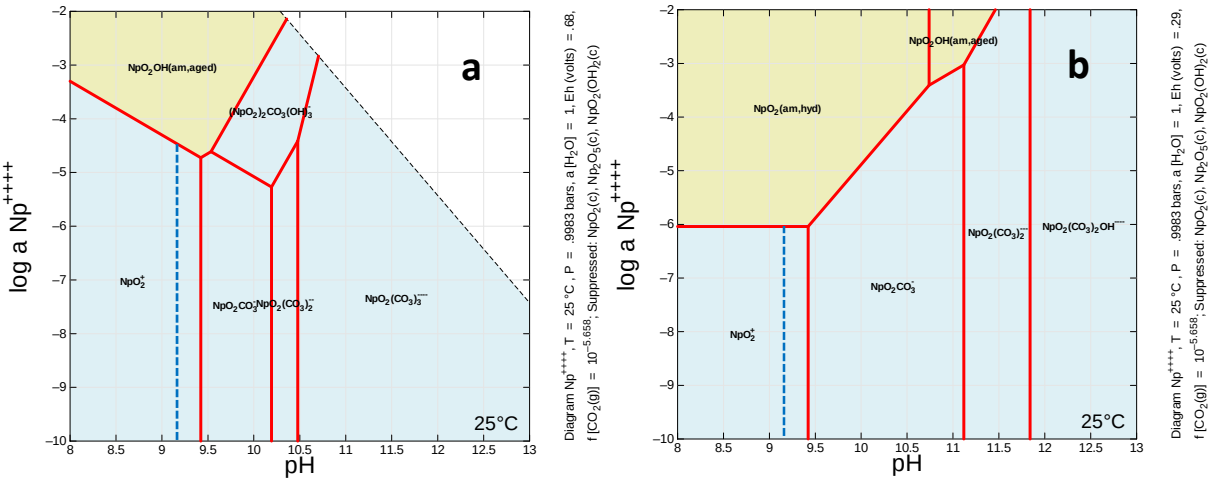

Figure 22: Solubility of NpO2OH(am,aged) and NpO2(am,hyd) versus pH for Oxidized Region III with a) Eh=+0.68 v and b) Eh=+0.29 v. Dashed line shows approximate pH at each condition.

In pore fluids of Condition A $NpO_{2(am, hyd)}$ is the dominant phases and has a constant solubility over a range of pH from 3.3 to 7.9 (Figure 23).

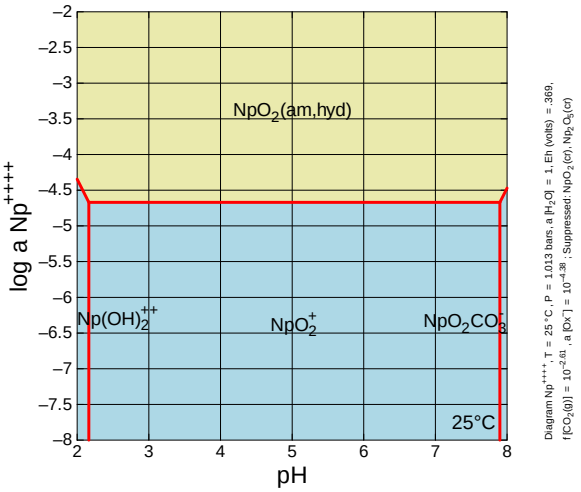

Figure 23: Solubility of $NpO_{2(am, hyd)}$ versus pH in pore fluids of Condition A.

Sensitivity to Eh

The sensitivity of neptunium solubility to Eh is strongly influenced by the relative stability of the phases $NpO_{2(am,hyd)}$ and $NpO_2OH_{(am,aged)}$. Figure 24 shows solubility versus Eh diagrams for Regions II (Figure 24a) and Oxidized Region III (figure 24b). When Eh<+0.12 v solubility is not sensitive to Eh in any of the chemical conditions. As Eh increases from +0.12 v, solubility increases until $NpO_2OH_{(am,aged)}$ becomes the stable phase. Once $NpO_2OH_{(am,aged)}$ is the stable phase, its solubility is insensitive to Eh until approximately +0.65 v for Region II conditions and +0.70 for Oxidized Region III. Figure 25 shows the sensitivity of neptunium solubility to Eh in

Condition A. At the Eh used for Condition A (dashed line) the solubility is sensitive to Eh, increasing as Eh increases and decreasing as Eh decreases.

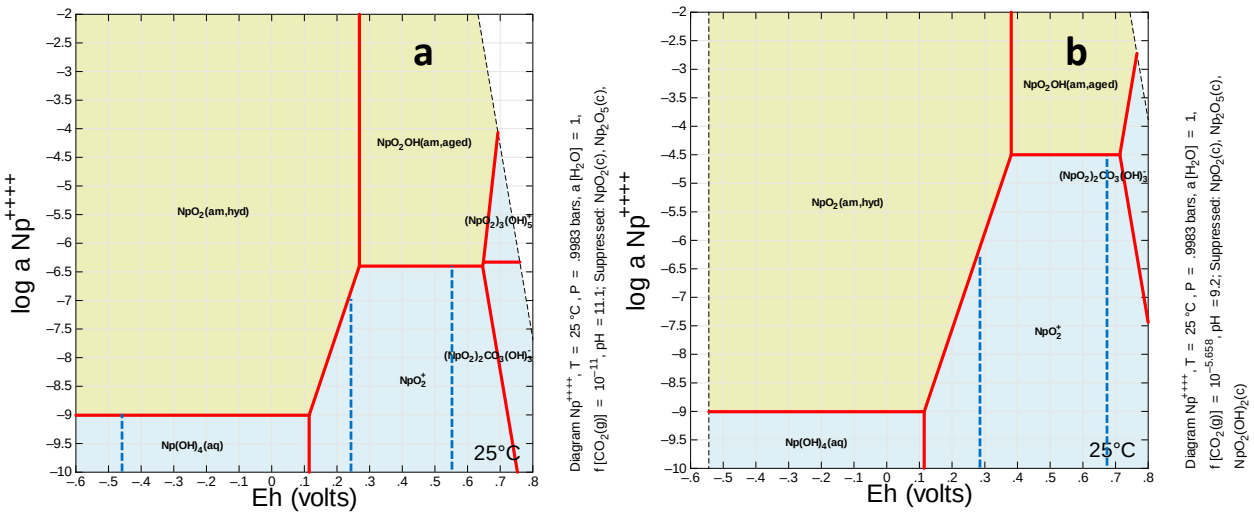

Figure 24: Solubility vs. Eh for NpO2(am,hyd) and NpO2OH(am, aged) at a) Reduced and Oxidized Region II and b) Oxidized Region III. Dashed line shows approximate Eh at each pertinent condition.

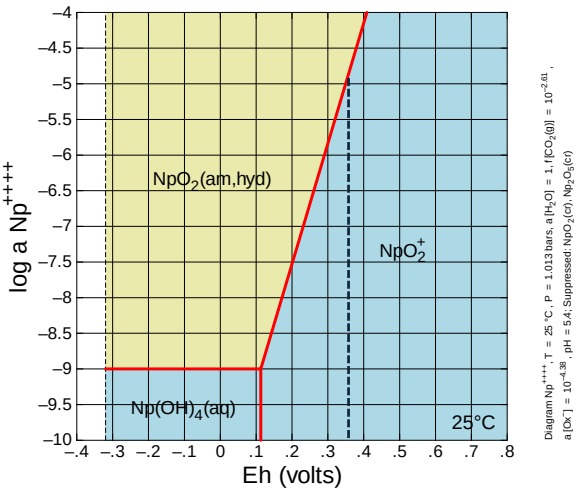

Figure 25: Solubility of NpO2(am, hyd) versus Eh in Condition A pore fluid. Dashed line shows approximate Eh of Condition A.

Sensitivity to Total Carbonate Concentration

In Reduced Region II the solubility of neptunium is not sensitive to total carbonate concentration (no figure shown). In the oxidized regions solubility is sensitive to total carbonate concentration because Np(V) and Np(VI) carbonate complexes become stable. Figure 26 shows the sensitivity in Oxidized Region II at an Eh in equilibrium with dissolved oxygen (Figure 26a) and at Eh=0.24 volts (Figure 26b). In both cases the solubility is not sensitive to total carbonate concentration in the log aCO_3^{-2} range of -8 to -4.9, despite the different solubility controlling

phases. The only difference in sensitivity is that at the more oxidizing conditions the $NpO_2(CO_3)_3^{-4}$ becomes stable at log aCO_3^{-2}~-2.2. The same relative sensitivity of solubility to total carbonate concentration applies to Oxidized Region III (Figure 27).

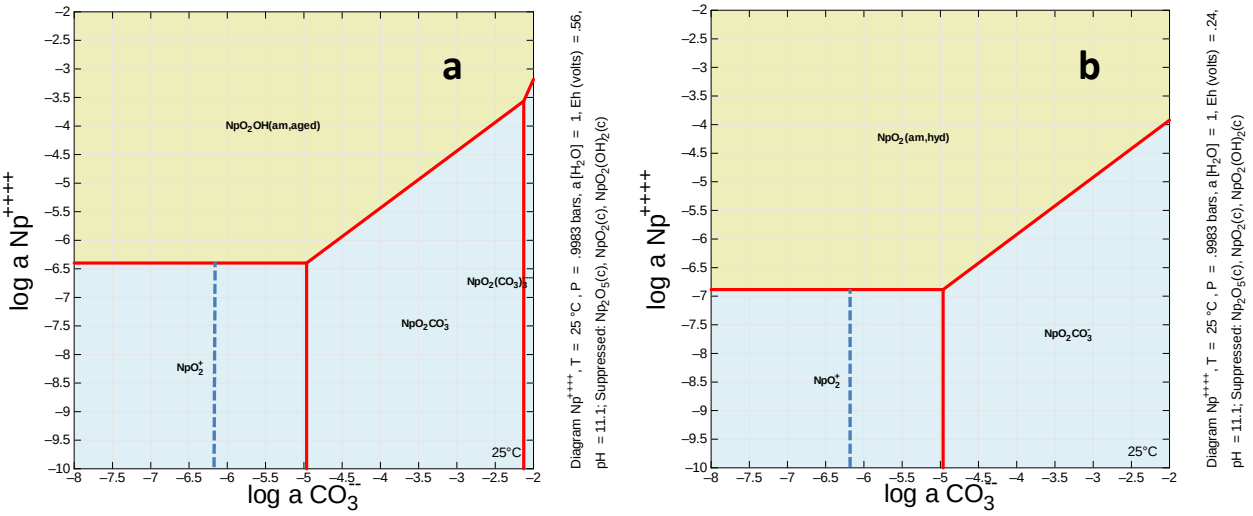

Figure 26: Sensitivity of neptunium solubility to carbonate concentration at a) Oxidized Region II, Eh=+0.56v and b) Oxidized Region II, Eh=+0.24v. Dashed line shows approximate total carbonate concentration at each condition.

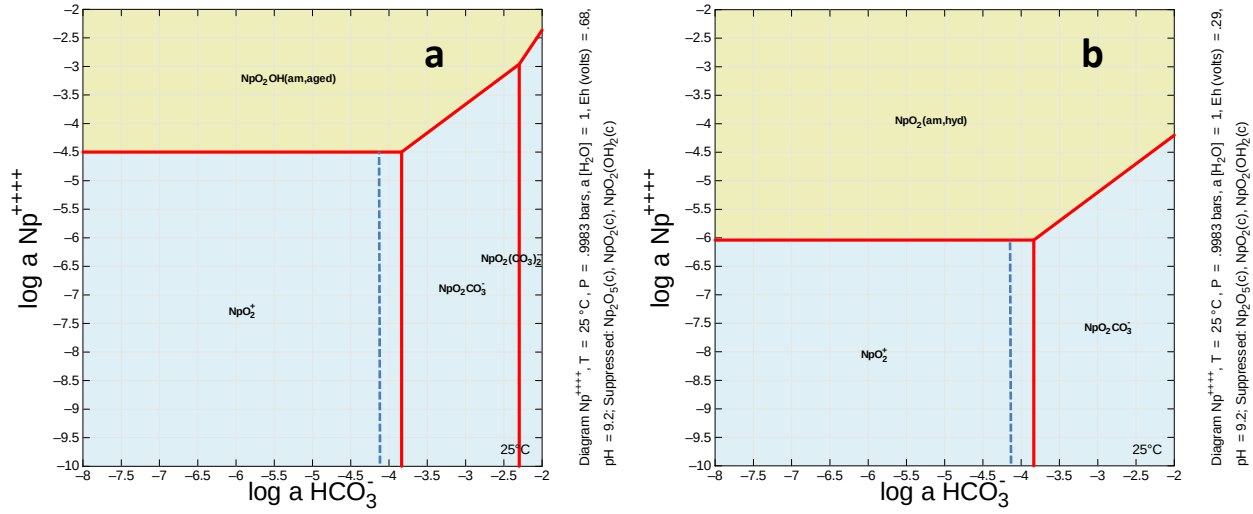

Figure 27: Sensitivity of neptunium solubility to carbonate concentration at a) Oxidized Region III, Eh=+0.68v and b) Oxidized Region III, Eh=+0.29v. Dashed line shows approximate total carbonate concentration at each condition.

The solubility of $NpO_{2(am, hyd)}$ is not sensitive to the dissolved inorganic carbon concentration in pore fluids of Condition A (no figure shown).

Sensitivity to Oxalate Concentration

Np solubility is not sensitive to oxalate concentration in Reduced Region II (no figure shown). In Oxidized Regions II and III solubility is only sensitive at oxalate concentration of one order of

magnitude and one half an order of magnitude greater than the concentrations used to estimate the solubilities (no figure shown)

Uranium

Solubility Controlling Phase

Two phases were chosen to control solubility of uranium at different redox conditions. For Reduced Region II, the phase $UO_{2(am,hyd)}$ was chosen, whereas $UO_3 \bullet 2H_2O$ (Schoepite) was chosen for oxidized regions. These phases are at the upper limit of uranium solubility under their respective conditions. The mineral uraninite (UO_2), less soluble than $UO_{2(am,hyd)}$, has been identified on weathered depleted uranium munitions (Mellini et al., 2005; Lind et al., 2009). Likewise, lower solubility forms of U(VI), for example $CaUO_4$ (Cantrell et al., 2008) or uranophane (Krupka and Serne, 1998), could control solubility in oxidizing cementitious conditions. Figure 28 shows Eh-pH diagrams under the different post-closure tank conditions.

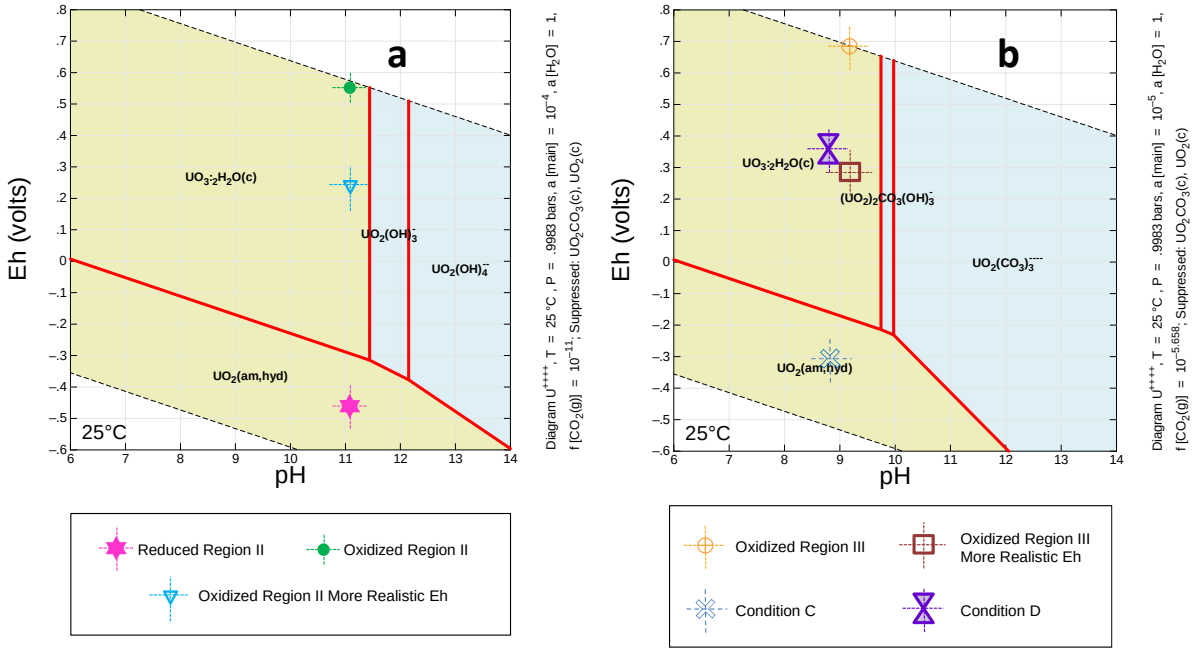

Figure 28: Eh-pH diagrams showing solubility controlling phases selected for uranium in a) Region II conditions and b) Region III conditions.

Sensitivity to pH

The sensitivity of uranium solubility to pH depends strongly on the redox conditions. In Reducing Region II with $UO_{2(am,hyd)}$ as the stable phase, solubility is constant over the pH range of 8 to 11.75 (Figure 29a). At pH=11.75 solubility increases until pH~12.2 while in equilibrium with the dominant aqueous species $UO_2(OH)_3^-$. At higher pH values $UO_2(OH)_4^{-2}$ is the dominant aqueous species and the slope of the solubility increase is steeper. Hence, at the Reducing Region II pH of 11.1, a decrease in pH has no effect on solubility and pH can increase 0.6 units before solubility begins to increase.

At Oxidized Region II conditions uranium solubility is sensitive at pH>8.1, controlled mostly by equilibrium of $UO_3 \bullet 2H_2O$ with the dominant aqueous species $UO_2(OH)_3^-$ (Figure 29b). The pH sensitivity is the same in this region whether Eh=+0.56 v or Eh=+0.24 v. Therefore, from the Oxidized Region II pH of 11.1, solubility increases with increases in pH and decreases with decreases in pH.

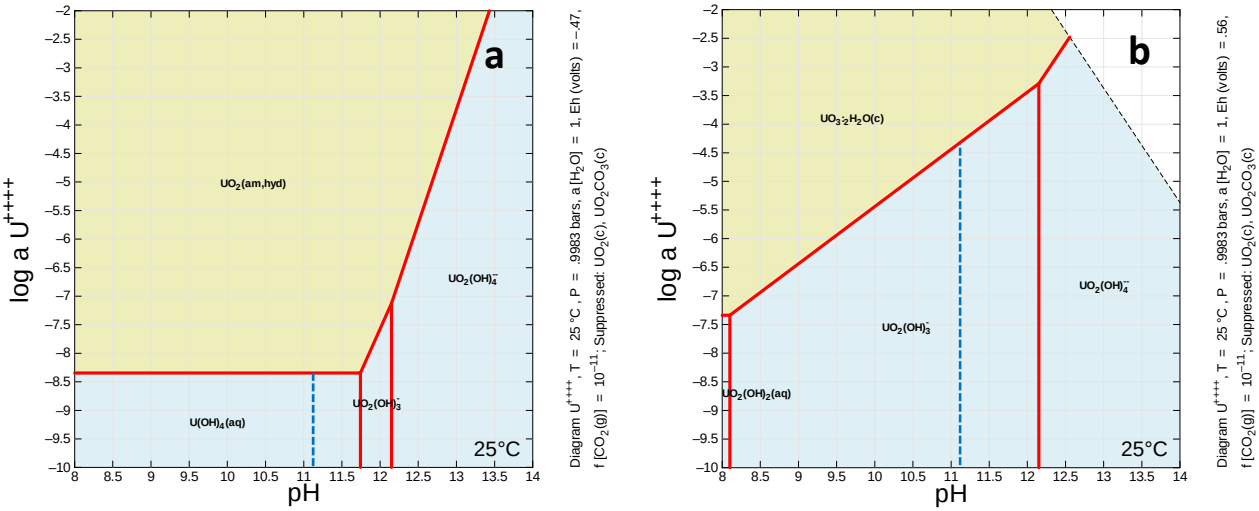

Figure 29: Sensitivity of uranium solubility to pH in a) Reducing Region II and b) Oxidizing Region II. Other parameters are to the side of each diagram. Dashed line shows approximate pH at each condition.

Likewise, uranium solubility in Oxidized Region III is sensitive to pH from pH=7.5 to 10 (Figure 30). Over that range solubility is controlled by equilibrium of $UO_3 \bullet 2H_2O$ with the dominant aqueous species $(UO_2)_2CO_3(OH)_3^-$. Choice of a more realistic Eh of +0.29 v makes no difference to the sensitivity. Thus, from the Oxidizing Region III pH of 9.2, decrease in pH results in a decrease in uranium solubility and increase in pH results in an increase in solubility. Beyond pH~9.6 uranium solubility becomes more sensitive to pH.

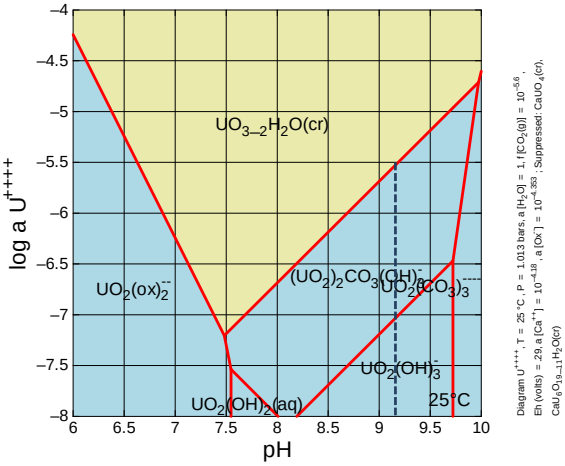

Figure 30: Sensitivity of uranium solubility to pH in Oxidized Region III. Dashed line shows approximate pH at the specified condition.

At the pH of 5.4 in pore fluids of Condition A, the solubility of $UO_3 \cdot 2H_2O$ is highly sensitive to pH changes (Figure 31). Increasing pH causes a decrease in solubility and a decrease in pH cause an increase in solubility.

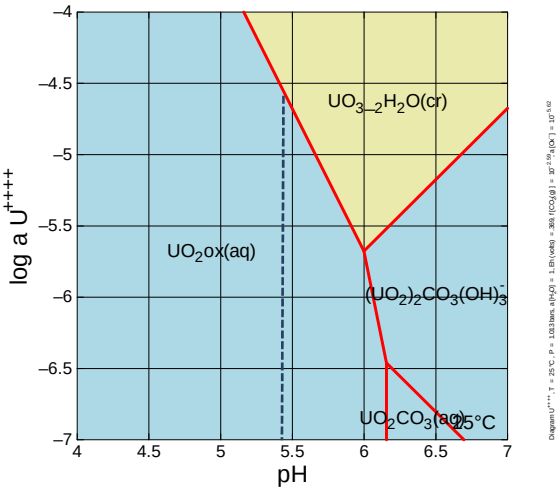

Figure 31: Solubility of $UO_3 \cdot 2H_2O$ versus pH for Condition A pore fluids. The dashed line shows approximate pH of Condition A pore fluids.

Sensitivity to Eh

Figure 32a shows that in Region II sensitivity of uranium solubility to Eh is almost a step change with the change in the thermodynamically stable solid phase. Below an Eh of -0.41 v, $UO_{2(am,hyd)}$ is stable and solubility does not vary with Eh. There is a steep rise in solubility over the Eh range of -0.41 to -0.30 v when $UO_3 \bullet 2H_2O$ becomes the stable phase. Solubility does not vary with Eh at Eh>-0.3 v. A similar behavior occurs in Region III (Figure 32b). The stability of $UO_{2(am,hyd)}$ is extended to a slightly higher Eh of approximately -0.24 v. At an Eh of approximately -0.18 v, $UO_3 \bullet 2H_2O$ becomes stable with a nearly three order of magnitude rise in solubility occurring between -0.24 and -0.18 v.

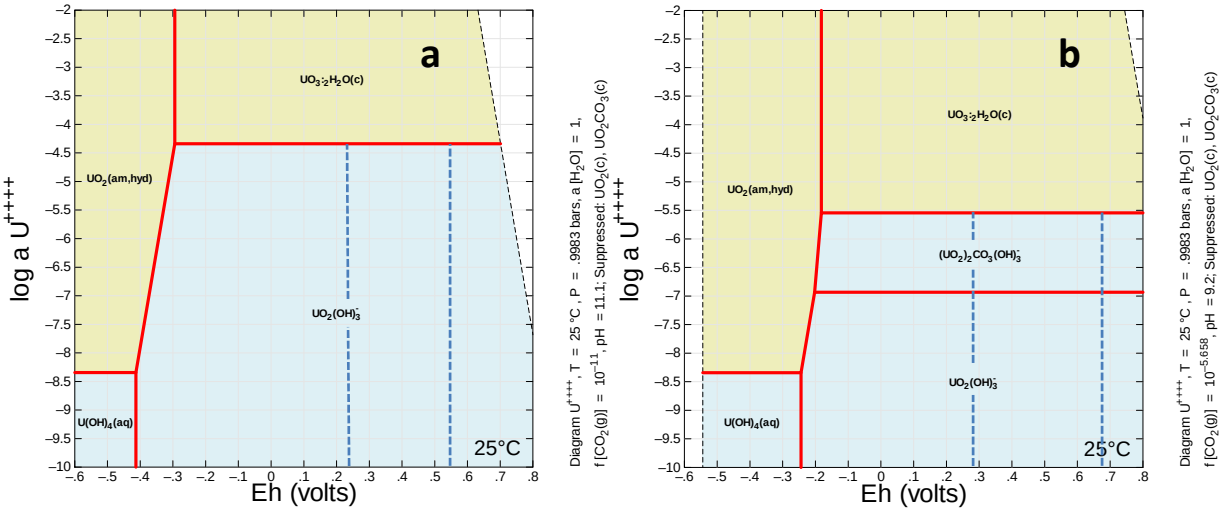

Figure 32: Sensitivity of uranium solubility to Eh in a) Region II and b) Region III; dashed lines show Eh values for Reduced Region II, Oxidized Region II (equilibrium with oxygen and more realistic), and Oxidized Region III (equilibrium with oxygen and more realistic).

The pattern of solubility sensitivity to Eh in pore fluids of Condition A is similar to that of the other chemical conditions (Figure 33). The solubility is constant at Eh below -0.14 volts with $UO_{2(am, hyd)}$ as the controlling solid. The solubility of uranium abruptly rises at Eh greater than -0.14 volts until equilibrium with $UO_3 \cdot 2H_2O$ is reached at an Eh of 0.04 volts and remains constant at higher Eh

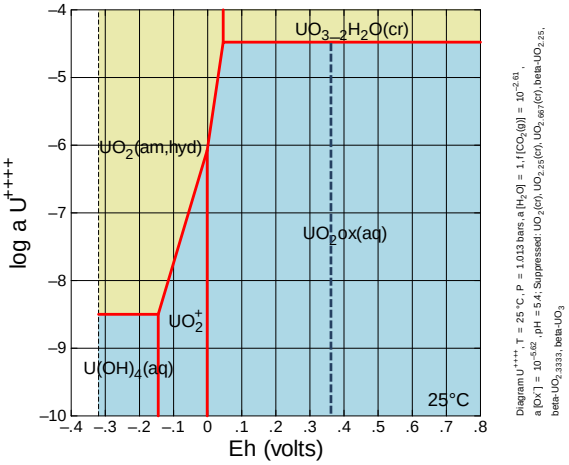

Figure 33: Solubility of UO3.2H2O versus Eh in pore fluids of Condition A. Dashed line shows Eh of Condition A pore fluids.

Sensitivity to Dissolved Inorganic Carbon

Figure 34a shows that uranium is not sensitive to carbonate concentration below log aCO_3~-2.3 at Reducing Region II conditions. At that point the aqueous complex $UO_2(CO_3)_3^{-4}$ becomes dominant and solubility rises with increase log aCO_3. In Oxidized Region II conditions (Figure 34b) uranium behavior is similar, though the solubility is significantly higher and $UO_2(CO_3)_3^{-4}$ becomes the dominant aqueous species at log aCO_3=-2.9. The dashed lines in Figures 34a and 34b show the log aCO_3 used to calculate solubilities in Table 11. In Region II the dissolved inorganic carbon concentration can increase by about 3 orders of magnitude before there is a significant increase in the solubility of uranium.

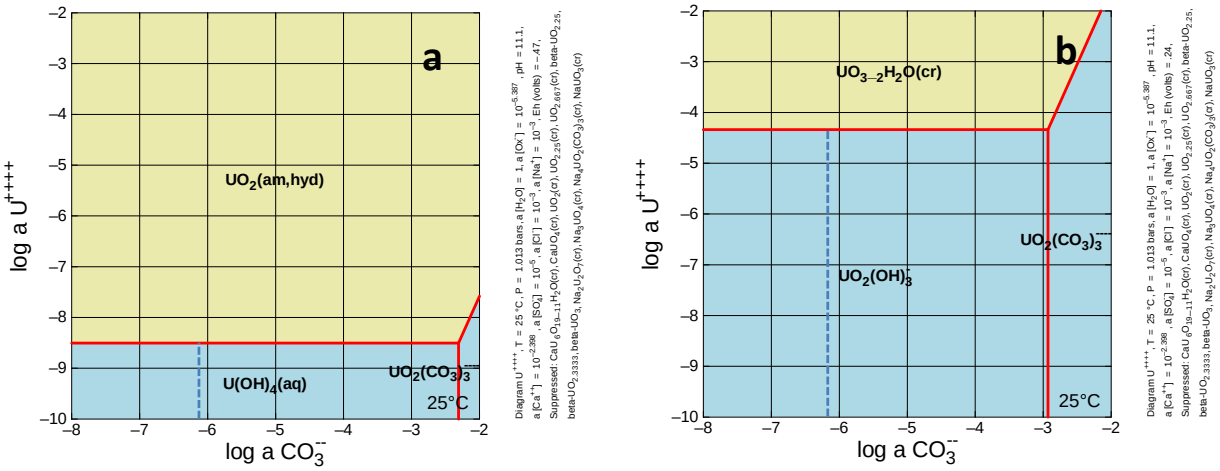

Figure 34: Influence of dissolved inorganic carbon on uranium solubility in a) Reduced Region II and b) Oxidized Region II; dashed lines show log aCO_3 at each condition.

Figure 35a shows the sensitivity of uranium solubility to dissolved inorganic carbon in Oxidized Region III. From log $aHCO_3$=-8 to -4.9 uranium solubility is constant. From log $aHCO_3$= -4.9 to -3.7, $(UO_2)_2CO_3(OH)_3^-$ is the dominant aqueous species and uranium solubility increases with increase in HCO3-. At log $aHCO_3$>-3.2, $UO_2(CO_3)_3^{-4}$ becomes the dominant aqueous species and the sensitivity of uranium solubility to dissolved inorganic carbon increases. The dashed line in Figure 35 shows the dissolved inorganic carbon concentration used to calculate solubilities in Table 11. It indicates that an increase in dissolved inorganic carbon in Oxidized Region III would increase solubility of uranium.

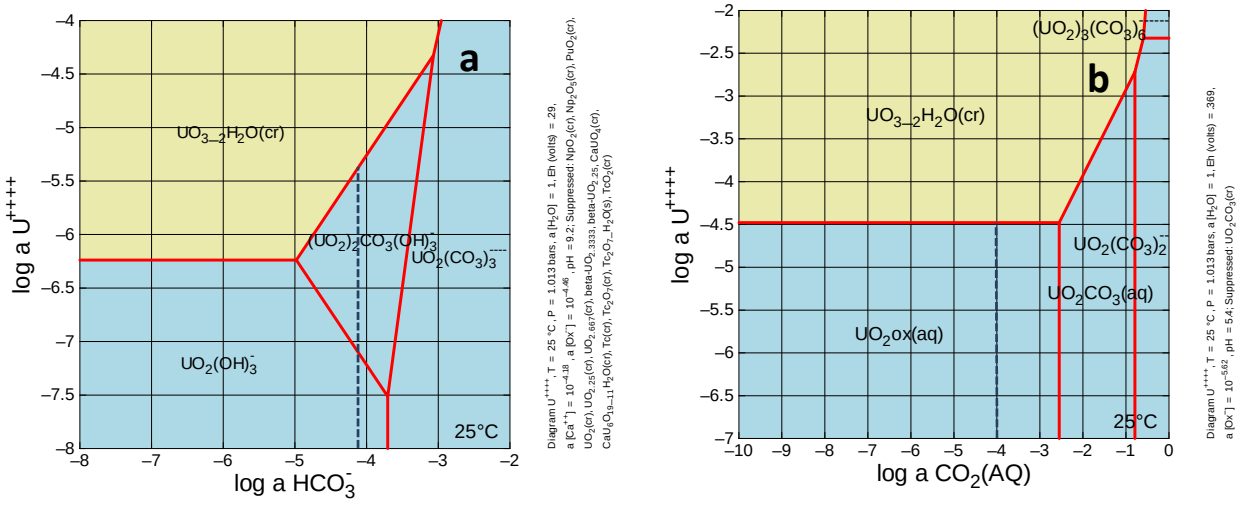

Figure 35: Sensitivity of uranium solubility to dissolved inorganic carbon in a) Oxidized Region III and b) Condition A; dashed line shows log aHCO3 and log aCO2(aq) used to calculate solubilities in Table 11.

Figure 35b shows that solubility of $UO_3 \cdot 2H_2O$ is not sensitive to dissolved CO_2 up to $\log aCO_{2(aq)}$=-2.6. At this point $UO_2CO_{3(aq)}$ becomes the dominant complex and further increases in $\log aCO_{2(aq)}$ cause higher solubilities of $UO_3 \cdot 2H_2O$.

Sensitivity to Oxalate Concentration

Uranium solubility is not sensitive to dissolved oxalate concentration in Reducing Region II and is only sensitive in Oxidized Region II at very high oxalate concentration (no figures shown). The same is true of Conditions C and D (no figures shown). However, uranium solubility does become sensitive to oxalate concentration in Oxidized Region III and Condition A. Figure 36a shows that solubility of $UO_3 \cdot 2H_2O$ is only sensitive to oxalate concentration above approximately $10^{-1.9}$. This concentration is over two orders of magnitude higher than that used to estimate solubility in Oxidized Region III. In contrast, $UO_3 \cdot 2H_2O$ solubility is sensitive to oxalate concentration in Condition A (Figure 36b). In fact, the aqueous complex $UO_2Ox_{(aq)}$ is the dominant oxalate species in Condition A.

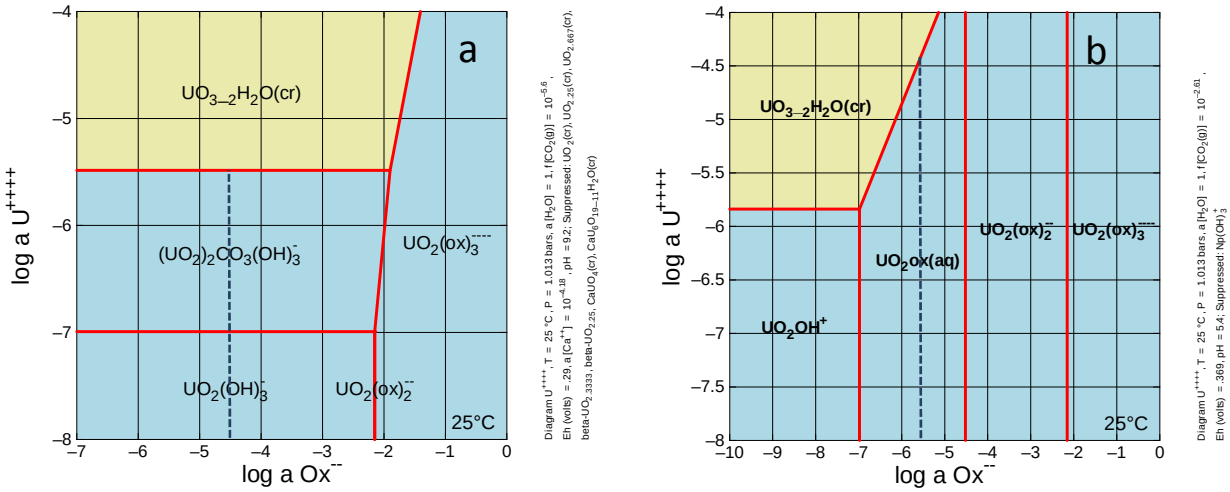

Figure 36 : Solubility of UO3.2H2O versus dissolved oxalate concentration in pore fluids of a) Oxidized Region III and b) Condition A. Dashed line shows concentration of oxalate used to calculate solubilities in Table 11.

Technetium

Solubility Controlling Phase

The solubility controlling phase selected for technetium under reducing conditions was $TcO_2 \bullet 1.6H_2O$. There is no solubility controlling phase for oxidizing conditions. An alternate solubility controlling phase under reducing conditions might be Tc_2S_7 because spectroscopic studies involving reducing grout indicated reduced technetium was primarily bound in a sulfide (Allen et al., 1996; Lukens et al., 2004). However, Guillaumont et al. (2003) does not accept the current thermodynamic data for Tc_2S_7, suggesting that colloidal interferences plague the various studies reviewed (Rard et al., 1999). The ambiguous data suggest a range of solubilities for Tc_2O_7 from approximately 10^{-8} moles/liter to extremely low values. Hence, $TcO_2 \bullet 1.6H_2O$ was used as the solubility controlling phase in Reduced Region II. Figure 37 shows the Eh-pH diagram for technetium at Region II conditions.

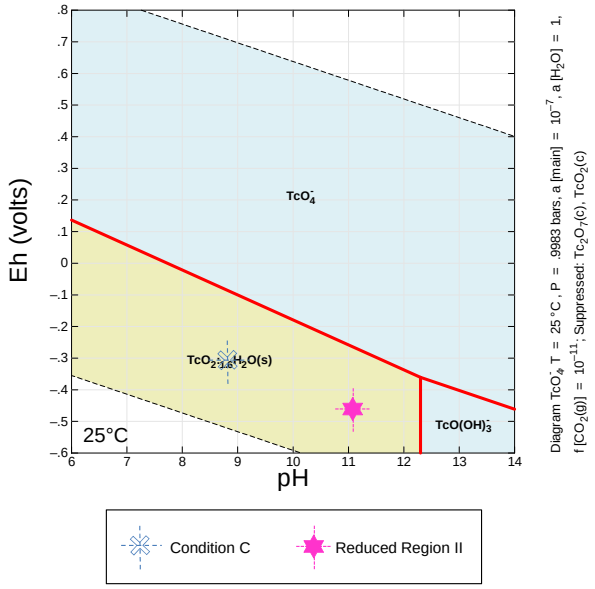

Figure 37: Eh-pH diagram for technetium at Region II conditions.

Sensitivity to pH

Figure 38 shows that in Reduced Region II technetium solubility does not vary with pH below pH=10.9. At pH>10.9 $TcO(OH)_3^-$ becomes the dominant aqueous species. Along the line representing equilibrium between $TcO_2 \bullet 1.6H_2O$ and $TcO(OH)_3^-$, solubility increases as pH increases at a slope of one order of magnitude per pH unit. At the Reducing Region II pH of 11.1 an increase in pH would result in an increase in solubility, whereas a decrease in pH would have no substantial effect.

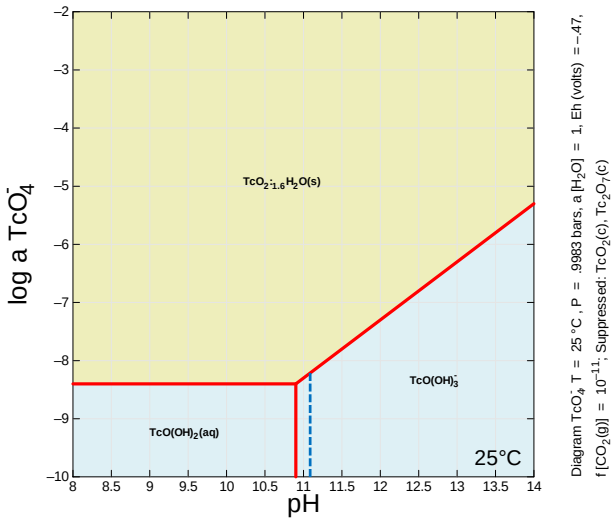

Figure 38: Sensitivity of technetium solubility to pH in Reducing Region II. Dashed line shows approximate pH at the specified condition.

Sensitivity to Eh

In Reducing Region II solubility of technetium is not sensitive to Eh below Eh=-0.29, but is highly sensitive at Eh above this value (Figure 39).

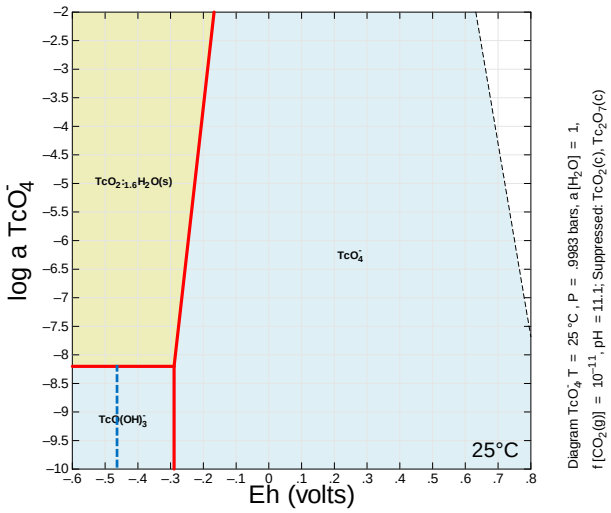

Figure 39: Sensitivity of technetium to Eh in Reducing Region II. Dashed line shows approximate Eh at each condition.

Sensitivity to Total Dissolved Carbon

The solubility of technetium in Reducing Region II is not sensitive to dissolved carbonate concentration (no figure shown).

Sensitivity to Oxalate Concentration

The solubility of technetium in Reducing Region II is not sensitive to dissolved oxalate concentration (no figure shown).

Plutonium

Sensitivity to pH

Solubility of plutonium is only sensitive to pH at values less than 9.1 in Reducing Region II (Figure 40). In Oxidizing Region II the sensitivity depends on the Eh (Figure 41). At Eh=0.24 volts there is no sensitivity to pH. At an Eh value of 0.56, in equilibrium with dissolved oxygen, solubility decreases as pH decreases below 11.1 – the pH used to estimate solubilities in Oxidized Region II. Above pH=11.1 the solubility of Pu is likely to be controlled by the Pu(VI) phase $PuO_2(OH)_2 \cdot H_2O$ and remain constant to higher pH values.

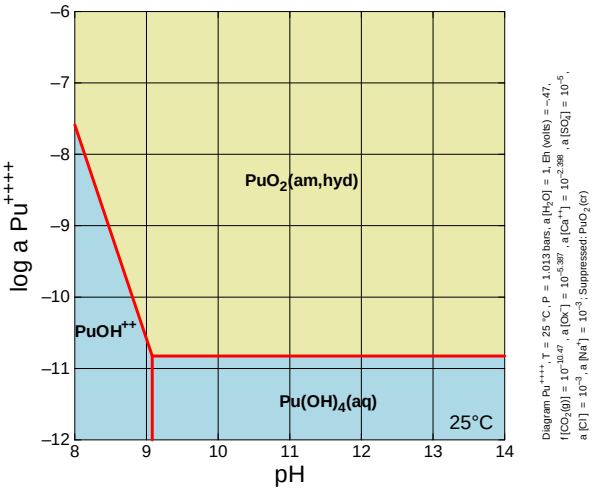

Figure 40: Solubility of Pu versus pH in pore fluids of Reducing Region II. Dashed line shows approximate pH used to calculate solubilities in Table 11.

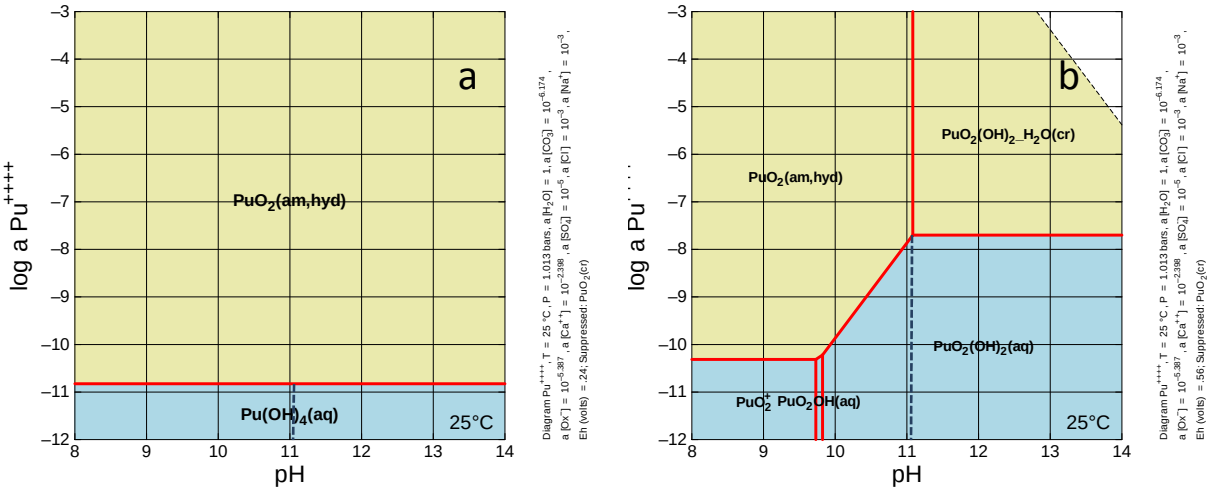

Figure 41: Solubility of Pu versus pH in Oxidized Region II for a) Eh=0.24 volts and b) Eh=0.56 volts.

The same pattern of Pu solubility sensitivity to pH occurs in Oxidized Region III (Figure 42). Solubility is not sensitive to pH when Eh=0.29 volts, but is when Eh is in equilibrium with dissolved oxygen at a value of +0.68 volts. At the higher Eh solubility is likely to be controlled by the Pu(VI) phase $PuO_2(OH)_2 \cdot H_2O$ and remain constant to higher pH values. For the solubility estimations at the higher Eh values no credit was taken for precipitation of $PuO_2(OH)_2 \cdot H_2O$ and solubility values for $PuO_{2(am,\ hyd)}$ were reported.

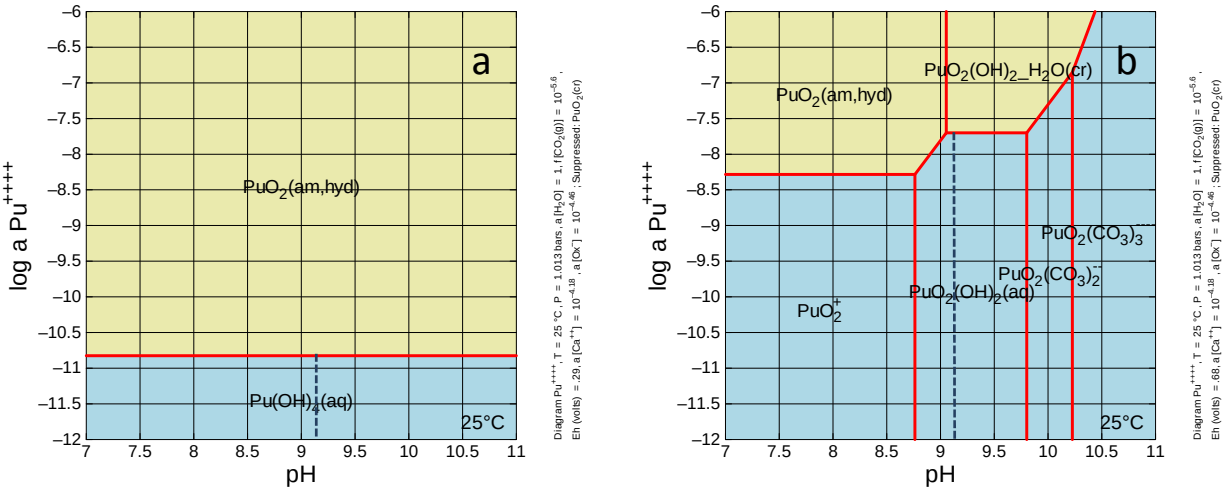

Figure 42: Solubility of Pu versus pH in pore fluids of Oxidized Region III at a) Eh=0.29 volts and b) Eh=0.68 volts. Dashed line shows approximate pH used to estimate solubility values reported in Table 11.

In pore fluids of Condition A the solubility of Pu is sensitive to pH (Figure 43). The pH of Condition A pore fluids is 5.4 and at pH values below this solubility of Pu increases, whereas at pH values greater than 5.4 Pu solubility decreases. From a pH of approximately 6.2 to pH=8 the solubility of Pu is not sensitive the pH.

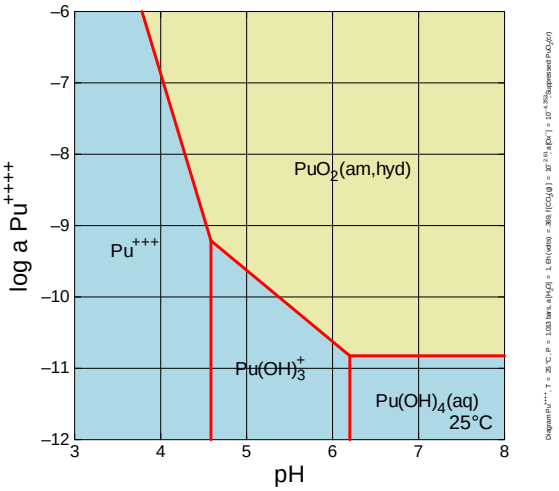

Figure 43: Solubility of Pu versus pH in Condition A pore fluids. Dashed line shows approximate pH of Condition A pore fluids.

Sensitivity to Eh

Figure 44 shows the sensitivity of Pu solubility to Eh at Region II conditions. The solubility is not sensitive to Eh in the range of -0.50 volts to +0.45 volts. At Eh values greater than 0.45 volts the solubility is sensitive to Eh, increasing as Eh increases. At an Eh of approximately +0.57 volts the Pu(VI) phase $PuO_2(OH)_2 \cdot H_2O$ likely controls solubility.

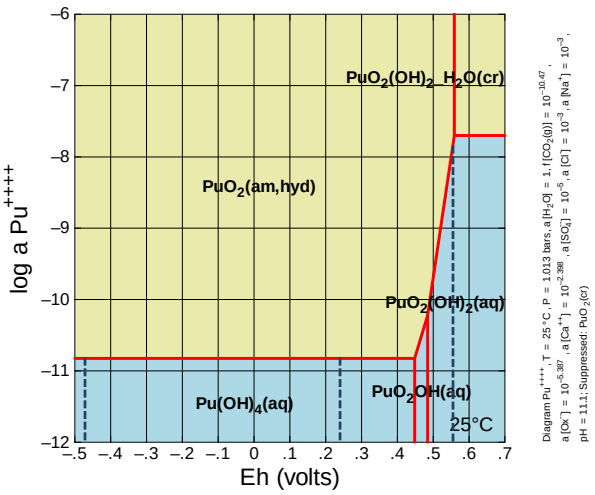

Figure 44: Solubility of Pu versus Eh in Region II conditions. Dashed lines show Eh values of -0.47, +0.24, and +0.56 volts.

In Oxidizing Region III conditions the sensitivity of Pu solubility to Eh also varies (Figure 45a). There is no sensitivity to Eh up to a value of approximately +0.53 volts. At higher Eh values solubility increases. In Condition A pore fluids solubility of Pu is not sensitive to Eh in the range of +0.23 to +0.57 (Figure 45b). Outside that range Pu solubilities increase.

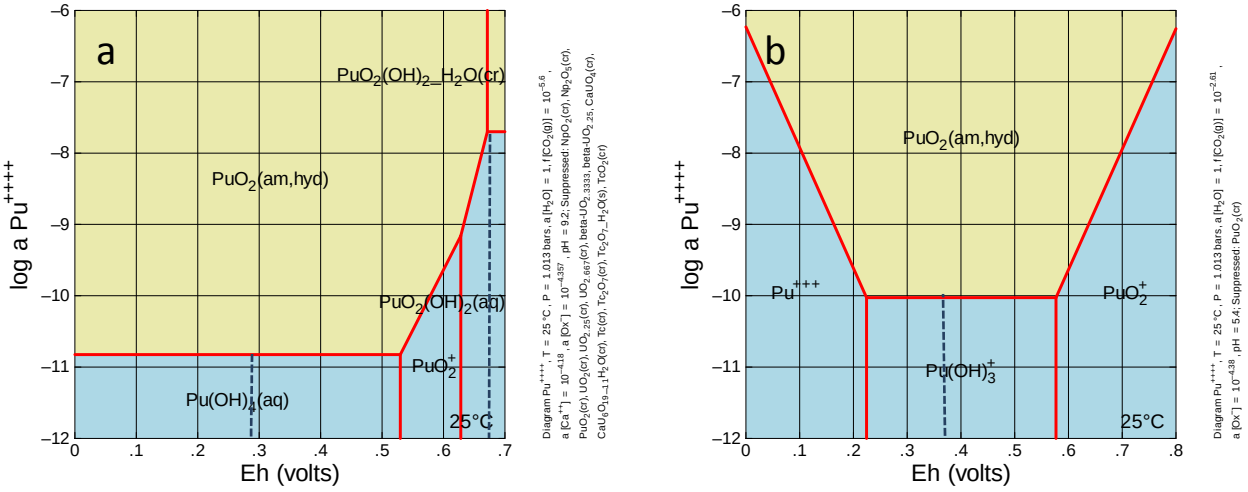

Figure 45: Pu Solubility versus Eh for a) Oxidized Region III and b) Condition A pore fluids. Dashed lines represent approximate Eh values used to estimate solubilities; Table 11 solubilities were estimated using +0.24 volts for Oxidizing Region III and 0.37 volts for Condition A.

The wide range of insensitivity of Pu solubility to Eh is important. The estimated solubility is the same regardless of the Eh value selected for the estimates up to high Eh values -- +0.45 volts for Oxidized Region II and +0.53 volts for Oxidized Region III. Though it is possible that Eh values will be greater than these upper thresholds, based on natural analogues and measured values in oxidized cements it seems unlikely.

Sensitivity to Dissolved inorganic carbon Concentration

Figure 46 shows that the solubility of Pu is not sensititive to carbonate concentration in pore fluids of Reduced Region II. Figure 47 shows that Pu solubility insensitive to carbonate concentration except at high carbonate concentrations ($logaCO3^{-2}$≥-3) when Eh=+0.56 (equilibrium with dissolved oxygen) in Oxidized Region II.

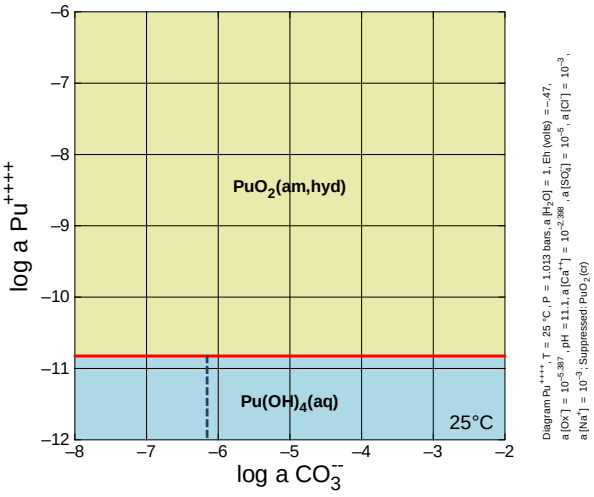

Figure 46: Solubility of Pu versus dissolved inorganic carbon in Reduced Region II pore fluids. Dashed line shows approximate $logaCO_3^{-2}$ used to calculate solubilities in Table 11.

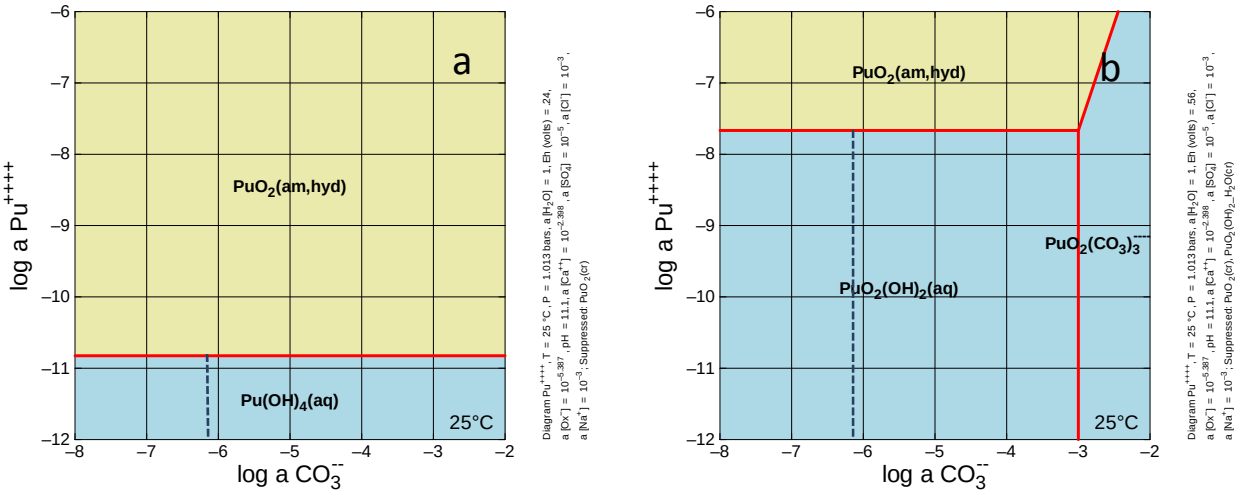

Figure 47: Solubility of Pu versus dissolved inorganic carbon concentration in Oxidized Region II pore fluids at a) Eh=+0.24 volts and b) Eh=+0.56 volts.

Figure 48 shows the sensitivity of Pu solubility to dissolved inorganic carbon concentration in Oxidized Region III pore fluids. At an Eh of +0.29 volts Pu solubility is not sensitive to bicarbonate concentration. However, at an Eh value of +0.56 volts the solubility does become

sensitive to bicarbonate concentration above log$aHCO_3$-=-3.6. In pore fluids of Condition A, solubility of Pu is not sensitive to dissolved inorganic carbon (Figure 49).

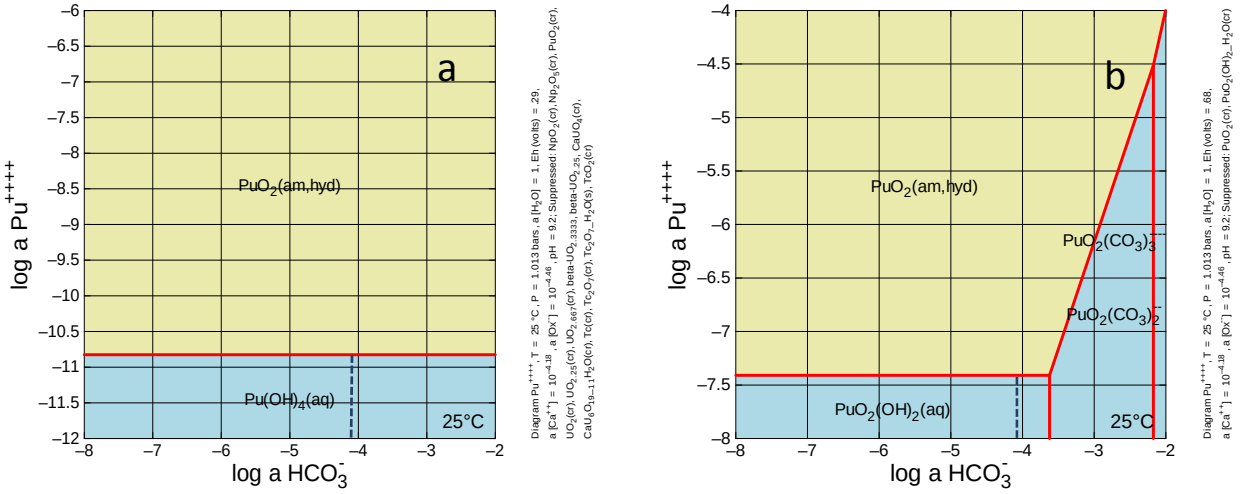

Figure 48: Solubility of Pu versus dissolved carbonate concentration in Oxidized Region III pore fluids at a) Eh=+0.24 volts and b) Eh=+0.68 volts. Dashed line shows dissolved inorganic carbon concentration used to estimate solubilities.

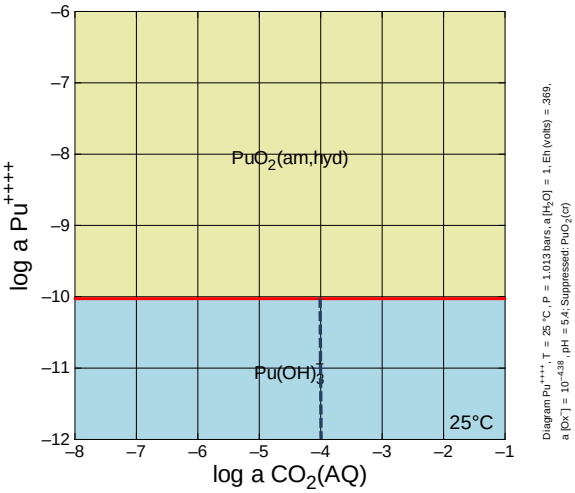

Figure 49: Solubility of Pu versus dissolved inorganic carbon concentration in pore fluids of Condition A. Dashed line shows log$aCO_{2(aq)}$ used to estimate solubility in Table 11.

Sensitivity to Oxalate Concentration

Solubility of Pu is not sensitive to dissolved oxalate concentration in Reduced Region II (Figure 50) or Oxidized Region II (Figure 51) conditions. Figure 52 and Figure 53 show that the same is true for Oxidized Region III pore fluids and Condition A pore fluids.

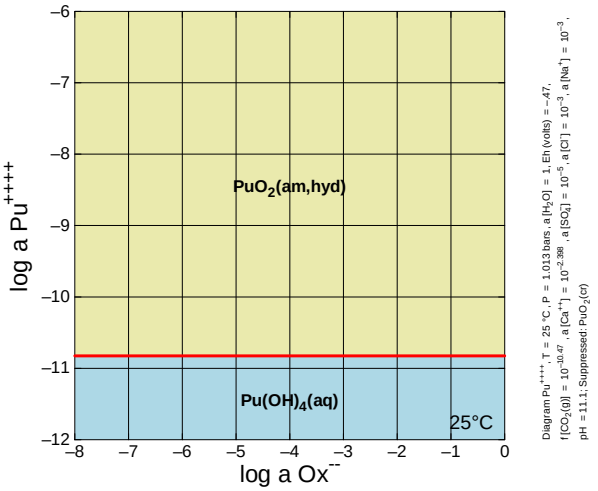

Figure 50: Solubility of Pu versus dissolved oxalate concentration in pore fluids of Reduced Region II. Dashed line shows oxalate concentration used to estimate solubility in Table 11.

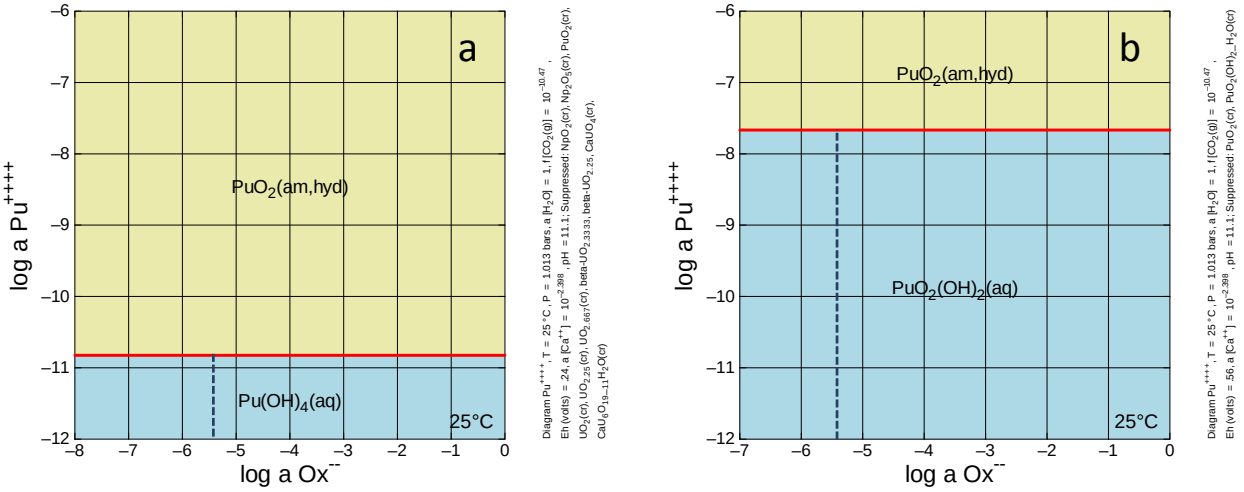

Figure 51: Solubility of Pu in Oxidized Region II pore fluids at a) Eh=+0.24 volts and b) Eh=+0.56 volts. Dashed line shows oxalate used to estimate solubilities in Table 11.

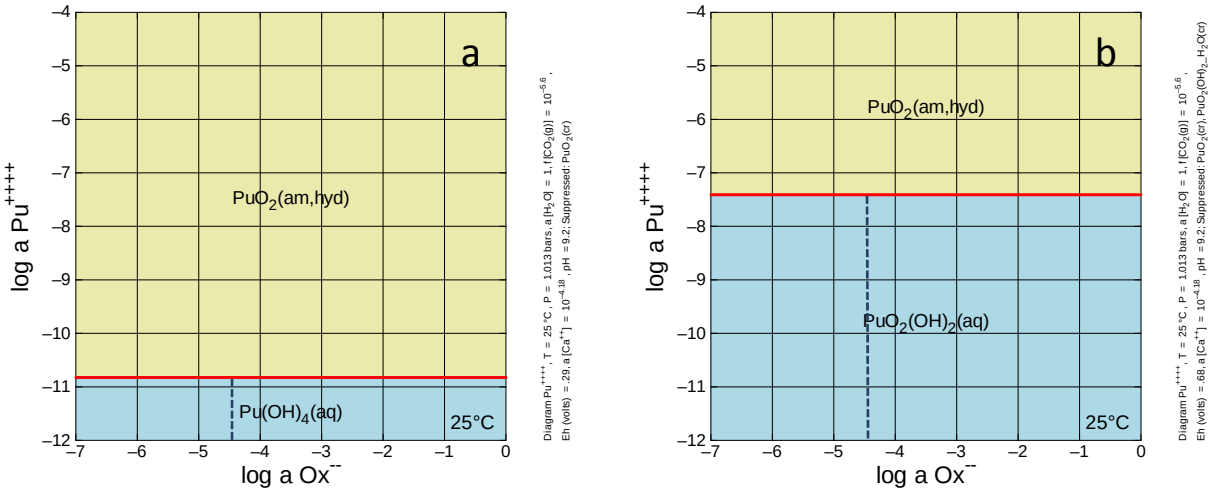

Figure 52: Solubility of Pu versus dissolved oxalate concentration in Oxidized Region III pore fluids at a) Eh=+0.24 volts and b) Eh=+0.68 volts. Dashed line shows oxalate concentration used to estimate solubility in Table 11.

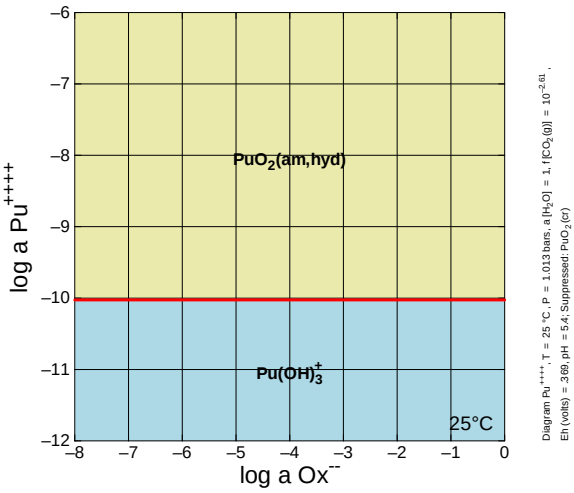

Figure 53: Solubility of Pu versus dissolved oxalate concentration in pore fluids of Condition A. Dashed line shows oxalate concentration used to calculate solubility in Table 11.

Effect of Isotope Dilution on Solubility

Some of the radionuclides of concern, notably those of Ni, Sr, and Se, have stable counterparts that occur in the waste. In general the mass concentrations of the stable counterparts are substantially higher than the mass concentration of the radionuclides of interest. The solubility of an element in Table 11 is the sum of all the isotopes of that element in solution. Hence, use of the solubility in waste release modeling of a particular isotope that has a stable counterpart overestimates the actual concentration of the isotope of interest in solution. The degree of

overestimation depends on the ratio of the mass concentrations of the isotope of interest to its stable counterpart. For example Dean (2012) gives inventories for stable Ni (1073 moles), ^{59}Ni (1.8 moles), and ^{63}Ni (0.2 moles). Thus, for Ni the isotope dilution effect leads to a significant overestimation of the solubility for ^{59}Ni and ^{63}Ni. It is possible that the same effect would occur for Pu isotopes if ^{244}Pu is present in the residual waste. Even if ^{244}Pu was a small fraction of the activity it could be a significant fraction of the total mass of Pu because of its very low specific activity. In this case, the solubility for Pu in Table 11 would be an overestimate of the solubility of ^{239}Pu.

Uncertainty in Apparent Solubilities of Coprecipitated Elements

The primary uncertainty associated with estimated apparent solubilities of coprecipitated elements is whether the assumption that the ratio of the element to iron in fluid equilibrating with the host phase is the same as it is in the solid host phase. It is possible that elements of interest are preferentially leached from the host phase. Nevertheless, it is also possible that iron is preferentially leached or that sorption of the element to the iron host phase is strong and the element is not easily released to the aqueous phase.

Additional uncertainty is introduced by the phase change of the host phase from magnetite to maghemite. During the phase change a coprecipitated trace element may be released to the aqueous phase. The element cannot be released at a concentration that is higher than the solubility of a solubility controlling discrete phase of that element. The potential effect of the phase change on release of an element can be estimated by considering one cm^3 of residual waste. The moles of magnetite in the one cm^3 can be estimated from the conservative estimate of 4000 gallons of residual waste left in a tank (Dean, 2012) and the iron inventory (Dean, 2012). The conversion of magnetite to maghemite will not occur until oxygenated water flows through the one cm^3 of waste. Assuming the porosity of the waste is the same as the grout and the dissolved oxygen concentration of the infiltrating water is 2.19E-4 moles/liter, the number of pore volumes required to convert all of the magnetite to maghemite can be calculated. Each pore volume is assumed to become saturated with an element at an Eh of -0.26 volts, poised by the equilibrium between magnetite and maghemite, and the mass in the aqueous phase is then lost from the waste. Table 15 shows the worst case loss (averaged over all H-Area tanks) of coprecipitated Np, Pu, Tc, and U during the conversion of magnetite to maghemite. It is considered the worst case because it does not take into account any sorption or occlusion of the elements from passing pore fluids. Furthermore, if the oxidized iron phase was hematite the loss of Tc and U would be much less because their solubilities would be lower because the Eh would be -0.44 volts, poised by equilibrium of magnetite and hematite.

Table 15: Average worst case loss of coprecipitated Np, Pu, Tc, and U from an iron host phase during the conversion of magnetite to maghemite with a comparison to the loss if hematite was the oxidized host phase.

	Maghemite			Hematite		
Element	Solubility Controlling Phase	Solubility (M)	% Lost During Magnetite/ Maghemite Conversion	Solubility Controlling Phase	Solubility (M)	% Lost During Magnetite/ Hematite Conversion
Np	$NpO_{2(am,hyd)}$	1E-9	1	$NpO_{2(am,hyd)}$	1E-9	1
Pu	$PuO_{2(am,hyd)}$	3E-11	<1	$PuO_{2(am,hyd)}$	3E-11	<1
Tc	$TcO_2 \cdot 1.6H_2O$	2E-7	68	$TcO_2 \cdot 1.6H_2O$	1E-8	8
U	$UO_3 \cdot 2H_2O$	6E-5	76	$UO_{2(am,hyd)}$	5E-9	<1

There are geologic analogues for the conversion of magnetite to hematite that suggest the conversion does not cause complete redistribution of trace constituents between the host and aqueous phases. Banded iron formations (BIFs) are composed, in part, of iron minerals that have undergone transformations from iron hydroxide to hematite to magnetite and back to hematite (Ohmoto et al., 2006). Yet, the final hematite still maintains some of the chemical characteristics of the original iron mineral precipitation. Rare earth elements, lead isotopes, and oxygen isotopes all reflect, to some degree, original processes that formed BIFs (e.g., Planavsky et al., 2010; Frei and Polat, 2007; Gutzmer et al, 2006). This is not to say that the trace element concentrations and isotopic ratios are unaffected by mineralogic alterations, but rather that wholesale redistribution of elements did not take place in hematite of many banded iron formations. This is despite multiple mineral transformations and greater than one billion years of aging.

Effect of Step-Changes in the Grout Degradation Model on Solubility

The work of Atkinson (1985) and numerous others since (e.g., Berner, 1988; Reardon, 1990; Atkins et al., 1992, Bennet et al., 1992) show that hydrous calcium silicate gels (C-S-H) in cement dissolve incongruently yielding a carbonation versus pH curve in which pH continuously changes during carbonation until the calcium to silica ratio of the C-S-H is approximately 0.8 (Harris et al., 2002; Pabalan et al., 2009). This is difficult to implement in an equilibrium reaction path model. Hence, the four C-S-H type phases indicated by Kulik (2011) were used to represent different calcium to silica ratios and the step-changes in the model are the result of transition from one phase to the other. Table 16 shows the calcium to silica ratios of the four minerals – two types of jennite and two types of tobermorite. In the model presented here it is assumed that after several hundred to several thousands of years in 100% relative humidity the grout is fully hydrated and in mineralogical equilibrium. This is different from most experimental degradation of cement pastes in which full hydration and equilibrium have not been attained. There is enough reactive silica from the blast furnace slag and fly ash that when the

grout is in mineralogical equilibrium there is no portlandite. The hydrous calcium silicates in the initial equilibrium mineralogy consist of near equal amounts of JenH and TobD. The JenH initially controls pH at 11.6, but is rapidly (80 pore volumes) converted into TobD. TobD then controls the pH at 11.1 until it is exhausted and Oxidized Region III ensues. The effect of the step changes is to average out the gradual pH changes as the calcium to silica ratio changes. The work of Harris et al. (2002) suggests that at a pH of approximately 10.5 is when incongruent dissolution ceases and a constant pH is maintained until the C-S-H is completely dissolved. The model presented here uses a constant pH of 11.1 to calculate solubilities in Reduced Region II and Oxidized Region II, rather than varying the pH from 11.6 to 10.5.

Table 16: Calcium to silica ratios of the hydrous calcium silicate phases of Kulik (2011).

Mineral	Ca/Si
JenD	2.25
JenH	1.33
TobD	1.25
TobH	0.67

To examine the effect of this "averaging" of pH values on the solubilities of Np, Pu, U, and Tc simulations were run at pH values of 10.5, 11.1, and 11.6 and for each pH the Eh was varied from -0.5 to +0.6 volts. Figure 54 shows the Np solubility versus Eh curves for the three pH values. For Np significant differences in the solubilities only occurs at high Eh values. This suggests that the difference between the step change model and a more realistic degradation model would be inconsequential for Np solubilities except at high Eh.

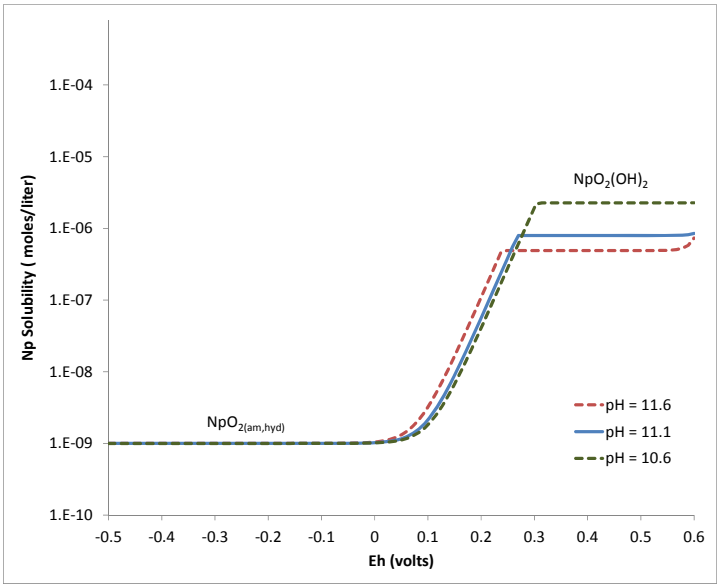

Figure 54: Solubility of Np versus Eh for pH values 10.5, 11.1, and 11.6.

For Pu two sets of curves are presented in Figure 55. Figure 55a assumes no precipitation of a Pu(VI) phase at high Eh values. Figure 55b allows $PuO_2(OH)_2 \cdot H_2O$ to precipitate and control

solubility at high Eh. Below and Eh value of +0.4 volts the curves for the three pH values are essentially the same suggesting that under these conditions the step change model and a more realistic model would produce the same solubility. Above an Eh value of +0.4 volts the curves diverge and there is somewhat less than a two order of magnitude difference between a solubility at pH=11.6 and pH=10.5 for a constant Eh. Hence, at the initial degradation of the JenH the step change model underestimates the solubility by approximately an order of magnitude. At the end of incongruent dissolution of the hydrous calcium silicate the step change model overestimates the solubility by approximately one order of magnitude. In between the error introduced by the step change model is less.

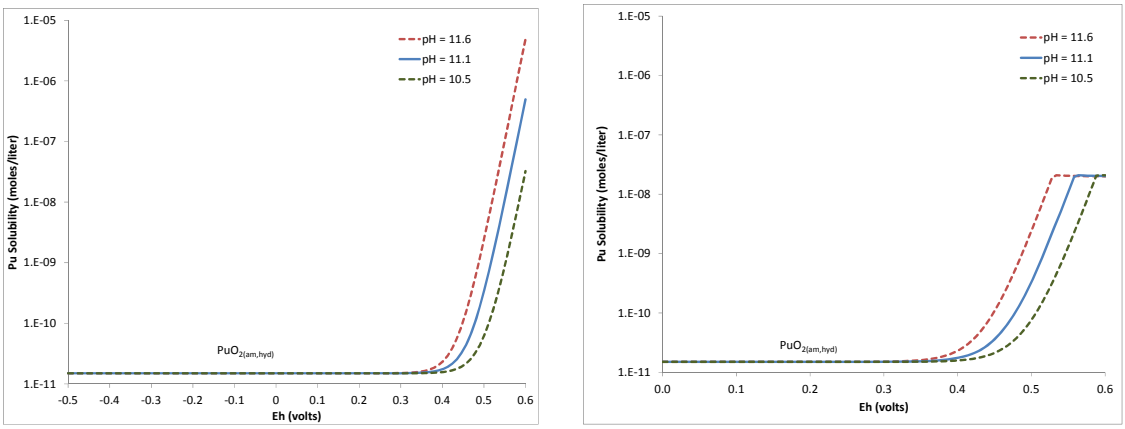

Figure 55: Solubility of Pu versus Eh for pH values of 10.5, 11.1, and 11.6.

Uranium behaves differently (Figure 56). At reducing conditions above an Eh value of -0.4 the difference between solubilities at pH values of 10.5 and 11.6 is nearly three orders of magnitude. At an Eh value of approximately -0.25 volts (depending on pH) $UO_3 \cdot 2H_2O$ precipitates. From that point on the difference between the pH=11.6 and pH=10.5 curves is one order of magnitude. The constant pH value of 11.1 tends to average out the errors in the solubilities as the grout degrades.

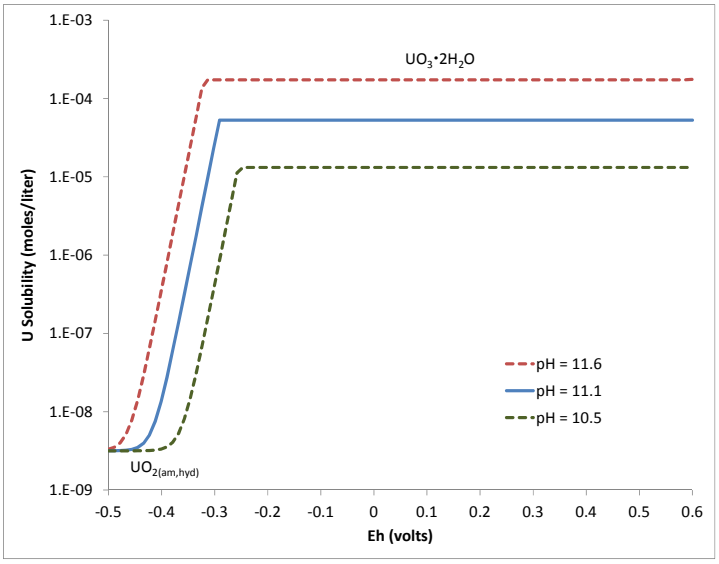

Figure 56: Solubility of U versus Eh for pH values of 10.5, 11.1, and 11.6.

Only reducing conditions are considered for Tc (Figure 57). For pH=11.1 the solubility of Tc is constant from -0.5 to -0.3 volts and increases abruptly at higher Eh values. In that range the difference in solubility at pH=11.6 and pH=10.5 is less than one order of magnitude and the error introduced by the constant pH of 11.1 is at maximum less than one half an order of magnitude.

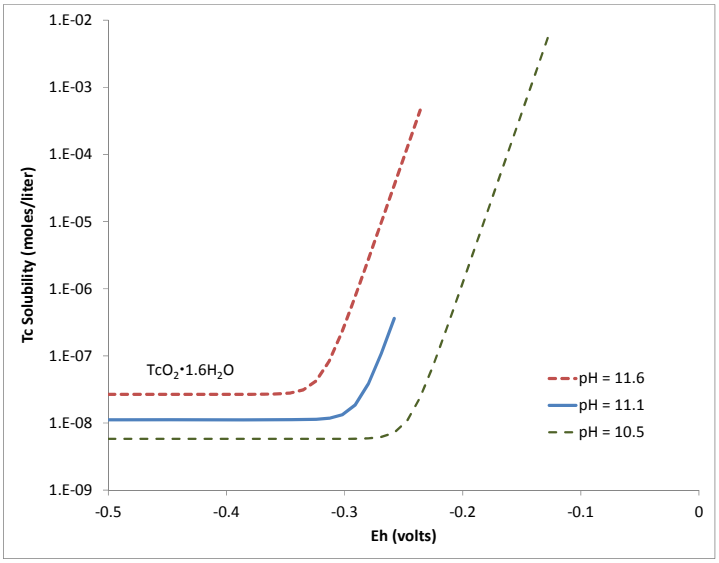

Figure 57: Solubility of U versus Eh for pH values of 10.5, 11.1, and 11.6.

Comparison of Solubilities with Other Studies

Comparison of solubilities estimated from thermodynamic data and specific conditions to solubilities compiled by others must be done with the recognition that conditions may differ and objectives may differ. For example, Krupka and Serne (1998) report estimated maximum solubilities of several radionuclides, whereas Kaplan (2006) reports “best” values. Table 17 lists estimated solubility values for some important radionuclides reported here compared to recommended values in Kaplan (2006) and Krupka and Serne (1998). Kaplan (2006) report values for generic cementitious material that was “young” (pH=12.5), “moderately aged” (pH=10.5), and “aged” (pH=5.5) in both reducing and oxidizing conditions. The compilation of Kaplan (2006) was based primarily on experimental rather than calculated values. Krupka and Serne (1998) list calculated maximum values for a range of pH and associated Eh values related to cementitious systems. The conditions most pertinent for this comparison are pH=11/Eh=0.27 (similar to Oxidized Region II) and pH=9/Eh=0.36 (similar to Oxidized Region III).

Table 17: Comparison of solubilities of key elements reported by this study to other compilations. All solubilities are in moles/liter.

Element	Reduced Region II		Oxidized Region II			Oxidized Region III		
	This Study	Kaplan (2006)	This Study	Kaplan (2006)	Krupka & Serne (1998)	This Study	Kaplan (2006)	Krupka & Serne (1998)
Am	10^{-9}	10^{-8}	10^{-9}	10^{-8}	10^{-11}	10^{-9}	10^{-7}	10^{-9}
Ni	10^{-9}	10^{-7}	10^{-7}	10^{-7}	10^{-8}	10^{-5}	10^{-6}	10^{-5}
Np	10^{-9}	10^{-6}	10^{-7}	10^{-8}	10^{-4}	10^{-6}	10^{-7}	10^{-3}
Pu	10^{-11}	10^{-10}	10^{-11}	10^{-8}	10^{-10}	10^{-11}	10^{-7}	10^{-10}
U	10^{-8}	10^{-7}	10^{-4}	10^{-7}	10^{-3}	10^{-5}	10^{-6}	10^{-4}
Tc	10^{-8}	10^{-10}	X	X	X	X	X	X

Given the caveats mentioned above values within an order of magnitude of each other should be considered good agreement. In reducing conditions the greatest discrepancies with Kaplan (2006) are Ni and Np. The difference for Ni arises because Kaplan (2006) did not consider sulfide phases because of lack of demonstrated presence in cementitious systems. However, Thoenen (1998) does consider the mineral millerite (NiS (c) alpha – used here as solubility controlling phase) a possible control on Ni concentrations in groundwater. For Np, Kaplan (2006) notes that the experimental values of Ewart (1992) are considerably lower than many calculated values. Pabalan (2009) suggests Np solubility values in reducing conditions between 10^{-8} and 10^{-9}, depending on Eh.

There is general agreement between the studies in the oxidized conditions as well. A notable exception is Np solubilities reported by Krupka and Serne (1998). However, they note that their recommended values are much higher than the experimental solubilities reported by Ewart et al. (1986), which tend to agree more with those presented here. They go on to note that Ewart et al. (1992) could fit a thermodynamic model to the Np(IV) experimental results by suppressing the anionic hydrolysis product $Np(OH)_5^-$. Subsequently in compiling the NEA thermodynamic database Lemire et al. (2001) stated that "$Np(OH)_5^-$ is not an important hydrolysis species for neptunium (IV)" and rejected any thermodynamic values.

The Pu solubility values in oxidized conditions recommended by Kaplan (2006) are higher than those in this study and for comparable conditions in Krupka and Serne (1998). This appears to be because the values reported by Kaplan (2006) came from studies that calculated the solubilities in equilibrium with dissolved oxygen. The value from this study is actually $10^{-10.5}$ (reported in Table 17 as 10^{-11}) and so agrees well with the value of 10^{-10} from Krupka and Serne (1998).

Another noteworthy comparison is to the solubility values calculated by Pabalon et al. (2009). They compared solubility calculations using the "thermo.com.v8.R6+" to calculations using the NEA database for Np, Pu, Tc, and U. Their solubilities calculated using the NEA database agree very well with those presented here.

Summary of Solubility Uncertainty

The sources of uncertainty in the solubility estimates include the thermodynamic data and uncertain conditions in the pore fluids contacting the waste as the tanks age. Examination of the effects of uncertainty in the thermodynamic data suggests an uncertainty in the solubilities that varies from approximately one to two orders of magnitude for four important elements. This uncertainty varies between elements and pore fluid compositions. This is shown in Figure 18.

There is uncertainty associated with the composition of the pore fluids in Table 10 which introduces uncertainty into the solubility estimates. Solubilities may be particularly sensitive to pH, Eh, dissolved inorganic carbon, and oxalate concentration. The sensitivities of Np, Pu, U, and Tc solubilities to these parameters were examined using diagrams that plot the solubility of a controlling phase against the parameter of interest. Some general trends are:

- In reducing conditions Tc is the only element that is sensitive to pH -- increased pH causes increased solubility
- In oxidizing conditions Np and U are sensitive to pH
- For Np, Pu, Tc, and U, Eh changes produce near step changes in solubility
    - For Np, Pu, and U in reduced phases, as Eh increases to a threshold value and over a narrow range of Eh the solubility of the reduced phase increases and a more soluble oxidized phase becomes stable
    - For Tc at Eh values greater than the threshold value, solubility increases over a narrow Eh range to a point where no solubility control is exerted
- Pu(IV) is insensitive to Eh up to values of Eh=+0.45 volts in Region II conditions
- Np(IV) is insensitive to Eh up to values of Eh=+0.10 volts
- The elements are most sensitive to dissolved inorganic carbon in Oxidized Region III and Condition A pore fluids
- Uranium is most sensitive to oxalate concentrations
    - Np is sensitive in oxidized regions at oxalate concentration greater than used for estimating solubilities
    - Pu and Tc solubilities are not sensitive to oxalate concentration

References

Allen, P.G., G.S. Siemering, D.K. Shuh, J.J. Bucher, N.M. Edelstein, C.A. Langton, S.B. Clark, T. Reich, and M.A. Denecke, 1997. Technetium speciation in cement waste forms determined by X-ray absorption fine structure spectroscopy. *Radiochimica Acta*, 76, 77-86.

Atkins, M., D.G. Bennett, A.C. Dawes, F.P. Glasser, A. Kindness, and D. Read, 1992b. "A thermodynamic model for blended cements." *Cement and Concrete Research*, 22, 497-502.

Atkins, M. and F.P. Glasser, 1992. Application of Portland cement-based materials to radioactive waste immobilization. *Waste Management*, 12, 105-131.

Bennett, D.G., D. Read, M. Atkins, and F.P. Glasser, 1992. A thermodynamic model for blended cements. II: Cement hydrate phases; thermodynamic values and modelling studies. *Journal of Nuclear Materials*, 190, 315-325.

Berner, U.R., 1988. Modelling the incongruent dissolution of hydrated cement minerals. *Radiochimica Acta*, 44/45, 387-393.

Bethke, C.M.and S. Yeakel, 2009. The Geochemist's Workbench® (geochemical modeling software), Release 8.0 Reference Manual, University of Illinois.

Bradbury, M. H., Sarott, F., 1995. Sorption Database for the Cementitious Near-Field of a L/ILW Repository for Performance Assessment, PIT-MISC-0075, ISSN 1019-0643, Paul Scherrer Institut, Switzerland.

Cantrell, K.J., K.M. Krupka, W.J. Deutsch, and M.J. Lindberg, 2006. Residual waste from Hanford tanks 241-C-203 and 241-C-204. 2. Contaminant Release Model, *Environmental Science and Technology*, 40, 3755-3761.

Cantrell, K.J., K.M. Krupka, W.J. Deutsch, M.J. Lindberg, H.T. Schaef, K.N. Geiszler, and B.W. Arey, 2008. Hanford Tank 241-C-103 Residual Waste Contaminant Release Models and Supporting Data. PNNL-16738, Pacific Northwest National Laboratory, Richland WA.

Dean, B., 2012, H-Area Tank Farm Closure Inventory for use in Performance Assessment Modeling, SRR-CWDA-2010-00023, Rev.3, Savannah River Remediation, Aiken, SC.

Denham, M., 2007. Conceptual Model of Waste Release from the Contaminated Zone of Closed Radioactive Waste Tanks. WSRC-STI-2007-00544, Rev. 2, Washington Savannah River Company, Aiken, SC.

Denham, M. and M. Millings, 2012. Estimated Solubilities of Americium, Neptunium, Uranium, and Technetium in Residual Waste in Post-Closure Aging of Tank 18F. SRNL-STI-2012-00241, Savannah River National Laboratory, Aiken, SC.

Flach, G. and J. Jordan, 2010. Conceptual approach for the H-Tank Farm Performance Assessment modeling with PORFLOW. SRNL-L6200-2010-00003, Savannah River National Laboratory, Aiken, SC.

Frei, R. and A. Polat, 2007. Source heterogeneity for the major components of ~3.7 Ga banded iron formations (Isua Greenstone Belt, Western Greenland): Tracing the nature of interacting water masses in BIF formation. Earth and Planetary Science Letters, 253, 266-281.

Furhmann, M., and Gillow, J., 2009, Fate of Contaminants with West Valley Grouts, BNL-82395-2009, Brookhaven National Laboratory, Upton, NY.

Gäfvert, T., C. Ellmark, and E. Holm, 2002. Removal of radionuclides at a waterworks. *Journal of Environmental Radioactivity*, 63, 105-115.

Glasser, F.P., 1997. Fundamental aspects of cement solidification and stabilization. *Journal of Hazardous Materials*, 52, 151-170.

Grenthe, I., J. Fuger, R.J.M. Konings, R.J. Lemire, A.B. Muller, C. N-T. Cregu, and H. Wanner, 1992. Chemical Thermodynamics of Uranium. North-Holland, Amsterdam.

Grigoriev, M.S., A.M. Fedoseev, A.V. Gelis, N.A. Budansteva, V.P. Shilov, V.P. Perminov, M.V. Nikonov, and N.N. Krot, 2001. Study of the interaction of Pu(IV) and Np(IV, V, VI) with iron hydroxides to predict the behaviro of actinides in environmental media. Radiochemica Acta, 89, 95-100.

Gu, B., S.C. Brooks, Y. Roh, and P.M. Jardine, 2003. Geochemical reactions and dynamics during titration of a contaminated groundwater with high uranium, aluminum, and calcium. *Geochimica et Cosmochimica Acta*, 67, 2749-2761.

Guillaumont, R., T. Fanghänel, J, Fuger, I. Grenthe, V. Neck, D.A. Palmer, M. H. Rand, 2003. Update on Chemical Thermodynamics of Uranium, Neptunium, Plutonium, Americium, and Technetium. Nuclear Energy Agency, Organisation for Economic Co-Operation and Development. Elsevier, Amsterdam.

Gutzmer, J., J. Mukhopadhyay, N.J. Beukes, A. Pack, K. Hayashi, and Z.D. Sharp, 2011. Oxygen isotope composition of hematite and genesis of high-grade BIF-hosted iron ores. Geological Society of America Memoirs 2006; 198; 257-268.

Hamm, L. and L. Collard, 2010, A Closer Look at HYF Tank elevations Versus Water Table (GSA Flow Model and Well Data Considered. SRNL-L5200-2010-00001, Savannah River National Laboratory, Aiken, SC.

Harris, A.W., Manning, M.C., Tearle, W.M., and Tweed, C.J., 2002, Testing of models of the dissolution of cements — leaching of synthetic CSH gels, Cement and Concrete Research, 32, 5, 731-749.

Hay, M.S., 1997. Analysis of Tank 19F Solids by X-ray Diffraction (U). SRT-LWP-97-111. Westinghouse Savannah River Company, Aiken, SC.

Hay, M.S., P.E. O'Rourke, and H.M. Ajo, 2012. Summary of XRD and SEM Analysis of Tank 18 Samples. SRNL-L3100-2012-00017, Savannah River National Laboratory, Aiken, SC.

Hay, M. S., K. P. Crapse, S. D. Fink, and J. M. Pareizs, 2007. "Characterization and Actual Waste Tests with Tank 5F Samples," WSRC-STI-2007-00192, Rev. 1, Aiken, SC: Savannah River National Laboratory. Washington Savannah River Company.

Heath, T., 2007. The HATCHES User Manual. Serco Assurance, Oxfordshire, England.

Hobbs, D.T., 1999. Precipitation of uranium and plutonium from alkaline salt solutions. *Nuclear Technology*, 128, 103-112.

Hobbs, D.T., 2012. Form and Aging of Plutonium in Savannah River Site Waste Tank 18. SRNL-STI-2012-00106, Savannah River National Laboratory, Aiken, SC.

Höglund, L.O., 2001. Project SAFE: Modelling of long-term concrete degradation processes in the Swedish SFR repository. SKB Report R-01-08, Swedish Nuclear Fuel and Waste management Co., Stockholm, Seden.

Hummel, W., U. Berner, E. Curti, F.J. Pearson, and T. Thoenen, 2002. "Nagra/PSI Chemical Thermodynamic Data Base 01/01." Techical Report 02-16, National Cooperative for the Disposal of Radioactive Waste.

Kaplan, D.I., 2006. Geochemical Data Package for Performance Assessment Calculations Related to the Savannah River Site (U). WSRC-TR-2006-00004 Rev. 0, Washington Savannah River Company, Aiken, SC.

Kaplan, D.I., T. Hang, and S. Aleman, 2005. Estimated Duration of the Reduction Capacity within a High Level Waste Tank (U), WSRC-RP-2005-01674, Washington Savannah River Company, Aiken, SC.

Krupa, K.M., and Serne, R.J., 1998, Effects on Radionuclide Concentrations by Cement/Ground-Water Interactions in Support of Performance Assessment of Low-Level Radioactive Waste Disposal Facilities, NUREG/CR-6377, PNNL-11408, U.S. Nuclear Regulatory Commission, Washington, DC.

Krupka, K.M., K.J. Cantrell, H.T. Schaef, B.W. Arey, S.M. Heald, W.J. Deutsch, and M.J. Lindberg, 2009. Characterization of Solids in Residual Wastes from Single-Shell Tanks at the Hanford Site, Washington, USA. Presentation to Waste Management 2009.

Kulik, D.A., 2006. "Improving the structural consistency of C-S-H solid solution thermodynamic Lothenbach, B., and F. Winnefeld. "Thermodynamic modelling of the hydration of Portland cement." *Cement and Concrete Research*, 36, 209-226.

Langmuir, D., 1997. Aqueous Environmental Geochemistry. Prentice Hall, Upper Saddle River, NJ.

Langton, C.A., 2007. Chemical Degradation Assessment of Cementitious Materials for the HLW Tank Closure Project (U). WSRC-STI-2007-00607, Rev. 0. Washington Savannah River Company, Aiken, SC.

Langton, C.A., 2009. Saltstone Matrix Characterization and Stadium Simulation Results: SIMCO Technologies, Inc. Task 6 Report. SRNL-STI-2009-00477, Rev. 0. Savannah River National Laboratory, Aiken, SC.

Lemire, R.J., J. Fuger, H. Nitsche, P. Potter, M.H. Rand, J. Rydberg, K. Spahui, J.C. Sullivan, W.J. Ullman, P. Vitorge, and H. Wanner, 2001. Chemical Thermodynamics of Neptunium and Plutonium. North-Holland, Amsterdam.

Lind, O.C., B. Salbu, L. Skipperud, K. Janssens, J. Jaroszewicz, and W. De Nolf, 2009, Solid state speciation and potential bioavailability of depleted uranium particles from Kosovo and Kuwait. *Journal of Environmental Radioactivity,* 100, 301-307.

Lothenbach, B. and F. Winnefeld, 2006. Thermodynamic modeling of the hydration of Portland cement. *Cement and Concrete Research*, 36, 209-226.

Lozano, J.C., F. Fernandez, and J.M.G. Gomez, 1997. Preparation of alpha-spectrometric sources by coprecipitation with Fe(OH)3: Application to actinides. *Applied Radiation and Isotopes.*, 48, 383-389.

Luke, K., and Lachowski, E., 2008, Internal Composition of 20-Year-Old Fly Ash and Slag-Blended Ordinary Portland Cement Pastes, Journal of the American Ceramic Society, 91, 12, 4084-4092.

Lukens, W.W., J.J. Bucher, D.K. Shuh, and N.M. Edelstein, 2004. Evolution of technetium speciation in reducing grout. *Environmental Science & Technology*, 39, 8064-8070.

Mellini, M. and F. Riccobono, 2005. Chemical and mineralogical transformations caused by weathering in anti-tank DU penetrators ("the silver bullets") discharged during the Kosovo war. *Chemosphere*, 60. 1246-1252.

Millings, M., J. Noonkester, and L. Bagwell, 2012a. Summary Dissolved Oxygen in Water Table Wells at SRS. SRNL-L3200-2011-00011, Savannah River National Laboratory, Aiken, SC.

Millings, M., 2012b, Summary Carbon Dioxide in Water Table Wells and the Vadose Zone at SRS, SRNL-L3200-2012-00017, Savannah River Nuclear Solutions, Aiken, SC.

Nakata, K., S. Nagasaki, S. Tanaka, Y. Sakamoto, T. Tanaka, and H. Ogawa, 2002. Sorption and reduction of neptunium(V) on the surface of iron oxides. *Radiochimica Acta*, 90, 665-669.

Noyes, R., 1994. Operations in Environmental Engineering. William Andrews Publishing.

Ohmoto, H., Y. Watanabe, K.E. Yamaguchi, H. Naraoka, M. Haruna, T. Kakegawa, K. Hayashi, and Y. Kato, 2010. Chemical and biological evolution of early earth: Constraints from banded iron formations. Geological Society of American Memoir 198, 291-331.

Pabalan, R.T., Glasser, F.P., Pickett, D.A., Walter, G.R., Biswas, S., Juckett, M.R., Sabido, L.M. , and Myers, J.L., 2009, Review of Literature and Assessment of Factors Relevant to Performance of Grouted Systems for Radioactive Waste Disposal, CNWRA 2009-001, Center for Nuclear Waste Regulatory Analyses, for U.S. Nuclear Regulatory Commission, Washington, DC.

Park, J-Y. and B. Batchelor, 2002. General chemical equilibrium model for stabilized/solidified wastes. *Journal of Environmental Engineering*, 128, 653-661.

Poirer, M.R., 2009, Analysis of Samples from Chemical Cleaning in Tank 5F, SRNL-L3100-2008-00020, Rev.3, Savannah River Nuclear Solutions, Aiken, SC.

Planavsky, N. A. Beffer, O.J. Rouxel, B. Kamber, A. Hofmann, A. Knudsen, and T.W. Lyons, 2010. Reare earth element and yttrium compositions of Archean and Paleoproterozoic Fe formations revisited; New perspectives on the significance and mechanisms of deposition. Geochimica et Cosmochimica Acta, 74, 6387-6405.

Rard, J.A., M.H. Rand, G. Anderegg, and H. Wanner, 1999. Chemical thermodynamics of Technetium. North-Holland, Amsterdam.

Reardon, E.J., 1990. An ion interaction model for the determination of chemical equilibria in cement/water systems., *Cement and Concrete Research*, 20, 175-192.

Roberts, K.A. and D.I. Kaplan, 2009. Reduction Capacity of Saltstone and Saltstone Components. SRNL-STI-2009-00637, Savannah River National Laboratory, Aiken, SC.

Roine, A., 2009. HSC Chemistry® Version 7.0 User's Guide, Volume 1/2 Chemical Reaction and Equilibrium Software with Extensive Thermochemical Database and Flowsheet Simulation. 09006-ORC-J, Outotec Research Oy, Finland.

Slater, S.A., D.B. Chamberalin, A.A. Aase, B.D. Babcock, C.Conner, J. Sedlet, and G.F. Vandegrift, 1997. Optimization of magnetite carrier precipitation process for plutonium waste reduction. *Separation Science and Technology*, 32, 127-147.

Stefanko, D.B. and C.A. Langton, 2011. Tanks 18 and 19-F Structural Flowable Grout Fill Material Evaluation and Recommendations. SRNL-STI-2011-00551, Savannah River National Laboratory, Aiken, SC.

Strom, R.N. and D.S. Kaback, 1992. Groundwater Geochemistry of the Savannah River Site and Vicinity (U). WSRC-RP-92-450, Westinghouse Savannah River Company, Aiken SC.

Thoenen, T., 1998, Solubility limitation of contaminant trace metals: an assessment for nickel in sulphidic groundwaters, Proceedings of Goldschmidt Conference, Toulouse, France.

Wakoff, B. and K.L. Nagy, 2004. Perrhenate uptake by iron and aluminum oxyhydroxides: An analogue for pertechnetate incorporation in Hanford waste tank sludges. *Environmental Science and Technology*, 38, 1765-1771.

Appendix 1: List of Minerals Used in Grout Degradation Simulations

Mineral	**Chemical Formula**
Brucite	$Mg(OH)_2$
C4AH13	$Ca_4Al_2O_7 \cdot 13H_2O$
Calcite	$CaCO_3$
Ettringite	$Ca_6Al_2(SO_4)_3(OH)_{12} \cdot 26H_2O$
$Fe(OH)_{3(am)}$	$Fe(OH)_{3(am)}$
Fe-Ettringite	$Ca_6Fe_2(SO_4)_3(OH)_{12} \cdot 26H_2O$
Gibbsite	$Al(OH)_3$
Gypsum	$CaSO_4 \cdot 2H_2O$
JenD	$Ca_{1.5}Si_{0.67}O_{2.84} \cdot 2.5H_2O$
JenH	$Ca_{1.33}Si_{1.0}O_{3.33} \cdot 2.17H_2O$
Maghemite	Fe_2O_3
Magnetite	Fe_3O4
Monocarboaluminate	$Ca_4Al_2O_6(CO_3) \cdot 11H_2O$
OH-Hydrotalcite	$Mg_4Al_2(OH)_{14} \cdot 3H_2O$
Portlandite	$Ca(OH)_2$
Amorphous Silica	SiO_2
TobD	$Ca_{0.88}Si_{0.67}O_{2.22} \cdot 1.83H_2O$
TobH	$Ca_{0.66}Si_2O_{4.66} \cdot 1.5H_2O$

Appendix 2 – Thermodynamic data for Ni, Np, Pu, U, Tc, and cement minerals

Reaction	Log K	Ref.
Cementitious Minerals		
Ettringite + $12H^{+} = 6Ca^{+2} + 2Al^{+3} + 3SO_4^{-2} + 38H_2O$	56.67	a
Fe-Ettringite + $12H^{+} = 6Ca^{+2} + 2Fe^{+3} + 3SO_4^{-2} + 38H_2O$	49.79	a
JenH + $2.66H^{+} = 1.33Ca^{+2} + Si(OH)_{4(aq)} + 1.5H_2O$	22.10	b
JenD + $3H^{+} = 1.5Ca^{+2} + 0.67Si(OH)_{4(aq)} + 2.66H_2O$	28.72	b
TobH + $1.32H^{+} + 1.84H_2O = 0.66Ca^{+2} + 2Si(OH)_{4(aq)}$	5.42	b
Portlandite + $2H^{+} = Ca^{+2} + 2H_2O$	22.80	b
Calcite = $Ca^{+2} + CO_3^{-2}$	-9.59	a
TobD + $1.66H^{+} = 0.83Ca^{+2} + 0.67Si(OH)_{4(aq)} + 1.32H2O$	13.56	a
OH-Hydrotalcite + $14H^{+} = 4Mg^{+2} + 2Al^{+3} + 17H_2O$	73.74	a
Brucite + $2H^{+} = Mg^{+2} + 2H_2O$	16.84	a
Monocarboaluminate + $12H^{+} = 4Ca^{+2} + 2Al^{+3} + CO_3^{-2} + 17H_2O$	70.29	a
C4AH13 +$14H^{+} = 4Ca^{+2} + 2Al^{+3} + 20H_2O$	104.20	a
Gibbsite + $3H^{+} = Al^{+3} + 3H_2O$	7.76	a
Silica(am) + $2H_2O = Si(OH)_{4(aq)}$	-2.71	a
Maghemite + $6H^{+} = 2Fe^{+3} + 3H_2O$	2.54	c
Magnetite + $8H^{+} = Fe^{+2} + 2Fe^{+3} + 4H_2O$	10.13	d
Pyrite + $H_2O = Fe^{+2} + 2HS^{-} + 0.5O_{2(aq)}$	-60.53	d

a—Lothenbach and Winnefeld (2006)

b—Kulik (2011)

c—Roine (2009)

d—HATCHES v. NEA18

Plutonium Thermodynamic Data Calculated from Free Energy of Formation Obtained from NEA

Species	Reaction	logK
Aqueous Species		
Pu+3	Pu+3 + 0.25O2(aq) +H+ = Pu+4 + 0.5 H2O	3.80
Pu+4		
PuOH+2	PuOH+2 + H+ = Pu+3 + H2O	6.90
PuOH+3	PuOH+3 + H+ = Pu+4 + H2O	-0.60
PuO2+	PuO2+ +3H+ = Pu+4 + 0.25O2(aq) +1.5H2O	-4.04
PuO2+2	PuO2+2 + 2H+ = Pu+4 + 0.5O2(aq) + H2O	-9.71
Pu(OH)2+2	Pu(OH)2+2 +2H+ = Pu+4 + 2H2O	-0.60
Pu(OH)3+	Pu(OH)3+ + 3H+ = Pu+4 + 3H2O	2.30
PuO2OH(a)	PuO2OH(a) + H+ = PuO2+ + H2O	9.73
PuO2OH+	PuO2OH+ + H+ = PuO2+2 + H2O	5.50
PuO2(OH)2(a)	PuO2(OH)2(a) + 2H+ = PuO2+2 + 2H2O	13.20
Pu(OH)4(a)	Pu(OH)4(a) + 4H+ = Pu+4 + 4H2O	8.50
PuO2CO3(a)	PuO2CO3(a) = PuO2+2 + CO3-2	-9.50
PuO2CO3-	PuO2CO3- = PuO2+ + CO3-2	-5.12
PuO2(CO3)2-2	PuO2(CO3)2-2 = PuO2+2 + 2CO3-2	-14.70
PuO2(CO3)3-4	PuO2(CO3)3-4= PuO2+2 + 3CO3-2	-18.00
PuO2(CO3)3-5	PuO2(CO3)3-5 = PuO2+ + 3CO3-2	-5.03
Pu(CO3)4-4	Pu(CO3)4-4 = Pu+4 + 4CO3-2	-37.00
Pu(CO3)5-6	Pu(CO3)5-6 = Pu+4 + 5CO3-2	-35.65
Solid Phases		
PuO2(am,hyd)	PuO2(am,hyd) +4H+ = Pu+4 + 2H2O	-1.99
PuO2(cr)	PuO2(cr) + 4H+ = Pu+4 + 2H2O	-8.03
PuO2CO3(s)	PuO2CO3(s) = PuO2+2 + CO3-2	-14.65

Neptunium Thermodynamic Data Calculated from Free Energy of Formation Obtained from NEA

Aqueous Species		
Species	**Reaction**	**logK**
Np+3	Np+3 + H+ + 0.25O2(aq) = Np+4 + 0.5H2O	17.7956
Np+4	Basis Species	
NpO2+	NpO2+ + 3H+ = Np+4 + 1.5 H2O + 0.25O2(aq)	-11.2790
NpO2+2	NpO2+2 + 2H+ = Np+4 + H2O + 0.5O2(aq)	-13.1788
NpOH+2	NpOH+2 + H+ = Np+3 + H2O	6.8001
NpOH+3	NpOH+3 + H+ = Np+4 + H2O	-0.5499
Np(OH)2+2	Np(OH)2+2 + 2H+ = Np+4 + 2H2O	-0.3500
NpO2OH(aq)	NpO2OH(aq) + H+ = NpO2+ + H2O	11.3007
NpO2OH+	NpO2OH+ + H+ = NpO2+2 + H2O	5.0997
NpO2(OH)2-	NpO2(OH)2- + 2H+ = NpO2+ + 2H2O	23.5992
Np(OH)4	Np(OH)4 + 4H+ = Np+4 + 4H2O	8.3048
(NpO2)2(OH)2+2	(NpO2)2(OH)2+2 + 2H+ = 2NpO2+2 + 2H2O	6.2698
(NpO2)3(OH)5+	(NpO2)3(OH)5+ + 5H+ = 3NpO2+2 + 5H2O	17.1192
NpO2CO3(aq)	NpO2CO3(aq) = NpO2+2 + CO3-2	-9.3204
NpO2CO3-	NpO2CO3- = NpO2+ + CO3-2	-4.9623
NpO2(CO3)2-2	NpO2(CO3)2-2 = NpO2+2 + 2CO3-2	-16.5155
NpO2(CO3)2-3	NpO2(CO3)2-3 = NpO2+ + 2CO3-2	-6.5338
Np(CO3)3-3	Np(CO3)3-3 = Np+3 + 3CO3-2	-15.6593
NpO2(CO3)3-4	NpO2(CO3)3-4 = NpO2+2 + 3CO3-2	-19.3711
NpO2(CO3)3-5	NpO2(CO3)3-5 = NpO2+ + 3CO3-2	-5.5001
Np(CO3)4-4	Np(CO3)4-4 = Np+4 + 4CO3-2	-36.6844
Np(CO3)5-6	Np(CO3)5-6 = Np+4 + 5CO3-2	-35.6158
(NpO2)3(CO3)6-6	(NpO2)3(CO3)6-6 = 3NpO2+2 + 6CO3-2	-49.8408
NpO2(CO3)2OH-4	NpO2(CO3)2OH-4 + H+ = NpO2+ + 2CO3-2 + H2O	5.3057
(NpO2)2CO3(OH)3-	(NpO2)2CO3(OH)3- + 3H+ = 2NpO2+2 + CO3-2 + 3H2O	2.8535
Solid Phases		
NpO2(c)	NpO2(c) + 4H+ = Np+4 + 2H2O	-9.7540
NpO2(am,hyd)	NpO2(am,hyd) + 4H+ = Np+4 + 2H2O	-0.7000
Np2O5(c)	Np2O5 + 2H+ = 2NpO2+ + H2O	3.6965
NpO2(OH)2(c)	NpO2(OH)2(c) + 2H+ = NpO2+2 + 2H2O	5.4693
NpO3.H2O(c)	NpO3.H2O(c) + 2H+ = NpO2+2 + 2H2O	5.4693
NpO2CO3(s)	NpO2CO3(s) = NpO2+2 + CO3-2	-14.5971
NpO2OH(am,aged)	NpO2OH(am,aged) + H+ = NpO2+ + H2O	4.7

Americium Thermodynamic Data Calculated from Free Energy of Formation Obtained from NEA

Aqueous Species		
Species	**Reaction**	**logK**
Am+2	Am+2 + H+ + 0.25O2(aq) = Am+3 + 0.5H2O	60.3689
Am+3	Basis species	0.0000
Am+4	Am+4 + 0.5H2O = Am+3 + H+ + 0.25O2(aq)	22.7171
AmO2+	AmO2+ +2H+ = Am+3 + 0.5O2(aq) + H2O	15.3892
AmO2+2	AmO2+2 + H+ = Am+3 + .75O2(aq) + 0.5H2O	20.8771
AmOH+2	AmOH+2 + H+ = Am+3 + H2O	7.2000
Am(OH)2+	Am(OH)2+ +2H+ = Am+3 + 2H2O	15.0999
Am(OH)3(aq)	Am(OH)3 + 3H+ = Am+3 + 3H2O	26.1996
AmCO3+	AmCO3+ = Am+3 + CO3-2	-7.9996
AmO2CO3-	AmO2CO3- = AmO2+ + CO3-2	-5.1005
Am(CO3)2-	Am(CO3)2- = Am+3 + 2CO3-2	-12.8997
AmO2(CO3)2-3	AmO2(CO3)2-3 = AmO2+ + 2CO3-2	-6.7000
Am(CO3)3-3	Am(CO3)3-3 = Am+3 + 3CO3-2	-15.0003
AmO2(CO3)3-4	AmO2(CO3)3-4= AmO2+2 + 3CO3-2	-18.9783
AmO2(CO3)3-5	AmO2(CO3)3-5 = AmO2+ + 3CO3-2	-5.1005
Am(CO3)5-6	Am(CO3)5-6 = Am+4 + 5CO3-2	-39.1084
AmHCO3+2	AmHCO3+2 = Am+3 + CO3-2 + H+	-13.4270
Solid Phases		
AmO2(c)	AmO2(c) + 4H+ = Am+4 + 2H2O	-9.9938
Am2O3(c)	Am2O3(c) + 6H+ = 2Am+3 + 3H2O	53.1472
Am(OH)3(c)	Am(OH)3(c) + 3H+ = Am+3 + 3H2O	15.6005
AmCO3OH.0.5H2O(c)	AmCO3OH.0.5H2O(c) + H+ = Am+3 + CO3-2+ 1.5H2O	-8.3990
AmCO3OH(am,hyd)	AmCO3OH(am,hyd) + H+ = Am+3 + CO3-2 + H2O	-6.2

Uranium Thermodynamic Data Calculated from Free Energy of Formation Obtained from NEA

Aqueous Species		
Species	**Reaction**	**logK**
U+3	U+3 + H+ + 0.25O2(aq) = U+4 + 0.5H2O	30.8437
U+4	Basis species	0.0000
UO2+	UO2+ +3H+ = U+4 + 0.25O2(aq) +1.5H2O	-13.9367
UO2+2	UO2+2 + 2H+ = U+4 + 0.5O2(aq) + H2O	-33.9436
UOH+3	UOH+3 + H+ = U+4 + H2O	0.5399
UO2OH+	UO2OH+ + H+ = UO2+2 + H2O	5.2507
UO2(OH)2(aq)	UO2(OH)2(aq) + 2H+ = UO2+2 + 2H2O	12.1497
U(OH)4(aq)	U(OH)4(aq) + 4H+ = U+4 + 4H2O	10.0052
UO2(OH)3-	UO2(OH)3- + 3H+ = UO2+2 + 3H2O	20.2506
UO2(OH)4-2	UO2(OH)4-2 + 4H+ = UO2+2 + 4H2O	32.4001
(UO2)2OH+3	(UO2)2OH+3 + H+ = 2UO2+2 + H2O	2.7001
(UO2)2(OH)2+2	(UO2)2(OH)2+2 + 2H+ = 2UO2+2 + 2H2O	5.6205
(UO2)3(OH)4+2	(UO2)3(OH)4+2 + 4H+ = 3UO2+2 + 4H2O	11.8995
(UO2)3(OH)5+	(UO2)3(OH)5+ + 5H+ = 3UO2+2 + 5H2O	15.5505
(UO2)3(OH)7-	(UO2)3(OH)7- + 7H+ = 3UO2+2 + 7H2O	32.1990
(UO2)4(OH)7+	(UO2)4(OH)7+ + 7H+ = 4UO2+2 + 7H2O	21.8997
UO2CO3(aq)	UO2CO3(aq) = UO2+2 + CO3-2	-9.9402
UO2(CO3)2-2	UO2(CO3)2-2 = UO2+2 + 2CO3-2	-16.6097
UO2(CO3)3-4	UO2(CO3)3-4 = UO2+2 + 3CO3-2	-21.8392
UO2(CO3)3-5	UO2(CO3)3-5 = UO2+ + 3CO3-2	-6.9497
U(CO3)4-4	U(CO3)4-4 = U+4 + 4CO3-2	-35.1207
U(CO3)5-6	U(CO3)5-6 = U+4 + 5CO3-2	-33.9994
(UO2)3(CO3)6-6	(UO2)3(CO3)6-6 = 3UO2+2 + 6CO3-2	-54.0005
(UO2)2CO3(OH)3-	(UO2)2CO3(OH)3- + 3H+ = 2UO2+2 + CO3-2 + 3H2O	0.8570
(UO2)3O(OH)2(HCO3)+	(UO2)3O(OH)2(HCO3)+ + 3H+ = 3UO2+2 + CO3-2 + 3H2O	-0.6529
(UO2)11(CO3)6(OH)12-2	(UO2)11(CO3)6(OH)12-2 + 12H+ = 11UO2+2 + 6CO3-2 + 12H2O	-36.4152
Solid Phases		
UO2(c)	UO2(c) + 4H+ = U+4 + 2H2O	-4.8511
UO3.2H2O(c)	UO3.2H2O(c) + 2H+ = UO2+2 + 3H2O	4.8109
UO2CO3(c)	UO2CO3(s) = UO2+2 + CO3-2	-14.7597
UO2 (am, hyd)	UO2(am, hyd) + 4H+ = U+4 + 2H2O	1.66
Na4UO2(CO3)3©	Na4UO2(CO3)3(c) = 4Na+ + UO2+2 + 3CO3-2	-27.1805

Technetium Thermodynamic Data Calculated from Free Energy of Formation Obtained from NEA

Aqueous Species		
Species	**Reaction**	**logK**
TcO4-	Basis species	
TcO4-2	TcO4-2 + H+ + 0.25 O2(aq) = TcO4- + 0.5 H2O	32.2908
TcO+2	TcO+2 + 1.5H2O + 0.75O2(aq) = TcO4- + 3H+	31.0434
TcO(OH)+	TcO(OH)+ + H+ = TcO+2 + H2O	1.5000
TcO(OH)2(aq)	TcO(OH)2(aq) + 2H+ = TcO+2 + 2H2O	4.0000
TcO(OH)3-	TcO(OH)3- + 3H+ = TcO+2 + 3H2O	14.8999
TcCO3(OH)2(aq)	TcCO3(OH)2(aq) = TcO+2 + H2O + CO3-2	-15.2522
TcCO3(OH)3-	TcCO3(OH)3- + H+ = TcO+2 + 2H2O + CO3-2	-6.9518
Solid Phases		
TcO2(c)	TcO2(c) + 2H+ = TcO+2 + H2O	-8.3936
TcO2*1.6H2O(s)	TcO2*1.6H2O(s) + 2H+ = TcO+2 + 2.6H2O	-4.4001
Tc2O7(c)	Tc2O7(c) + H2O = 2TcO4- + 2H+	15.3103
Tc2O7*H2O(s)	Tc2O7*H2O(s) = 2TcO4- + 2H+	14.1050

Thorium Thermodynamic Data Calculated from Free Energy of Formation Obtained from NEA

Aqueous Species		
Species	**Reaction**	**logK**
Th+4	basis species	
Th(OH)+3	Th(OH)+3 + H+ = Th+4 + H2O	2.5000
Th(OH)2+2	Th(OH)2+2 + 2H+ = Th+4 + 2H2O	6.2006
Th(OH)4(aq)	Th(OH)4(aq) + 4H+ = Th+4 + 4H2O	17.4006
Th2(OH)2+6	Th2(OH)2+6 + 2H+ = 2Th+4 + 2H2O	5.8998
Th2(OH)3+5	Th2(OH)3+5 + 3H+ = 2Th+4 + 3H2O	6.8002
Th4(OH)8+8	Th4(OH)8+8 + 8H+ = 4Th+4 + 8H2O	20.3997
Th4(OH)12+4	Th4(OH)12+4 + 12H+ = 4Th+4 + 12H2O	26.5997
Th6(OH)14+10	Th6(OH)14+10 + 14H+ = 6Th+4 + 14H2O	36.8004
Th6(OH)15+9	Th6(OH)15+9 + 15H+ = 6Th+4 + 15H2O	36.8004
Th(CO3)5-6	Th(CO3)5-6 = Th+4 + 5CO3-2	-30.9996
Th(OH)2(CO3)2-2	Th(OH)2(CO3)2-2 + 2H+ = Th+4 + 2CO3-2 + 2H2O	-8.7976
ThOH(CO3)4-5	ThOH(CO3)4-5 + H+ = Th+4 + 4CO3-2 + H2O	-21.5989
Th(OH)4(CO3)-2	Th(OH)4(CO3)-2 + 4H+ = Th+4 + CO3-2 + 4H2O	15.6048
Solid Phases		
ThO2(c)	ThO2(c) + 4H+ = Th+4 + 2H2O	1.7647
ThO2(am,hyd,fresh)	ThO2(am, hyd, fresh) + 4H+ = Th+4 + 2H2O	9.3000
ThO2(am,hyd,aged)	ThO2(am, hyd, aged) + 4H+ = Th+4 + 2H2O	8.5000

Thorium Thermodynamic Data Calculated from Free Energy of Formation Obtained from NEA

Aqueous Species		
Species	**Reaction**	**logK**
Ni+2	basis species	
NiOH+	NiOH+ + H+ = Ni+2 + H2O	9.5400
Ni(OH)3-	Ni(OH)3- + 3H+ = Ni+2 + 3H2O	29.1999
Ni2OH+3	Ni2OH+3 + H+ = 2Ni+2 + H2O	10.5999
Ni4(OH)4+4	Ni4(OH)4+4 + 4H+ = 4Ni+2 + 4H2O	27.5198
NiHS+	NiHS+ = Ni+2 + HS-	-5.1800
NiSO4(aq)	NiSO4(aq) = Ni+2 + SO4-2	-2.3501
NiCO3(aq)	NiCO3(aq) = Ni+2 + CO3-2	-4.1999
Solid Phases		
NiO(c)	NiO(c) + 2H+ = Ni+2 + H2O	12.4829
NiS(c) (alpha)	NiS(c) + H+ = Ni+2 + HS-	-9.5062
NiS(c) (beta)	NiS(c) + H+ = Ni+2 + HS-	-10.1261
NiS2(c)	NiS2(c) + H2O = Ni+2 + 0.25H+ + 0.25SO4-2 + 1.75HS-	-26.3878
NiSO4(c)	NiSO4(c) = Ni+2 + SO4-2	4.7457
NiSO4.7H2O(c)	NiSO4.7H2O(c) = Ni+2 + SO4-2 + 7H2O	-2.2675
NiCO3(c)	NiCO3(c) = Ni+2 + CO3-2	-10.9921
NiCO3.5.5H2O(c)	NiCO3.5.5H2O(c) = Ni+2 + CO3-2 + 5.5H2O	-7.5222
Ni(OH)2(beta)	Ni(OH)2beta + 2H+ = Ni+2 + 2H2O	11.0288

Appendix 3 – Diagrams Showing Sensitivity of Solubility to pH, Eh, Dissolved Inorganic Carbon and Dissolved Oxalate for Conditions C and D

Condition C – Neptunium

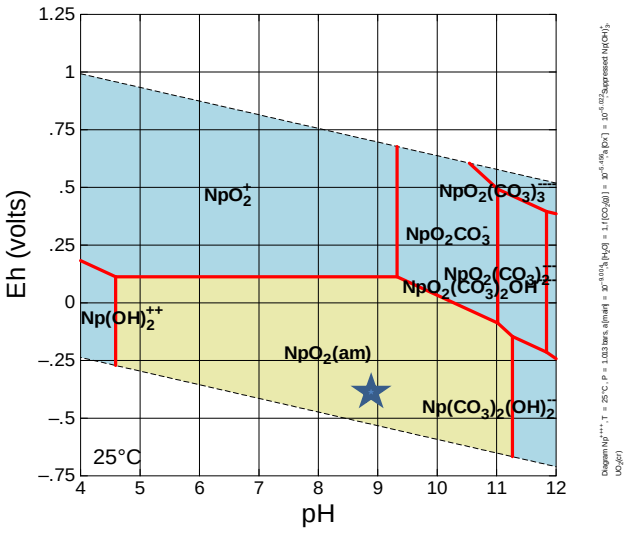

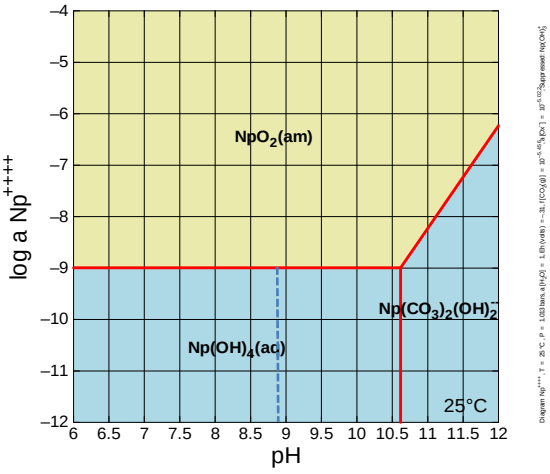

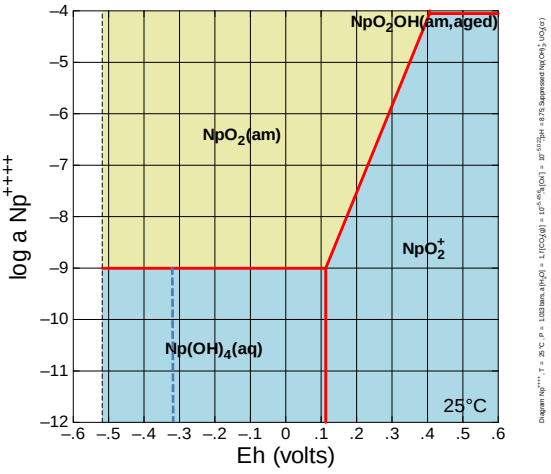

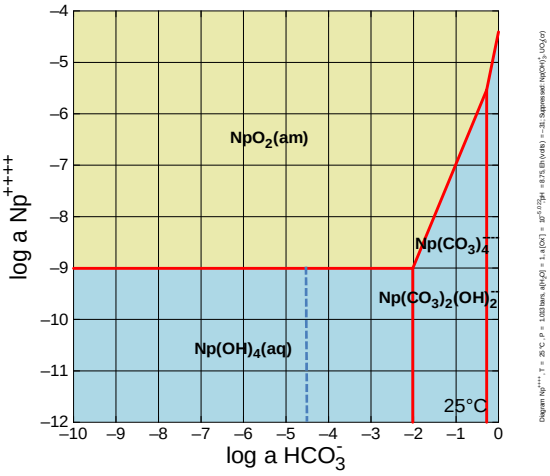

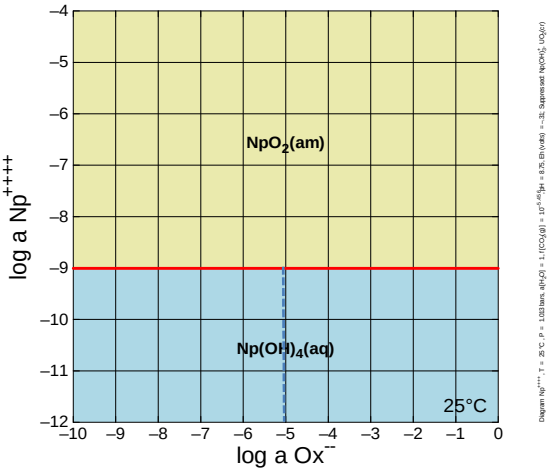

Condition C – Plutonium

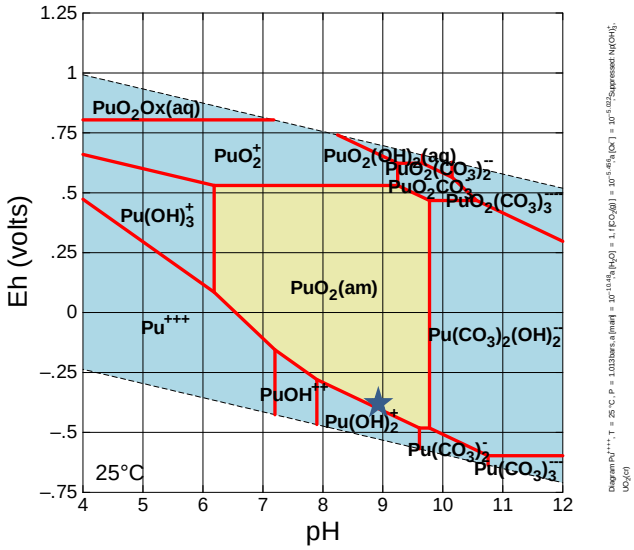

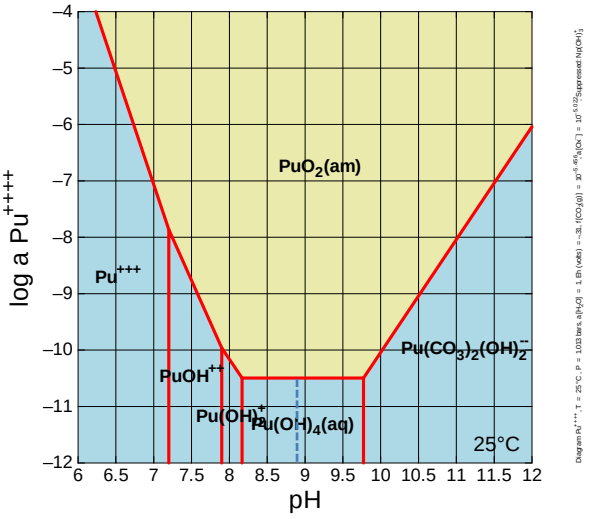

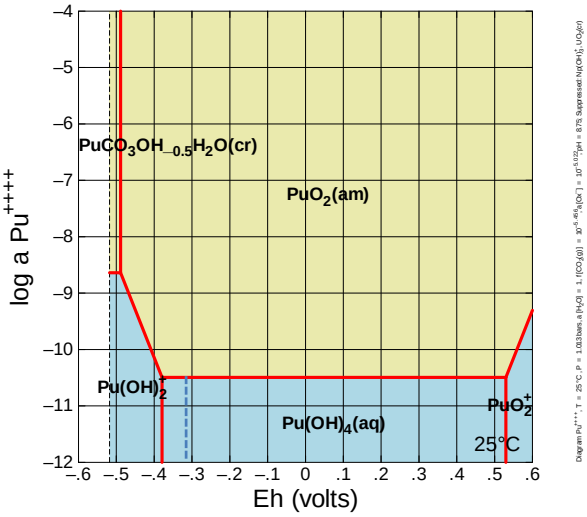

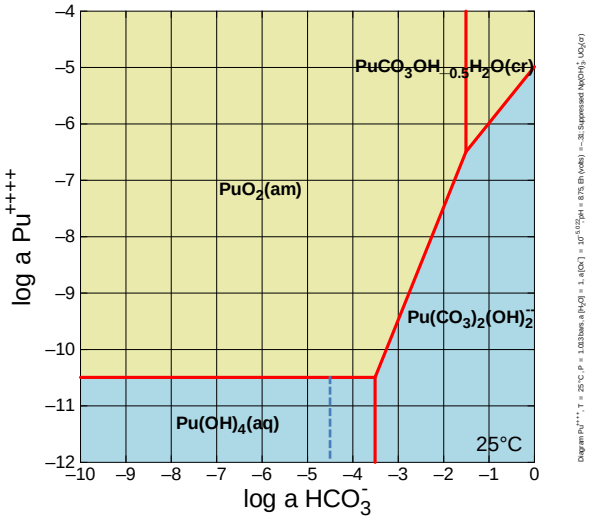

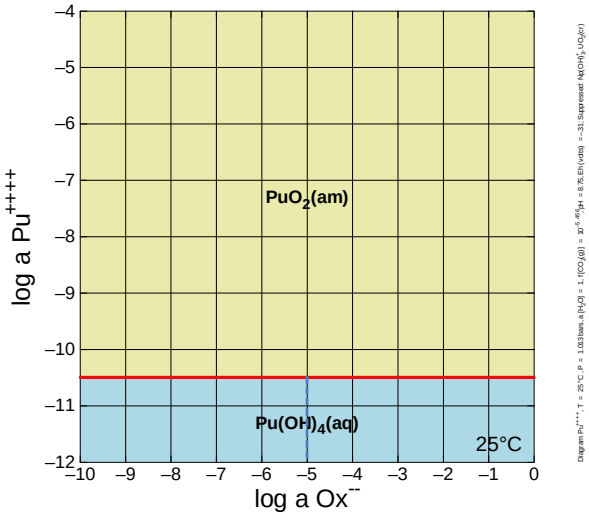

Condition C – Uranium

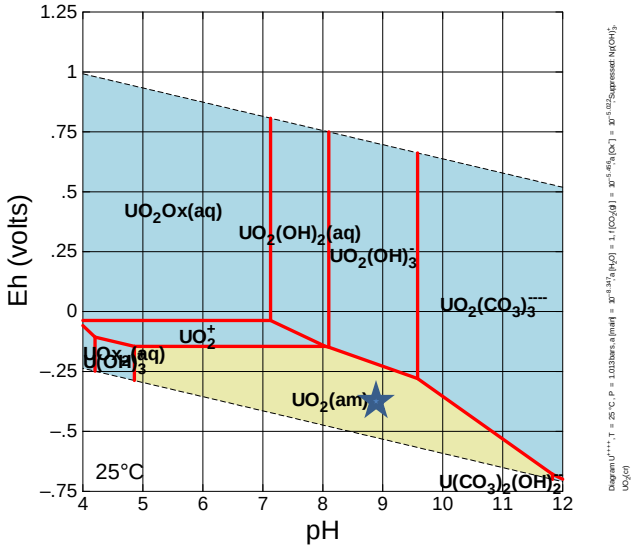

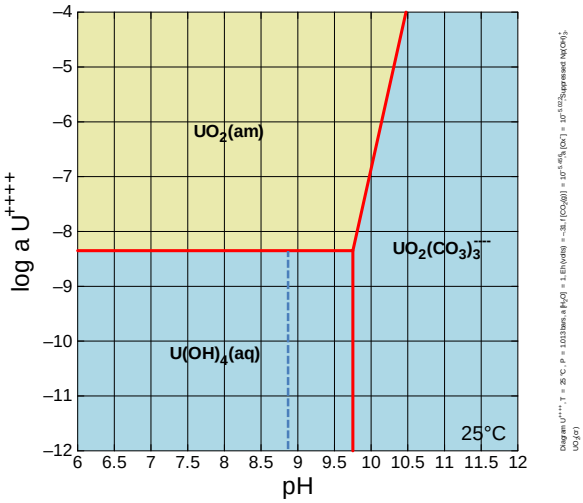

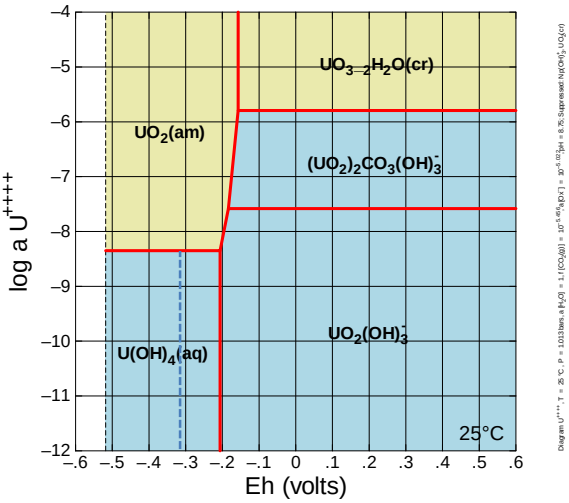

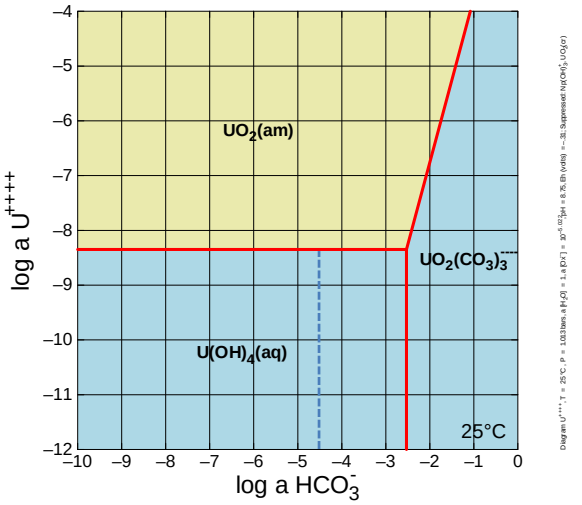

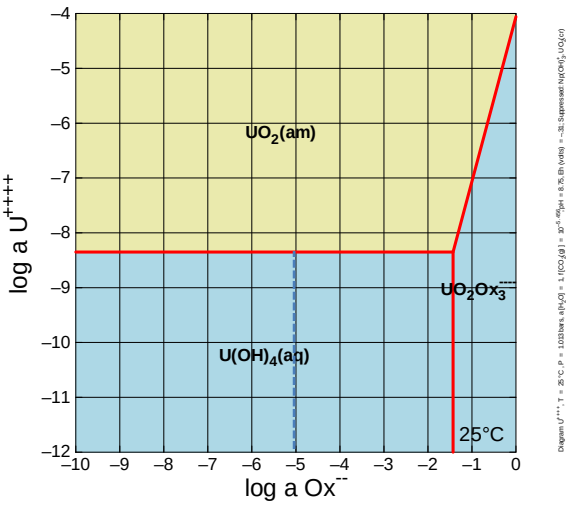

Condition C – Technetium

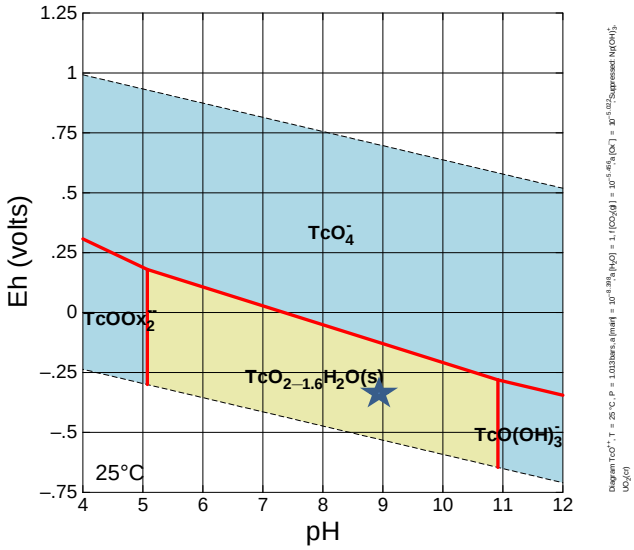

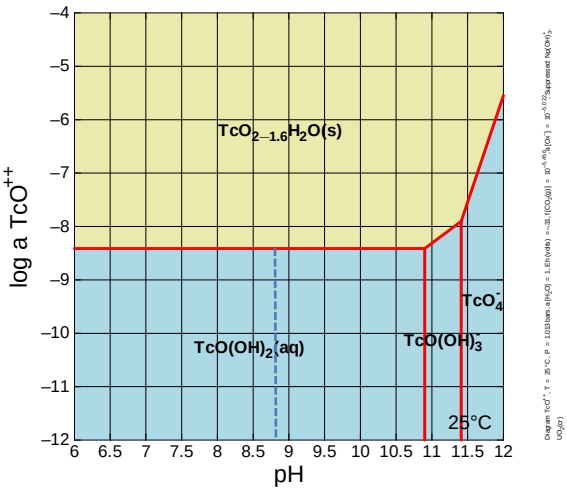

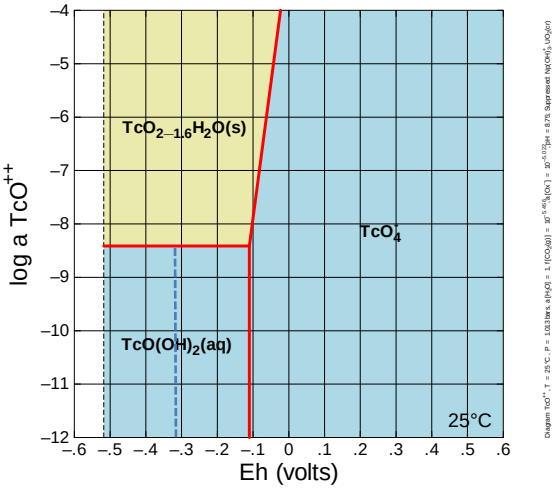

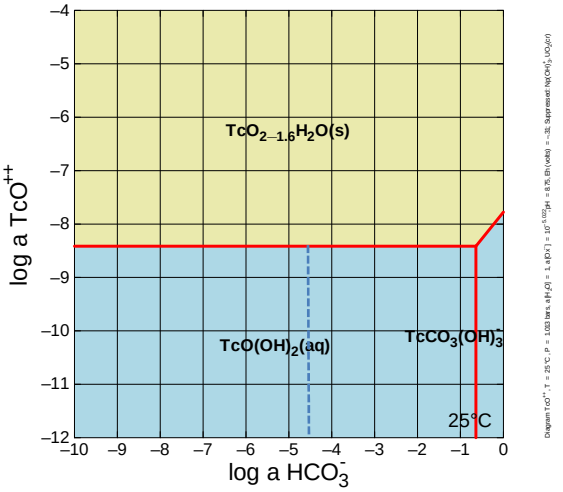

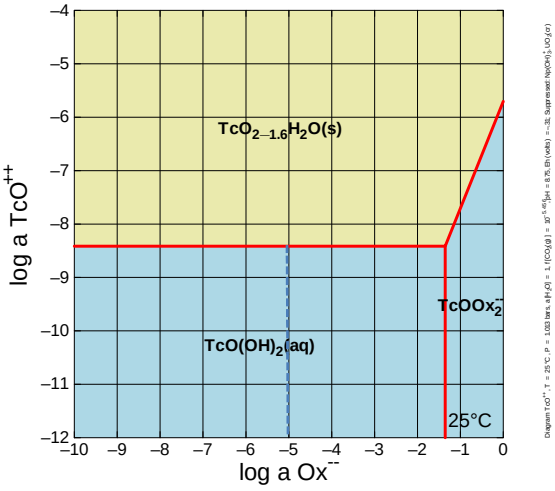

Condition D – Neptunium

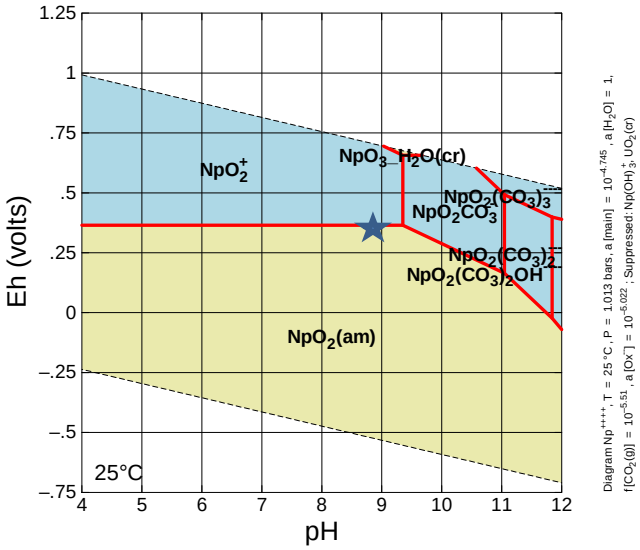

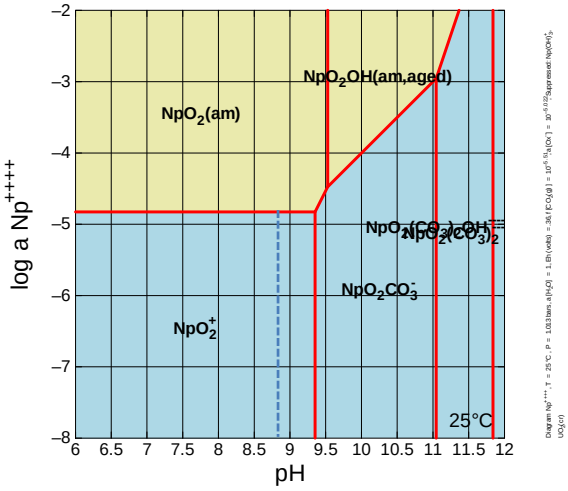

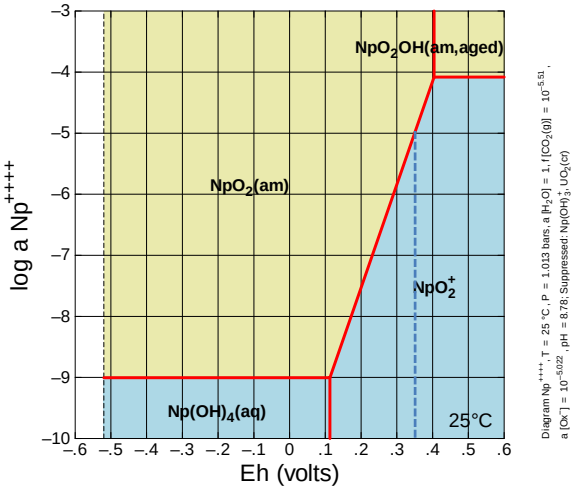

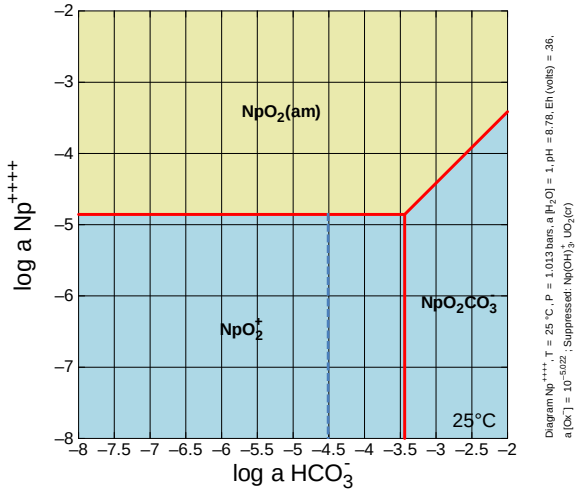

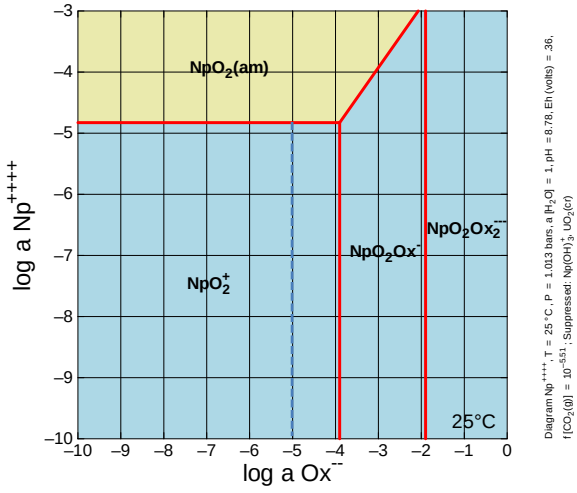

Condition D – Plutonium

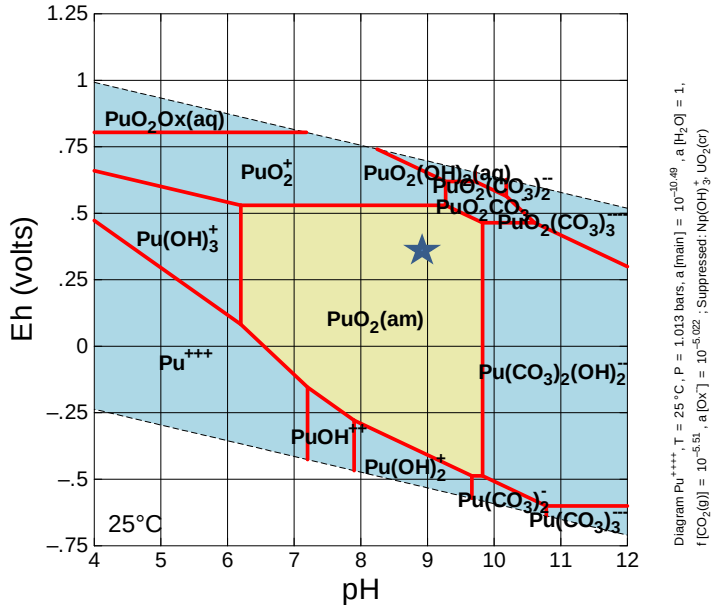

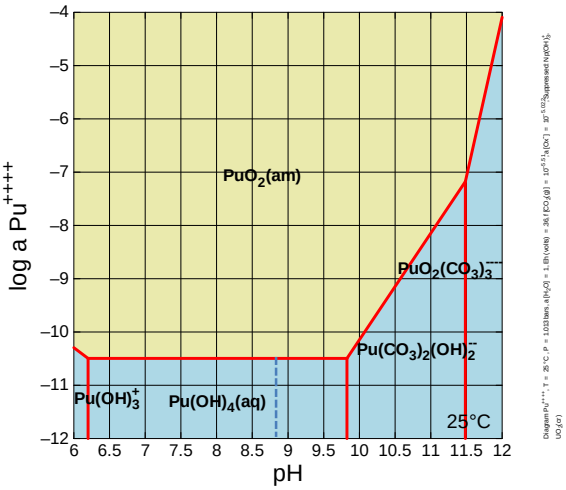

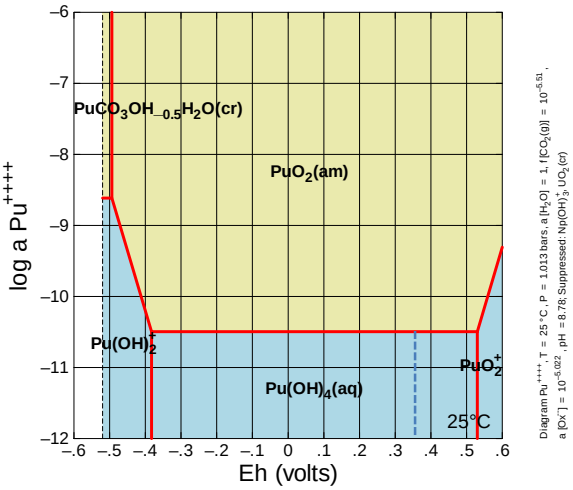

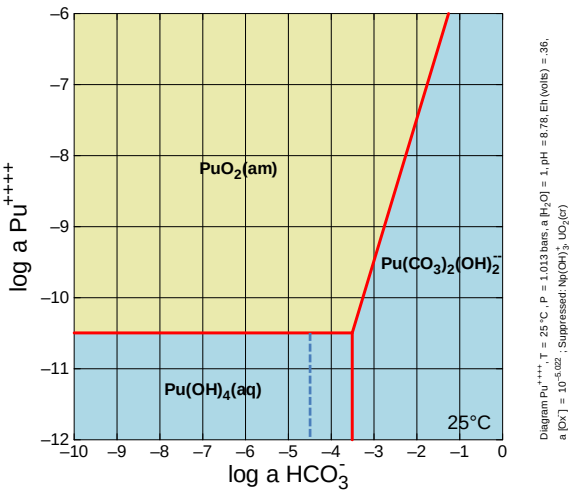

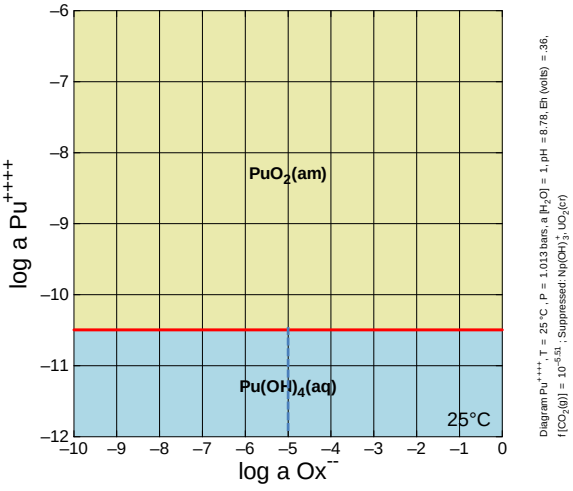

Condition D – Uranium